Spatial distribution and function of ion channels on neural axon

A dissertation presented to

the faculty of

the College of Arts and Sciences of Ohio University

In partial fulfillment

of the requirements for the degree

Doctor of Philosophy

Shangyou Zeng

March 2005

This dissertation entitled

Spatial distribution and function of ion channels on neural axon

by

Shangyou Zeng

has been approved for

the Department of Physics and Astronomy

and the College of Arts and Sciences by

Peter Jung

Associate Professor of Physics

Leslie A. Flemming

Dean, College of Arts and Sciences

SHANGYOU ZENG. Ph.D. March 2005. Physics

Spatial distribution and function of ion channels on neural axon (159pp.)

Director of Dissertation: Peter Jung

Voltage-dependent ion channels mediate action potentials in excitable membranes, and play an important role in signal generation and propagation in neurons. In different neurons and different parts of neurons, voltage-dependent ion channels are distributed heterogeneously to facilitate specific functions. In my dissertation, I focus on myelinated axons and unmyelinated axons, use deterministic HH equations, stochastic HH equations and cable equations to investigate the effect of the spatial organization of ion channels on neuronal function.

The spiking behavior of a small cluster of ion channels triggered by intrinsic noise and synaptic noise was investigated using stochastic HH equations. The mechanism in neuronal spike-generation by small and large ion channel clusters is different. For large ion channel clusters, action potentials are elicited by synaptic noise. In small ion channel clusters, channel noise dominates over synaptic noise. Action potentials are generated at a frequency that is determined by single-channel kinetics.

In some cases, ion channels are distributed in clusters along unmyelinated axons. Each ion channel cluster spikes spontaneously. The synchronization of ion channel clusters along unmyelinated axons was investigated. It has been shown that two ion channel clusters exhibit maximal synchrony when they have the same size. Furthermore there is an optimal size of ion channel clusters with maximal synchrony.

Blockage of internodal potassium channels of the immature axon will induce sustained oscillation activity by a single stimulus. The mechanism underlying the oscillation activity

and the function of internodal potassium channels were investigated. While the leakage current has no effect on axonal oscillations, increasing internodal sodium conductance as well as increasing internodal membrane capacitance can induce axonal oscillations. One function of internodal potassium channels is to stabilize the paranodal axolemma against nodal back-firing after a single impulse.

Experiments show that in some unmyelinated axons, ion channels are located in cluster. The effect of clustered ion channels on action potential propagation efficiency and speed was investigated. It has been shown that potassium channel localization is beneficial for increasing propagation efficiency and propagation speed of action potentials. Localization of sodium channels is advantageous to propagation efficiency only when axonal parameters are in a specific range.

Approved:

Peter Jung

Associate Professor of Physics

Acknowledgements

My dissertation would not have jumped off to a smooth start without the extensive succor from a variety of people around. Among them is Prof. Peter Jung, my supervisor and one of the four members of my dissertation committee, whose outstanding tutorship in the past four years has contributed to my steady advance of knowledge in physics. I am particularly impressed by his rigorous attitude and approach in science research, as well as by his solid academic background and sharp grasp of physical science. Prof. Jung's passion, dedication and aspiration for science have served a strong driving force behind my persistently assiduous study in the doctoral degree, putting me on the right track to complete my PhD dissertation, and giving me a steady ride for my future career in academia.

I also need to extend my thank-you note to Ohio University and its Physics & Astronomy Department for granting me full financial support, which totally shed my worries about funding the study and shown me a handy entry to an amiably excellent academic environment, thus gave me the full display of my talent on the academic work.

Meanwhile, Dr. William Holmes is another person on my thank-you list. It is he who funded my study, unloading my financial burden in the period when I was engaged in the dissertation writing. Besides, he instructed me last year on research projects, showing me the way into another brand new territory of research.

I am completely indebted to all the four professors in my dissertation committee: Prof. Peter Jung, Prof. William Holmes, Prof. David Tees and Prof. Daniel Phillips. Blessed by their constructive advice on my dissertation proposal, I have been put at ease to work on the dissertation. Furthermore, they spent lots of precious time reading my proposal and the draft version of my dissertation, always giving me thoughtful and insightful feedback.

On the other hand, I am grateful to all the faculty members of Ohio University that

have taught me in the past few years. Their rich knowledge and patient instructions have strengthened my academic background and expanded my horizon on science. I am fully convinced that their excellent teaching philosophy, methods and approaches will leave a lasting impact on my teaching career in the years to come.

I also need to thank department chair Prof. Wright Louis, department graduate chair Prof. David Drabold, advisor of the first academic year Prof. Sergio Ulloa and advisor of the second academic year Prof. Kenneth Hicks, for they have created an excellent academic environment that facilitated and advanced my hunt on academic research. I appreciate all my TA instructors, for they put me in the right course of self-discipline, perseverance and dedication, the rightful attitude toward scientific research and studies.

Meanwhile, I am thankful to Dr. Jianwei Shuai, Mr. Muhammad Afghan and Mrs. Suhita Nadkarni, as well as all the others who have provided me succor one way or the other in the last several years. Though I did not list all of their names right here, I just want to let them know that their heartfelt support left me indebted for the rest of my life.

I also appreciate the government and people of the United States for offering me the great opportunity to pursue my PhD degree. The last several years not only saw me upgrade my scientific knowledge, but also familiarized me with the great culture created by the great country and the great people. Upon them, I have found the virtues planted deeply in all human beings: consciences, integrity, kindness, compassion, patriotism, diligence and love.

I am deeply indebted to my family in China. I am grateful to my parents for bringing me up, nurturing me in a love-caring ambience and giving me access to top-notched college education. My parents have devoted their love to me unreservedly. And it is their strong support and love that made my study trip to the United States a reality in the first

place, placing me on a solid path to finish my doctoral program and getting me ready for a bright future career on teaching and research in the field of physics. Their selfless love will always accompany my academic journey, motivating me to gear up for new challenges and embrace new success and breakthroughs in the future.

Last but not least, I appreciate deeply my great home country and compatriots. The well-established, broad and profound culture created by my great ancestors and compatriots in the past five thousand years through unremitting struggle, persevering pursuit, unceasing vitality and unquenched faith has deeply affected my minds, feelings, qualities and values and engraved everlasting marks on my soul and spirit. She was one of the most powerful motility and spiritual support for me to withstand miseries and overcome difficulties in the past years. The huge determination, courage, devotion and faith displayed by them during the very long, arduous and magnificent course of pursuing Chinese nation's independence, emancipation and revival have manifested the noble, optimistic and never giving up spirit of human beings confronting miseries, difficulties and challenges, and will encourage me to finish my rest life's journey forever.

Contents

List of Tables

List of Figures

Chapter 1

Introduction

1.1 Morphology of the neuron

Neurons are the basic unit to send and receive electro-chemical signals to and from the brain and in the nervous system. There are approximately 100 billion nerve cells in the brain. The diameter of neural cell bodies varies from 1 μm to 100 μm(1). The length of neural axons ranges from dozens of microns to several meters. The typical neuron has four morphologically defined regions (Fig.1.1): the cell body (also called soma), the dendrites, the axon and the presynaptic terminals of the axon(1).

A neuron's dendritic tree is connected to thousands of neighboring neurons. When one of the neighboring neurons fires, a chemical or electrical signal is transmitted. After one of the dendrites receives the signal, a positive or negative voltage change is induced. The dendritic tree integrates the signals spatially and temporally. Spatial summation occurs when several weak signals sum into a single large one, while temporal summation converts a rapid series of weak pulses from one source into a large signal. The amassed signal is then propagated to the cell body. The soma and the enclosed nucleus do not play a significant

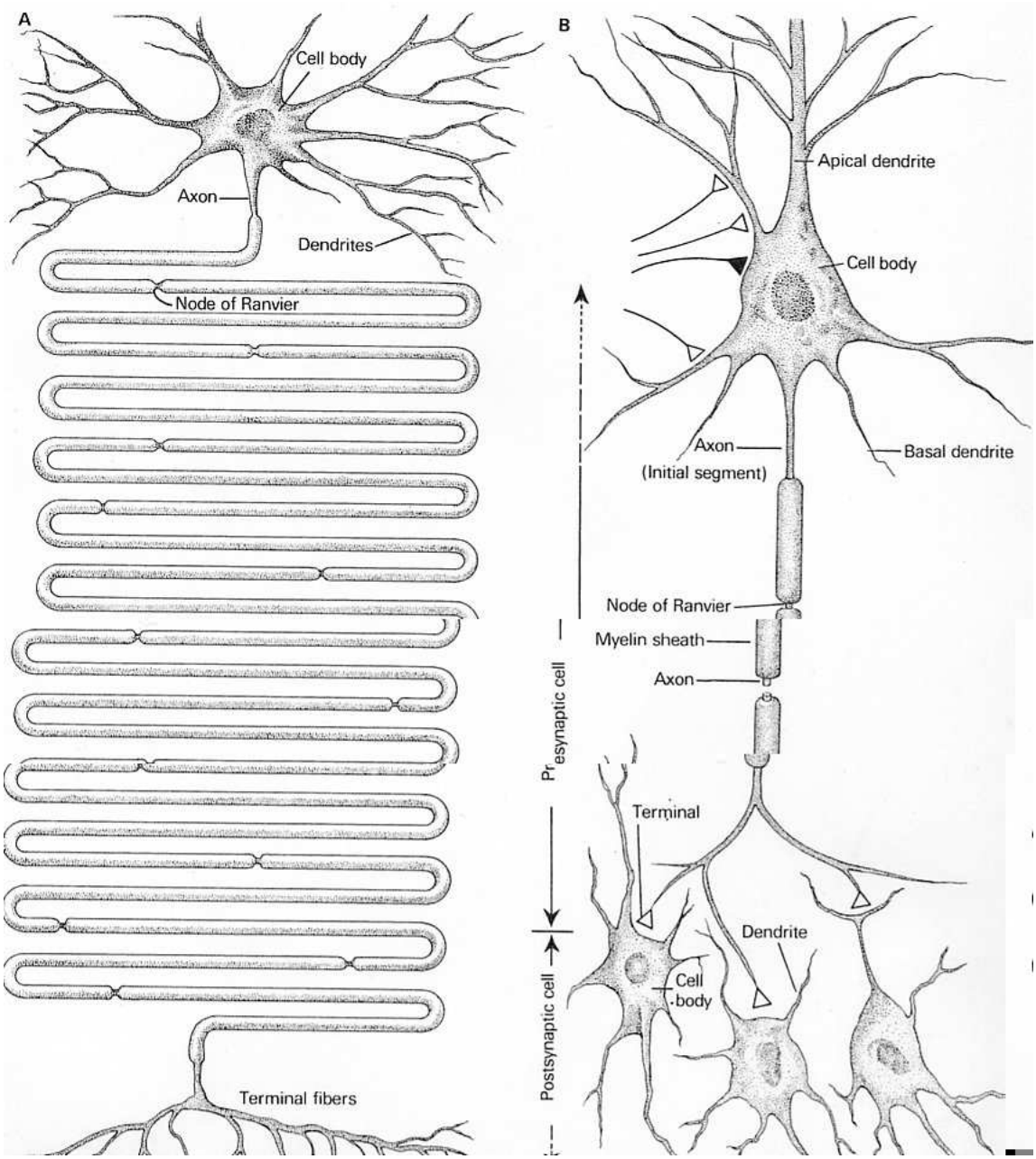

Figure 1.1: The main features of a typical neuron.
A. A neuron drawn to illustrate the relative extent of each region. B. Typical neuron drawn to illustrate its various regions and its points of contact with other nerve cells. Reprinted from (1).

role in regulating the incoming and outgoing signal. The main function of the soma is to perform a continuous maintenance required to maintain the neural function. In addition to the nucleus, the soma contains other cellular organelles. These organelles are located within the cell boundary in a fluid called cytoplasm. These organelles provide multiple functions, including protein production, energy production, transporting proteins through the cell membrane, enzyme production and hormone secretion, etc. Therefore the soma is the site of major metabolic activity in neurons. Soma diameters range widely from 5 μm to 100 μm in mammals. Neurons have a slightly expanded region at the initial end of the axon called the axon hillock. The axon hillock receives the aggregated signal integrated by the dendritic tree. If the aggregated signal is greater than the threshold value of the axon hillock, then the neuron fires an action potential, and the output signal is transmitted down along the axon. The amplitude of the output signal is constant, regardless of the strength of the input signal. The axon of a neuron is a singular fiber that carries information away from the soma to the presynaptic terminals of the axon. The axon is considerably longer than the dendrites of a neuron. The length of the axon ranges widely from dozens of microns to several meters. The signal propagates along the axon to the presynaptic terminals. After receiving the signal, the presynaptic terminals release chemicals called neurotransmitters. Neurotransmitters diffuse across the synaptic cleft to the dendritic tree of another neuron, and trigger a positive or negative charge at the postsynaptic dendrite.

1.2 Types of neurons

There are many kinds of neurons. They are different in shape and function. According to their function, spinal cord neurons are categorized as sensory neurons, motor neurons and interneurons(1). Sensory neurons carry messages from the body's sensory receptors to

the CNS (central nervous system). They are specialized to be sensitive to special physical stimuli, such as light, sound, chemicals or pressure. Motor neurons carry messages from the CNS to muscles or glands. Interneurons form the largest group in the nervous system. They receive input signals from sensory and other neurons, and send signals to motor and other neurons. Neurons also vary in shape, more particularly, in the number and form of processes. On the basis of process number arising from the cell body, neurons are categorized into three groups: unipolar, biploar, and multipolar(1). Unipolar neurons have one primary process that gives rise to many branches. Some branches serve as the dendritic tree to receive information, some branches serve as axons and presynaptic terminals. Unipolar neurons are predominant in the nervous systems of invertebrates. In bipolar neurons, the somas give rise to one process in each end. One process, called the dendrite or peripheral process, collects information from the periphery, the other process, called the axon or central process, carries information to the central nervous system. The bipolar cells in the retina are the classic examples. Multipolar neurons predominate in the vertebrate nervous system. These cells have many processes. Some processes serve as the dendritic tree branches, while one process serves as the axon. In a typical multipolar neuron, many dendrites emerge from all parts of the soma. The pyramidal cell and the Purkinje cell are the classic examples of the class.

1.3 Ion channels

Electrical signals in the nervous system are carried by dissociated ions: sodium, potassium, calcium and chlorine. Movement of ions across the plasma membrane induces changes of the electrical potential across the membrane. These potential changes are the primary signals that convey information from one part of the neuron to another part of the neuron, from

this neuron to another neuron, and from one part of the body to another part of the body. But since the cell membrane is almost impermeable to ions, it is necessary to use some specialized cellular devices to transport ions in and out of the neuron throught the membrane. The specialized devices are ion channels. Ion channels are formed by aggregation of proteins. Ionic current through ion channels is often driven by the ionic concentration gradient across the neuron membrane and the electric potential. The energy derives from the chemical forces of diffusion, osmosis, and electrochemical equilibrium.

Ion channels can be classified into two categories: passive or active(1). Passive ion channels are always open, but active channels have gates that can be either open or closed. The opening and closing of active ion channels is controlled by neurotransmitters, membrane potential or various other physical stimuli. Passive ion channels are important to determine the resting membrane potential, while active ion channels are responsible for the generation of action potentials and synaptic potentials. Ion channels, whether passive or active, can also be classified by their permeability. Each channel behaves as if it has a selective filter which permits some specific ions to pass through, but blocks other ions. In addition, there may be several different ion channels permeable for one type of ion. For example, some passive K^+ channels are responsible for the resting K^+ flux, and some active K^+ channels are responsible for the repolarization of the membrane after an action potential. Most ion channels are not perfectly selective, several types of ions may be permeable to the same type of ion channel. For example, K^+ channels pass one Na^+ ion for about 12 K^+ ions(1).

Passive channels, which are responsible for establishing the membrane resting potential, are located in the dendrite, the soma, and the axon. Chemically-gated channels, which are controlled by the neurotransmitter, are located on the dendrite and the soma, and are

responsible for producing synaptic potentials. Synaptic potentials are integrated by the dendritic tree, propagate to the soma, and serve as the input signal. Although there are lots of voltage-dependent channels in the dendrites and the soma, most voltage-gated channels are located on the axon hillock, along unmyelinated axons, and at the nodes of Ranvier in myelinated axons. These channels are responsible for the generation and propagation of action potentials.

The most important voltage-gated channels are Na^+, K^+, and Ca^{2+} channels. Na^+ channels are almost all voltage-gated. When the inside of the neuron becomes more positive, Na^+ channels activate or open, and allow Na^+ ions to pass through. Most Na^+ channels also close or inactivate in a few milliseconds even through the membrane potential remains at a level positive to the potential which activated them. Na^+ channels serve to let positive charge into the neuron to mediate the rising phase of the action potential. Na^+ channels are used in places where fast and reliable voltage changes are needed, such as generation of action potentials in the axon hillock and propagation of action potentials along the axon. K^+ channels, like Na^+ channels, open when the inside of the neuron becomes more positive. Some require a more positive voltage to open than most Na^+ and Ca^{2+} channels, and stay open as long as the voltage remains positive enough. Others open with small depolarizations and inactivate quickly. Activated K^+ channels allow positive charge to move from the neuron to the extracellular space , and mediate the repolarizing process of the action potential. Ca^{2+} channels, like Na^+ channels, activate when the inside voltage becomes more positive, and most inactivate spontaneously even through the voltage stimulus is maintained. They tend to open more slowly than Na^+ channels. Ca^{2+} channels also mediate the rising phase of the action potential as Na^+ channels, but they have some other cellular functions, such as: muscle contraction, hormone and neurotransmitter secretion,

etc. With the patch-clamp technique developed by Neher and Sakmann(2), it is possible to measure the electrical current through ion channels directly. The experiment shows that individual ion channels open and close randomly at constant membrane voltage, described by opening and closing rates(2; 3).

1.4 Location of channels

Action potentials are propagated by the axon to the synaptic terminal of neurons. The axon is a thin, tube-like process that arises from the neuronal cell body and travels from distances ranging from micrometers to meters before terminating. Axons come in two flavors, those covered by layers of the lipid *myelin* and those that are not. Most axons of invertebrates are unmyelinated, such as the squid axon. In most unmyelinated axons, the ion channels are distributed uniformly along the axon to provide stable propagation of action potentials. In this case, the conduction in the axon is continuous, and the excitability along the axon membrane is almost constant. Some experimental papers(4; 5; 6) show that the ion channels are also located in clusters along some kinds of unmyelinated axons, such as rat retina axons, giant squid axons and Aplysia axons. The mechanism and special function of ion channel clusters along unmyelinated axons are unclear. The exact value of single channel conductance depends on many variables, in particular the composition of the extracellular fluid. The conductance of a single potassium ion channel of giant squid axon is approximately 20 pS(9). The conductance of a single sodium ion channel of giant squid axon ranges from 2 pS to 10 pS(7; 8). The density of potassium ion channels in unmyelinated axon is approximately 20 per μm^2(9). The density of sodium ion channels in unmyelinated axon ranges from 10 to 330 per μm^2(7; 8). In our simulations of ion channel clusters in unmyelinated axon, we choose the conductances of a single sodium ion channel

and a single potassium ion channel to be 20 pS, the density of sodium ion channels to be 60 per μm^2 and the density of potassium ion channels to be 20 per μm^2. These values are also used in many simulation papers(10; 11; 12).

1.5 Myelin

In vertebrates, many axon fibers are wrapped dozens or even hundreds of times with myelin. Because much of the axon is myelinated, the actual diameter of the axon is approximately 60% or 70% of the total diameter with the myelin(13). The myelin sheaths, which originate from the Schwann cell in the peripheral nervous system (PNS) and the oligodendrocytes in the central nervous system (CNS) (14), consist of a compacted spiral of glial membrane surrounding the axon. This anatomical arrangement provides a high transverse resistance and low capacitance. Myelinated fibers are periodically punctuated by nodes of Ranvier, where the myelin is interrupted. The nodes usually extend for approximately 1-2 μm along the axon fiber(1; 13). The distance between two nodes ranges from hundreds of μm to several millimeters(13). The axon membrane itself is highly differentiated at the nodes of Ranvier, exhibiting different properties in that region compared to other sites along the fiber. Due to the isolating effect of myelin, the capacitance and leakage current conductance of the myelinated fibers are only approximately one percent of those of the nodes(13).

In both mammalian and frog myelinated nerves, voltage-dependent sodium ion channels are present mainly in the nodal and not in the internodal axolemma(15). In frog myelinated nerves, voltage-dependent potassium ion channels are present both in the internodal and in the nodal membrane(15). However, in mammalian myelinated nerves, potassium channels are virtually absent from the nodal membrane(16), being present only in the internodal axolemma. Because sodium ion channels are clustered in the nodal region of

myelinated axons, conduction does not proceed continuously along the cable, but jumps in a discontinuous manner from one node to the next. This *saltatory conduction* was clearly demonstrated by Huxley and Stampfli(17) and Tasaki (18). Sodium ion channel clusters in the nodal region provide the physiological basis for saltatory conduction. The function of the internodal potassium channels in the juxtaparanodal (nodal side of transition ranges from nodes of Ranvier to internodal regions) membrane remains unclear. The density of potassium ion channels in the juxtaparanodal regions is 12 per μm^2(19; 20). The density of sodium ion channels in the node ranges from 700 per μm^2 to 1500 per μm^2(21; 22). The conductance of each sodium ion channel in rat axon is 14.5 pS (21), and the conductance of each potassium ion channel in the rat axon is 20 pS(19; 20).

1.6 Hodgkin-Huxley equations

The electrical behavior of the excitable nerve membrane was first quantitatively formalized by Hodgkin and Huxley(23). In the Hodgkin-Huxley (HH) equations, the voltage dependent ion channel conductance is described by a set of deterministic nonlinear differential equations. When the density of ion channels is high, the HH equations are a good approximation to describe the average behavior of the large number of ion channels, which individually open and close stochastically. When the patch of membrane is small, the membrane exhibits spontaneous spiking(24; 25). In this case, the stochastic HH equations are more appropriate for describing the electric behavior of the membrane. Theoretical work shows that when the number of ion channels is small, then the stochastic HH equations can simulate all the unique behaviors of small numbers of ion channel clusters (10; 11; 26); when the ion channel number is large, the stochastic HH equation results will approach the deterministic limit, and generate the properties of the deterministic HH equations(27; 28).

There are two main sources of noise that arise in the nerve membranes: the noise due to the stochastic opening and closing of ion channels and synaptic noise due to stochastic arrival of neurotransmitter and spontaneous presynaptic release of neurotransmitters. When the area of the neuronal membrane is small, the noise effect due to the stochastic opening and closing of ion channels is dramatic. On the other hand, the neuronal membrane is also driven by the synaptic noise. The synaptic noise comes from multiple sources, including the probabilistic release of quantal transmitter, the random diffusion of transmitter, stochastic chemical reaction in synaptic cleft and unpredictable responses of ligand-gated ion channels(29). Neurons in cortical and other neural cells receive a continuous barrage of synaptic input as a source of external noise(30).

Voltage-dependent ion channels mediate action potentials in excitable membranes, and play an important role in signal generation and propagation in neurons(31). In the last decades, using many methods such as: recombinant DNA technology, protein chemistry, X-ray diffraction and electron microscopy, experimentalists have identified the protein components of many voltage-dependent ion channels, derived their amino acid sequence, and cloned, expressed, and manipulated them(13) . On the basis of the HH equations, theorists have constructed many models to simulate and predict the electrical behaviors of neurons such as: spiking, sub-threshold behavior, bursting and oscillation(3; 13). In different neurons and different parts of neurons, voltage-dependent ion channels are distributed differently to facilitate corresponding functions(3; 13). In my thesis, I focus on myelinated and unmyelinated axons, use deterministic HH equations, stochastic HH equations and cable equations to investigate the effect of the spatial organization of ion channels on neuronal function. The thesis is organized as follows:

Chapter 2: Structure, properties and distribution of ion channels. In this chapter, I will

introduce the molecular structure of ion channels briefly, introduce biophysical properties of ion channels, and then demonstrate the ion channel distribution along unmyelinated and myelinated axons.

Chapter 3: Deterministic and stochastic HH equations. In this chapter, I will describe the corner stone of modern neuroscience: HH equations, then describe the stochastic HH equations, and describe several general solution methods of stochastic HH equations.

Chapter 4: Cable equation. In this chapter, I will introduce the cable equation, the solution of the cable equation under special boundary conditions, and the numerical solution of the cable equation.

Chapter 5: Mechanism for neuronal spike generation by small and large ion channel clusters. When the cluster of ion channels is small, it is more valid to use stochastic HH equations to describe the electrical behavior of the membrane. The mechanism for neuronal spike-generation by small and large ion channel clusters will be different. I will use stochastic HH equations to investigate the spiking behavior of a small cluster of ion channels triggered by intrinsic noise and external noise.

Chapter 6: Synchronization of ion channel clusters along the unmyelinated axon. Although in most cases, ion channels are distributed uniformly along unmyelinated axon, in some cases, ion channels are also distributed in clusters. Each cluster spikes spontaneously. In this chapter, I will investigate the synchronization of ion channel clusters along unmyelinated axons.

Chapter 7: Axonal oscillation in developing mammalian nerve axons. In myelinated axon, sodium channels are located at nodes, but potassium channels are located in juxtaparanodal regions. Blockage of internodal potassium channels in the immature axon will induce bursting activity by a single stimulus, but blockage of internodal potassium channels

of a mature axon has no the effect. In this chapter, I will investigate the sources to induce bursting activity and the function of internodal potassium channels.

Chapter 8: Effects of clustering ion channels along unmyelinated axons. Experiments show that in some unmyelinated axons, ion channels are located in clusters. In this chapter, I will investigate the effect of clustering ion channels on action potential propagation efficiency and speed.

Chapter 9: Summary

Chapter 2

Properties, structure and distribution of ion channels

An ion channel is an integral membrane protein or more typically an assembly of several proteins(13). They anchor within the membrane lipid bilayer of neurons, glia, and other cells. Their function is to facilitate the diffusion of ions across biological membranes. By controlling the diffusion of ions, ion channels provide the substrate for all biophysical phenomena relating to information processing, including mediating synaptic transmission, controlling membrane potential, invoking the action potential and supporting the propagation of the action potential. Channels are either open or closed. The conformational change between closed and open states induced by an external or internal signal is called gating. Channel gating can be due to changes in the membrane voltage or by binding of the neurotransmitter. Ion channels can be classified according to the chemical or physical modulators that control their gating activity. There are several different groups of ion channels as summarized below(13):

- Voltage-gated channels sense the transmembrane potential and their opening or closing is controlled by the transmembrane potential. Sodium, calcium and many potassium channels belong to this class of channel.

- Ligand-gated channels open in response to a specific ligand molecule on the surface of the membrane. AMPA receptor and other neurotransmitter-gated channels belong to this class of channel.

- Channels open in response to second messengers. Calcium-activated potassium channels belong to this class of channel.

- Channels open or close in response to compression. This kind of channel is believed to detect touch pressure or acoustic vibration.

Some channels respond to multiple stimuli. For example, the NMDA receptor is activated not only by interaction with its ligand, glutamate, but also by transmembrane potential and only conducts when glutamate is bound and the membrane is depolarized. Some calcium-sensitive potassium channels respond to both calcium and transmembrane potentials.

2.1 Biophysics of channels

A single channel opens or closes stochastically, and is controlled by membrane potential, stimuli of ligand molecules or compression. The channel is conducting, only when the channel is open. The switch-like behavior of a single channel is demonstrated in Fig.2.1. The current through a single channel can be described by a nonlinear model, called Goldman-Hodgkin-Katz equation, and Ohm's law(13; 32). In most cases, if the Nernst re-

versal potential is properly included, Ohm's law is sufficient to describe the relationship of voltage and current of a single open channel as follows(13; 32),

$$I_{ionic} = \gamma(V - V_{ionic}) \tag{2.1}$$

where γ is the channel conductance of a single channel, and V_{ionic} is the reversal potential of the specific kind of ion.

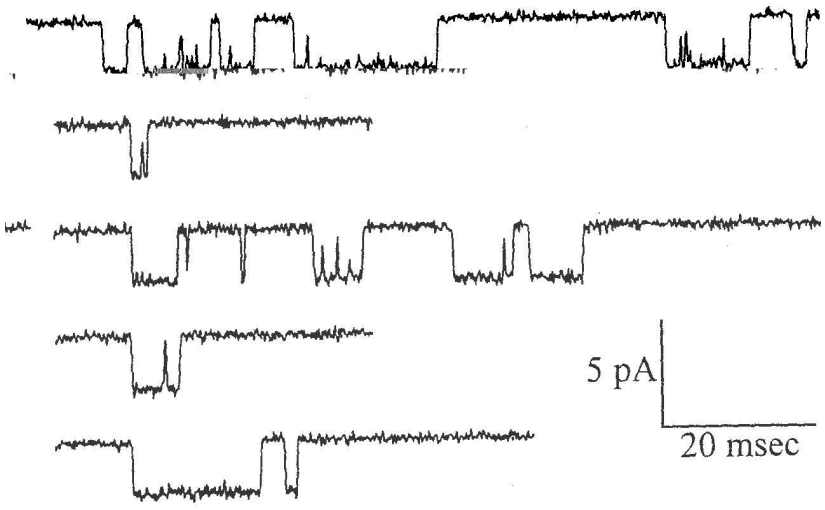

Figure 2.1: Current flowing through a single ion channel.
Several excerpts from a patch-clamp recording of a single acetylcholine-activated channel on a cultured muscle cell are shown. The openings of the channel (downward events) cause a unitary 3-nA current to flow, occasionally interrupted by a brief closing. Reprinted from (13).

The voltage dependence of some ion channels are plotted in Fig.2.2. In part A, the ion channel satisfies Ohm's law. In part B, the I-V relationship of calcium-dependent potassium channel is not exactly linear; for large potential excursions, the current through the ion

Table 2.1: Ion channel density and single channel conductance

Channel type	Preparation	γ(pS)	ion channel density $\eta(1/\mu m^2)$
Fast Na^+	Giant squid axon	14	330
Fast Na^+	Rat axonal node of Ranvier	14.5	700
Fast Na^+	Pyramidal cell body	14.5	4-5
Delayed rectifier K^+	Giant squid axon	20	18
Ca^{2+}-dependent K^+	Mammalian preparation	130-240	—-
Transient A current	Insect, snail, mammal	5-23	—-
Nicotinic ACh receptor	Mammalian motor endplate	20-40	10,000
$GABA_A Cl^-$ receptor	Hippocampal granule cells	14-23	—-

channel begins to saturate. There are many sources responsible for the nonlinearity. When the concentration gradient of ions is too steep, current flows more easily in one direction than in the other direction. A second source of nonlinearity is that ions move into the channel and block it. The value of γ ranges from one to several hundred pS for various ion channels(3; 13). The upper limit of γ is 300 pS, for no channel with larger conductance has been reported(3; 13). The density of ion channels varies widely depending on the nervous tissue. In the unmyelinated axon, such as the squid axon, the density of sodium channels is on the order of 300 per square micrometer, and that of potassium channels is on the order of 20 per square micrometer(3; 13). In the node of Ranvier, sodium channels are high localized, and can be as high as 2000 per square micrometer(3; 13). The single channel conductances and channel densities are listed in Table.2.1, which is reprinted from (13).

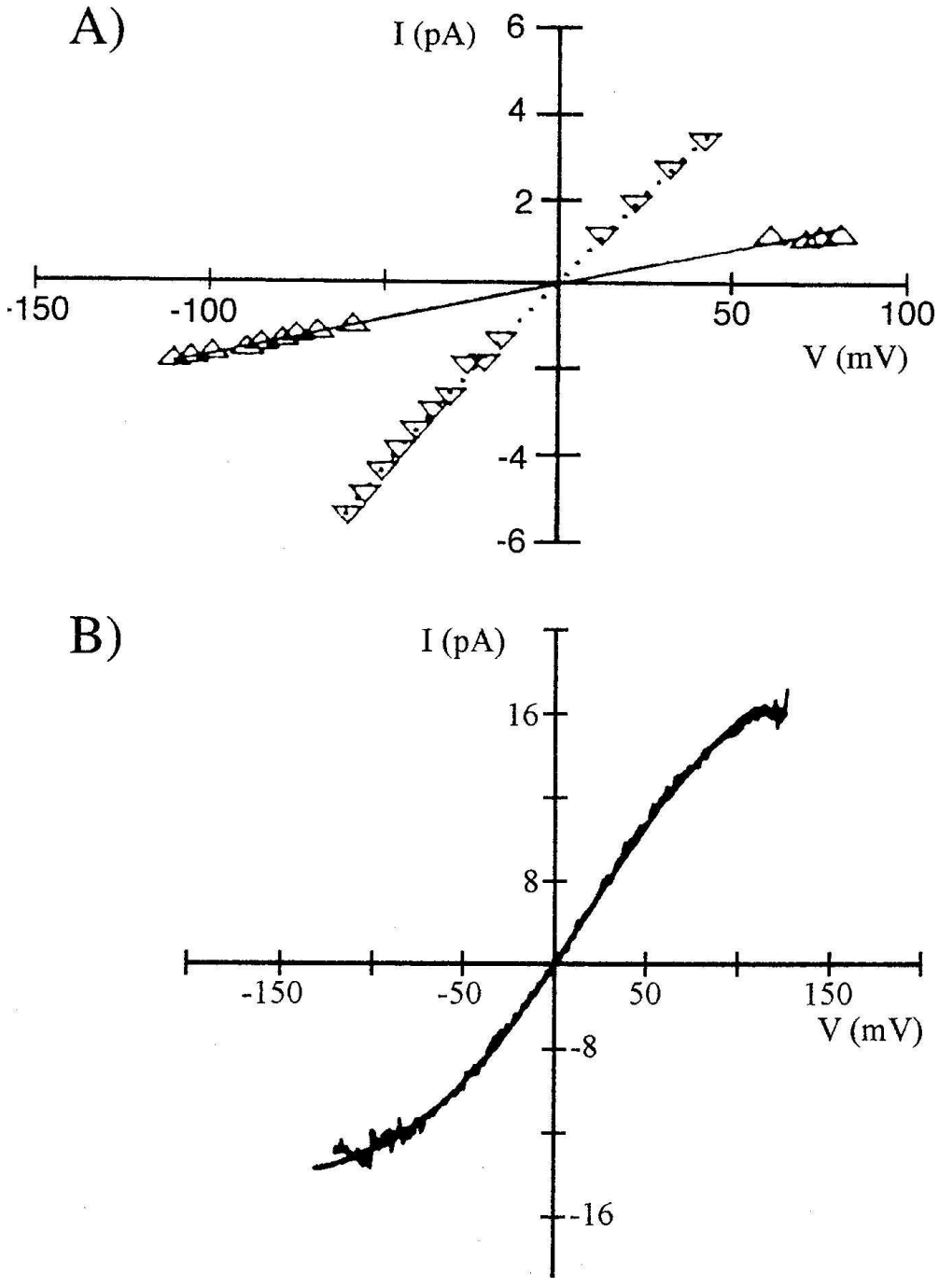

Figure 2.2: Voltage dependence of ionic channels.
(A) Current-voltage relationship of a single nicotinic ACh-activated channel. (B) I-V relationship for a single voltage- and calcium-dependent potassium channel in a symmetrical 160-mM potassium solution. Reprinted from (13).

2.2 Molecular structure of ion channels

The electromicrograph of an ACh-gated channel is shown in Fig.2.3A, a schematic graph of a voltage-dependent ion channel is shown in Fig.2.3B. Ion channels are quite large molecules, which consist of several thousand amino acids with molecular weight more than 300,000 Daltons(1 Dalton = $10^{-27}kg$). The most narrow part of an ion channel with a diameter about 3 $\mathring{A}$ determines the selectivity for certain ions. The conformational change in a part of the ion channel by electric fields induces the voltage-dependent gating of the channel, which is either open or closed. At the resting potential of -80 mV, the electrical field across the 40 $\mathring{A}$ thin membrane is as high as 200,000 V/cm. Charges moving through the membrane change the field, and change the configuration of the channel. The *gating current* causing the change of channel configuration is tiny compared to the current moving through the ion channel when it is open.

Recombinant DNA technology combined with protein chemistry, X-ray diffraction and electron microscopy(31; 33) provide the technology to characterize the activation and inactivation processes of sodium channels at the molecular level. The key points to determine the voltage-dependent activation are four homologous subunits (termed S4) which span the ion channel membrane in an α helix. Catterall(35; 36) presented a sliding helix model to explain the activation of voltage-dependent channels, and this model now has experimental support. Upon depolarization, each S4 subunit rotates by 60 degrees, and moves about 5 $\mathring{A}$. The rotation of the S4 subunit moves one charge across the membrane. The four subunits act together to cause a configuration change that makes the channel conductive.

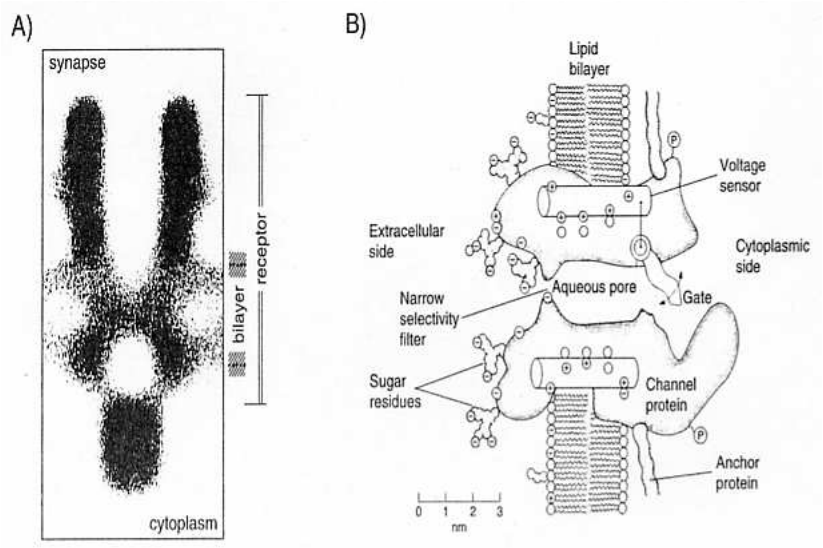

Figure 2.3: Molecular structure of an ionic channel.
(A) Electron-microscopic image using crystallographic methods of the axial section of one of the nicotinic acetylcholine receptors in the electric fish Torpedo. (B) Schematic view of a generic voltage-dependent ion channel. Reprinted from (13).

2.3 Developmental clustering of ion channels at nodes of Ranvier

The major impediment to evolution of a large body is the requirement of stable, efficient and rapid propagation of action potentials over long distances with minimal metabolic and space requirements. The elegant solution of this problem is to develop the myelin sheath and discontinuous localization of voltage-dependent ion channels. The myelin sheath is a high-resistance, low capacitance barrier for ions, and provides the physiological basis for rapid propagation of action potentials. Nodes of Ranvier interrupt the myelin sheath, and are distributed along the axon uniformly. In nodes of Ranvier, the density of voltage dependent Na^+ channels is as high as $2000/\mu m^2$(3). In contrast, voltage-dependent K^+ channels are excluded from nodes(34). Instead, K^+ channels are clustered beneath the myelin sheath in the regions adjacent to the paranodes(transition ranges from nodes of Ranvier to internodal regions), called the juxtaparanode. The total length of nodes, paranodes and juxtaparanodes is just a small fraction of the total axon length, but the precise establishment and maintenance of these domains are important for the propagation of action potentials. The cellular and molecular mechanisms responsible for the formation of nodes and myelin sheath, and the maintenance of these domains are important and interesting problems(37; 38; 39). Although the details of these events remain unclear, some recent experiments show that the specific interactions between neuronal axons and myelinated glial cells are critical to the localization of ion channels(37; 38; 39).

2.3.1 Adult axons

In myelinated axons of adults, the nodes of Ranvier are located almost equidistantly along the axon and are responsible for the regeneration of the action potential. The distance between two nodes, approximately 100 times the axonal diameter(40) , ranges from several hundred microns to several millimeters. Na^+ channels are highly localized in the nodal region, and the density reaches up to $2000/\mu m^2$. The internodal Na^+ channel density is about 5% of the above value estimated by loose patch clamp recordings(41; 42; 43). There is a sharp transition in Na^+ channel density from the node to paranodal regions. The distribution of K^+ channels is different from that of Na^+ channels in myelinated axons. Chiu and Ritchie(44; 45) showed that K^+ channels were absent from the nodal regions, but contributed to the voltage clamp currents. Roper(19) reported that the density of potassium channels at the paranodal region is six times higher than that of nodal and internodal regions. It is also shown that Kv1.1 and Kv1.2 (two kinds of potassium channel subunits) are present at high density in the juxtaparanodal axolemmal zone(46). The function of internodal potassium channels is not clear, but there are two main lines of speculation: one is that they stabilize the internodal axolemma(47; 48), the other is that they prevent back firing by a single impulse(45). Myelin serves to speed up the propagation and enlarge the propagation distance of single action potentials by reducing the membrane capacitance and by increasing the transverse resistance.

2.3.2 Localization of nodal Na^+ channels

In the vertebrate nervous systems, the segregation of ion channels in myelinated axons occurs during the first several days of development in the peripheral nervous system (PNS) and in the first several weeks in the central nervous system (CNS)(14). The localization

of sodium channels in the rat sciatic nerve(49) occurs as early as postnatal day P1, but the localization of sodium channels in the optic nerve has not been observed before P9(50). During maturation, the propagation speed of action potentials increases 50 times from 0.2 m/s to 10 m/s due to the thickening of myelin and Na channel clustering. The cells responsible for myelin formation are different for the CNS (oligodendrocytes) and the PNS (Schwann cells).

During the early developmental myelinating procedure of PNS axons, clusters of Na^+ channels first appear adjacent to the edge of Schwann cells. As the gap between two Schwann cells decreases, adjacent clusters of Na^+ channels fuse to form a new node of Ranvier. Many experimental results(49; 51; 52) show that the clustering of Na^+ channels in the PNS requires the onset of myelination by Schwann cells and the physical influence of axoglial contact. In the CNS, the onset of myelination occurs at P7, but clustering of Na^+ channels occurs at P9-P10(50). Quantitative analyses also show that during the developmental period from P5 to P60, the formation of axoglial junctions precedes the clustering of Na^+ channels by about 2 days. These results are consistent with the assumption that axoglial contact is essential for Na^+ channel clustering, and oligodendrocytes exclude the Na^+ channels from regions of axoglial contact to form the channel clusters(53). In regenerating myelinated axons, the distance between two nodes will decrease, but Na^+ channel number in each node remains constant. Thus, the total Na^+ channel number along the remyelinated axon will increase.

2.3.3 Localization of voltage-gated K^+ channels

In contrast to Na^+ channels, potassium channels are not located at the nodes of Ranvier, but are clustered in the region adjacent to paranodes called juxtaparanodes. Juxtaparanodal

K^+ channels are found in many nervous tissues such as brainstem(46), cerebellar white matter(54), spinal cord(55), optic nerve(56) and sciatic nerve(57). Blockage of juxtaparanodal K^+ channels by K^+ channel blockers such as 4-aminopyridine increases both the amplitude and duration of action potentials in the optic nerve, but has almost no effect on the conduction in myelinated PNS axons. The transient localization of K^+ channels in nodal and paranodal zones stabilizes action potential conduction and prevents back-firing by a single stimulus in PNS development(48).

The mechanisms to determine K^+ channel clustering at juxtaparanodal regions parallel those of Na^+ channels as described above, but there are several differences. In demyelinated PNS axons, Na^+ channels remain at the nodes of Ranvier, but K^+ channels clustered at juxtaparanodes diffuse laterally to the former nodal and paranodal zones that normally exclude K^+ channels. This suggests that the continuous presence of paranodal axoglial junctions is necessary to keep the localization of K^+ channels at juxtaparanodes. During remyelination, Na^+ channels migrate to the edge of Schwann cells and fuse to form the new node, but clusters of K^+ channels are not detected. Only after the new node is fully formed, is the clustering of K^+ channels observed. It is interesting to note that K^+ channels initially are located at the nodal regions, then diffuse to the paranodes, and finally are clustered at the corresponding juxtaparanodes. The clustering of juxtaparanodal K^+ is also observed in CNS regions, such as optic nerve(50) and spinal cord(58). The clustering of K^+ channels during developmental myelination of CNS axons is similar to that of the PNS axons. However, there are some differences and similarities between the clustering procedures of PNS axons and CNS axons. As in PNS, the clustering of K^+ channels is several days later than that of Na^+ channels(59).

Chapter 3

Deterministic and stochastic HH equations

Nerve cells have an all-or-nothing response to external stimuli. If the amplitude of external stimuli is less than a threshold value, the response of the nerve cell is weak, just a small perturbation of the membrane potential. If the amplitude of external stimuli is larger than a threshold, the response of the nerve cell is dramatic. The nerve cell will generate large amplitude voltage pulses that are called action potentials. An action potential propagates along the axon to the presynaptic terminals of the axon with constant amplitude and speed. Action potentials are so important that most propagation of information in the nervous system depends on them. The ionic mechanism underlying the generation and propagation of action potentials in the nervous system was quantified in giant squid axon by Hodgkin and Huxley(23; 60; 61; 62). They presented the HH model in their four papers. The HH model describes the electrical behavior of nervous membrane by a set of first-order ordinary differential equations and elucidates the all-or-nothing response of action potentials.

3.1 Electrical circuit for a patch of nerve membrane

Hodgkin and Huxley carried out research on the squid giant axon. In order to eliminate the effect of the spatial component of the neuronal structure, a conductive axial wire was inserted inside the axon. The technology, called “space clamp”, keeps the potential along the axon uniform. The total membrane current is the sum of the ionic currents and the capacitive current(13),

$$I_m(t) = I_{ionic}(t) + c_m \frac{dV(t)}{dt} \tag{3.1}$$

where I_{ionic} is the ion channel current, c_m is the specific membrane capacitance, and V is the membrane potential.

For most neuronal membranes, ionic currents mainly include sodium ion channel currents and potassium ion channel currents. Other ion channel currents are lumped as leakage current. Sodium ion channel conductance g_{Na} and potassium ion channel conductance g_K are voltage dependent. Leakage current conductance is voltage independent. Then the total ionic current is the sum of the sodium ion channel current, potassium ion channel current and the leakage current(13; 32),

$$I_{ionic} = I_{Na} + I_K + I_{leak} \tag{3.2}$$

Each kind of ionic current $I_i(t)$ is linearly related to the driving potential, which is equal to the membrane potential minus the corresponding reversal potential V_i(13; 32),

$$I_i(t) = g_i(V(t) - V_i) \tag{3.3}$$

Each voltage-dependent ionic current conductance is expressed as the maximal conductance multiplied by the fraction of open ion channels.

3.2 Dynamics of ion channels

Each voltage dependent ion channel is characterized by specific dynamics to determine the temporal change of activation and inactivation states.

3.2.1 Potassium ion channels

Hodgkin and Huxley modeled the potassium channel current as(23),

$$I_K = \bar{g}_K n^4 (V - V_K) \tag{3.4}$$

where $\bar{g}_K$ is the maximal potassium conductance with the value of $36mS/cm^2$ and V_K is the reversal potential of potassium channels with the value of $-77mV$(23). The term n^4 implies there are four gates in one potassium channel(13; 23). Only when all the four gates are open is the potassium ion channel open. Then n represents the open probability of one potassium gate and has a value between 0 and 1.

We can assume that each potassium gate has two states, the open state and the closed state. If the open probability is n, then the closed probability is 1-n. The transition between the open state and the closed state is governed by first order kinetics, and can be described by the following scheme(13; 32),

$$\text{n} \underset{\alpha_n}{\overset{\beta_n}{\rightleftharpoons}} \text{1-n}$$

where α_n is the voltage dependent transition rate from the closed state to the open state, and β_n is the voltage dependent transition rate from the open state to the closed state. All the transition rates have units of 1/msec. Then, the scheme can be expressed by a first order differential equation(13; 32),

$$\frac{dn}{dt} = \alpha_n(V)(1-n) - \beta_n(V)n. \tag{3.5}$$

Instead of using transition rates α_n and β_n, we can rewrite Eq.3.5 with a voltage dependent time constant $\tau_n(V)$ and a steady-state open fraction $n_\infty(V)$,

$$\frac{dn}{dt} = \frac{n_\infty - n}{\tau_n}, \tag{3.6}$$

where

$$\tau_n = \frac{1}{\alpha_n + \beta_n}, \tag{3.7}$$

and

$$n_\infty = \frac{\alpha_n}{\alpha_n + \beta_n}. \tag{3.8}$$

According to Hodgkin and Huxley, the opening and closing rates of potassium channels are(23)

$$\alpha_n(V) = \frac{0.01(55+V)}{-e^{-(55+V)/10}+1}, \tag{3.9}$$

and

$$\beta_n(V) = 0.125e^{-(V+65)/80}. \tag{3.10}$$

where the unit of V is mV.

Fig.3.1 shows the voltage dependence of the time constant for potassium ion channels.

τ_n has a bell shape. Fig.3.2 shows the voltage dependence of the steady-state value n_∞ of potassium ion channels. n_∞ increases monotonically with the membrane potential. Because of the fourth power relationship between g_K and n, the potassium conductance as a function of the membrane potential is much steeper than the steady-state value of a single n gate. The open fraction of potassium ion channels in the steady-state is identical to $n_\infty(V)^4$. At the resting potential, this fraction is very small, $n_\infty(0)^4 \approx 0.01$, and thus means only 1% of potassium channels are in the open state. The evolution of the potassium channel conductance is dictated by the solution of Eq.3.6(13),

$$n(t)^4 = (n_\infty - (n_\infty - n_0)e^{-t/\tau_n(V)})^4, \tag{3.11}$$

where n_0 is the initial steady-state value, and n_∞ is the final steady-state value.

3.2.2 Sodium ion channels

The dynamics of sodium ion channels is more complicated than that of potassium channels. In order to fit the dynamics of sodium channels, Hodgkin and Huxley used an activating sodium gate m and an inactivating sodium gate h to describe the sodium channel conductance (13; 23; 32),

$$I_{Na} = \bar{g}_{Na} m^3 h (V - V_{Na}), \tag{3.12}$$

where $\bar{g}_{Na}$ is the maximum sodium conductance with the value of $120 mS/cm^2$, V_{Na} is the sodium reversal potential with the value of 50 mV, and m and h are dimensionless variables with values from 0 to 1. Similar to the n gate of potassium channels, gate m and gate h

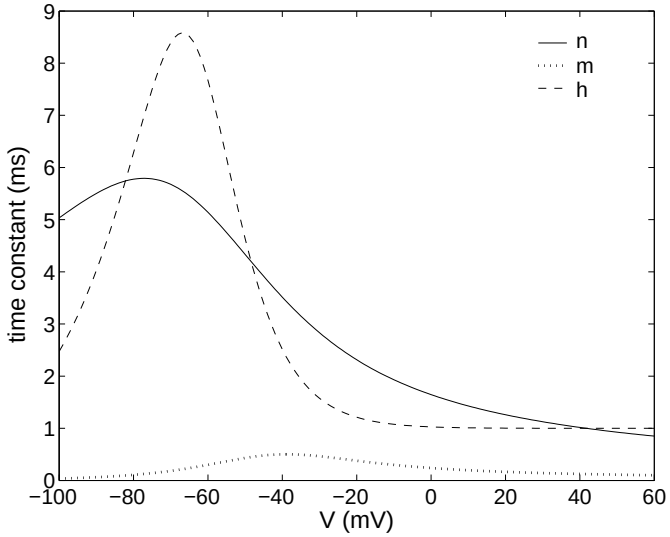

Figure 3.1: Time constants

Time constants of sodium activation gate m, sodium inactivation gate h and potassium activate gate n.

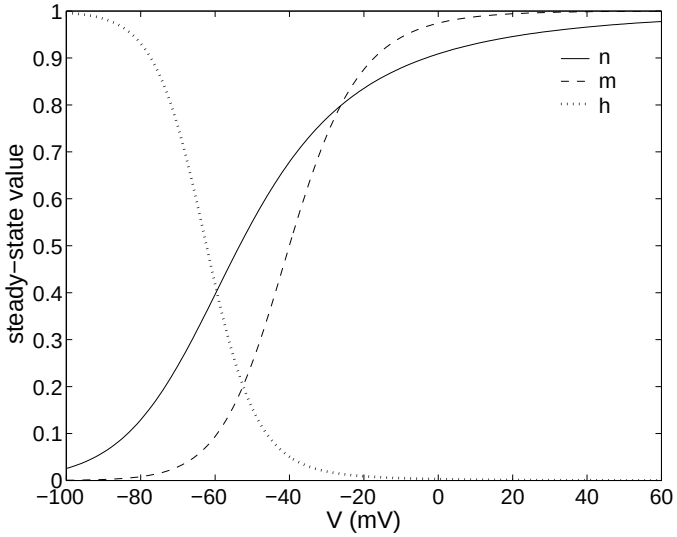

Figure 3.2: Steady-state value

Steady-state value of sodium activation gate m, sodium inactivation gate h and potassium activation gate n.

satisfy the following dynamics(13; 32),

$$\frac{dm}{dt} = \alpha_m(V)(1-m) - \beta_m(V)m, \tag{3.13}$$

and

$$\frac{dh}{dt} = \alpha_h(V)(1-h) - \beta_h(V)h. \tag{3.14}$$

Transition rates α_m, β_m, α_h and β_h are given by(23),

$$\alpha_m(V) = \frac{0.1(V+40)}{-e^{-(40+V)/10}+1} \tag{3.15}$$

$$\beta_m(V) = 4.0e^{-(V+65)/18} \tag{3.16}$$

$$\alpha_h(V) = 0.07e^{-(V+65)/20} \tag{3.17}$$

$$\beta_h(V) = \frac{1.0}{e^{(-35-V)/10}+1}. \tag{3.18}$$

The time constants of sodium channels are plotted in Fig.3.1 and similar to τ_n, both τ_m and τ_h are bell-shaped curves, while the value of τ_m is just 10% of that of τ_h. The steady-state values $m_\infty(V)$ and $h_\infty(V)$ of sodium channels are plotted in Fig.3.2. While m_∞ increases monotonically with increasing membrane potential as expected of an activation variable, h_∞ decreases monotonically with increasing membrane potential, the feature of an inactivation variable. When the membrane potential is at the resting potential, m is approximately 0, h is approximately 1. The steady-state sodium conductance at rest is less

than 1% of the maximal value. When the membrane potential is suddenly increased by the voltage clamp technique, m will change to a value close to its final value in a fraction of millisecond according to its short time constant, while h requires 5 msec or longer to decrease from its former high value to its final smaller value. In other words, two processes govern the sodium conductance: the activation process rapidly increases the sodium conductance upon depolarization, while the inactivation process decreases the sodium conductance upon depolarization slowly.

3.2.3 Complete model

Except for the sodium and potassium currents, other ion channel currents are lumped as leakage current. Unlike the sodium and potassium conductance, leakage conductance g_{leak} is a constant over time, without depending on the membrane potential. The value of g_{leak} provided by Hodgkin and Huxley is 0.3 mS/cm^2, corresponding to a passive membrane resistivity of $R_m = 3333\Omega cm^2$(23). The leakage current also has an associated reversal potential V_{leak}. Hodgkin and Huxley did not measure V_{leak} directly, but adjusted it so that the total membrane current at the resting potential was 0. V_{leak} came out to be -54.4 mV(23). The membrane capacitance C_m is 1 $\mu F/cm^2$. Then, the single equation describing current across a patch of neuronal membrane is(13; 32),

$$C_m\frac{dV}{dt} = \bar{g}_{Na}m^3h(V_{Na} - V) + \bar{g}_K n^4(V_K - V) + g_{leak}(V_{rest} - V) + I_{inj}(t) \qquad (3.19)$$

where I_{inj} is the current injected by an electrode. This nonlinear equation in combination with the first-order ordinary linear differential equations (Eq.3.5, Eq.3.13, Eq.3.14) specify the dynamics of neuronal membrane potential.

3.3 Generation of Action Potentials

One of the most remarkable behaviors of the neuronal membrane is its all-or-nothing response to external stimulus. If the amplitude of the external stimulus is below a threshold, the membrane will depolarize slightly and then return to the resting potential, while if the amplitude of the external stimulus is above a threshold, the stimulus will induce an action potential, whose shape is independent of the stimulus(13; 23; 32). The effect of an injected inward current pulse I_{inj} is to depolarize the membrane potential. The depolarization will increase m and n, but decrease h. Because the time constants τ_h and τ_n are an order of magnitude slower than the time constant τ_m, h and n can be considered as quasi-stationary, but m will increase initially. Consequently, the conductance of the potassium ion channels will remain approximately constant, and the conductance of sodium ion channels will increase initially. If the amplitude of the current pulse is below the threshold value, the system is at the sub-threshold case. Because the membrane potential is depolarized from rest, the value of $V - V_K$ will increase, and the potassium current I_K will increase concomitantly. The concomitant increase of I_K will outweigh the increase of I_{Na} due to the increase of g_{Na}, and the total current is outward. The net outward current will drive the membrane potential back to the resting potential. If the amplitude of the current pulse is increased over a threshold value, the depolarization of the membrane potential will reach a point where the increase of I_{Na} exceeds the increase of I_K. At this point, I_{Na} enters a positive feedback loop: the additional I_{Na} depolarizes the membrane potential, and the depolarization of membrane potential increases the value of m, which then increases I_{Na}. Driven by the positive feedback, the membrane potential will reach the reversal potential of V_{Na} rapidly. After a delay, the activation of the n gate and the inactivation of sodium channels will turn on, and drive the membrane potential back to the resting potential.

3.3.1 Voltage threshold for spike initiation

What is the most important factor to initiate spiking of neurons? Is it the potential threshold value V_{th}? The minimal amount of injected current I_{th}? A certain amount of electrical charge Q_{th}? These possibilities have been discussed by many authors in some different circumstances. In order to simplify the discussion, we just deal with the spike initiation in an ideal nonlinear membrane, without considering the complicated spatial structure of axons.

In order to answer this question, we need to consider the instantaneous I-V relationship $I_0(V)$ of the squid giant axon. We are interested in rapid synaptic injection, where the injection time is less than the passive membrane time constant. In the short period of time, we can consider the sodium inactivation gate h and the potassium activation gate n to be constant. Because the time constant of m is ten times faster than the constants of h and n, we can consider m reaching its steady-state value within the injection period. According to these principles, we plot the instantaneous I-V relationship $I_0(V)$ in Fig.3.3 , where $I_0(V)$ is the sum of the ion and leakage currents. In this figure, we keep n and h to be the value at the resting potential, and m to be the steady-state value. In other words,

$$I_0(V) = \bar{g}_{Na} m(V)^3 h(V_{rest})(V - V_{Na}) + \bar{g}_K n(V_{rest})^4 (V - V_K) + g_{leak}(V - V_L) \quad (3.20)$$

Fig.3.3 shows the inverted U-shape of I_0 near the resting potential, and three ionic currents I_{Na}, I_K and I_{leak}.

When there is no external input, the system rests at the resting potential -65mV(23). If a small depolarizing potential is applied, the system is moved to the right, generating a small outward current. Because the increase in I_K due to the increase in the driving potential

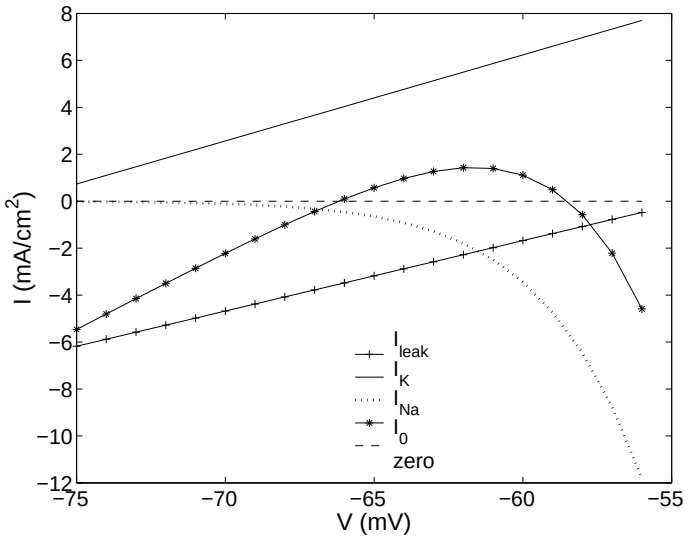

Figure 3.3: Current-voltage relationship around the resting potential

$V - V_K$ and the decrease in I_{leak} due to the decrease in the driving potential $V_L - V$ outweigh the increase in I_{Na} due to the increase of m, this pulls the membrane potential back to the resting potential corresponding to the subthreshold potential trajectory. Similarly, if a hyperpolarizing potential is applied, a negative inward current will be generated to pull the membrane potential back to the resting potential. The resting potential point is a stable attractor. $I_0(V)$ has a second zero point at $V = V_{th} \approx 5.0mV$. Because the slope of the I_0 curve around V_{th} is negative, the point V_{th} is an unstable point. A negative perturbation will carry the system to the resting potential, but a positive perturbation will induce a small inward current flow, which further depolarizes the membrane, and leads to a larger inward current. Then, the membrane potential depolarizes toward the reversal potential of the sodium current, and an action potential will be generated.

3.3.2 Refractory Period

When an action potential is generated, the membrane potential will be pulled back to the resting potential due to the inactivation of sodium channels and the activation of potassium channels. The potassium conductance remains activated following the spike pulse, and induces the membrane to undergo a hyperpolarization (a change in membrane potential in the negative direction, making the cell interior more negative). During this period where the h gates of the sodium channels remain inactivated and the potassium channels remain activated, it is more difficult to initiate an action potential than usual. The membrane is in the refractory period.

The refractory period is measured by the following method shown in Fig.3.4 . At $t = 0$, a 0.5 ms current pulse is injected into a patch of membrane to initiate an action potential. The amplitude of the minimal pulse is $I_1 = 14mA/cm^2$. The pulse triggers an action

potential which peaks at 4 ms. The membrane potential is repolarized to $V = V_{rest}$ at $t = 6ms$. The time that the potential is below the resting potential is set to $\Delta t = 0$. Then a second current pulse is injected to initiate another action potential. We begin to record the amplitude of the second pulse at $\Delta t = 2ms$. At this time, $I_2/I_1 = 21.4$, which means that the amplitude of second pulse has to be 21.4 times larger than that of the first pulse to generate an action potential. Because such a large amplitude is impossible physiologically, this period is called the absolute refractory period. When $\Delta t = 12ms$, $I_2/I_1 = 1$, and this period is called the relative refractory period. This is followed by a brief period of hyperexcitability, during which the amplitude of the second pulse need only be 82% of that of the first pulse.

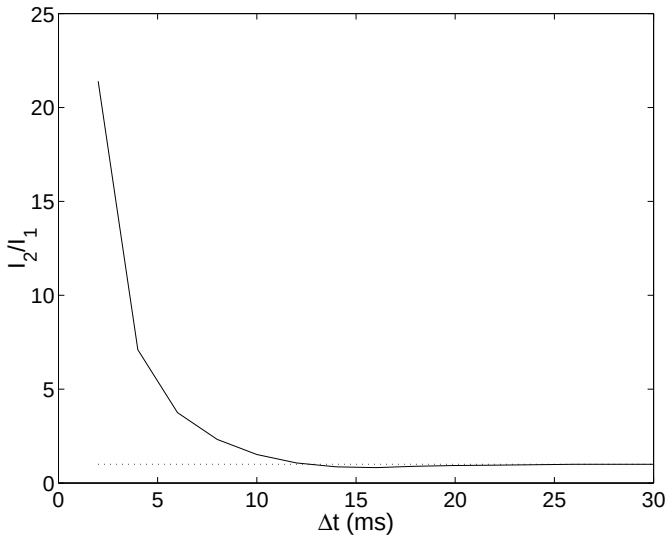

Figure 3.4: $\frac{I_2}{I_1}$ in refractory period

3.4 Stochastic Hodgkin-Huxley equations

If the number of ion channels is large, the dynamics of the m, n and h gates can be described by first-order differential equations. If the number of ion channels is small, differential equations are not a good description due to the stochastic behavior of ion channels. It is more accurate to use stochastic HH equations. To integrate Eq.3.19, the numbers of open sodium and potassium channels have to be determined at each instant. It is assumed that the subunits of the sodium and potassium channels are not cooperative and that they switch between the open and closed states according to a Markov process(13). There are several methods to simulate the patch of ion channels. Each method has some advantages and disadvantages.

3.4.1 Simple stochastic method

This method assumes that all gates open and close according to a two-state Markov process with voltage dependent opening and closing rates(12). For example, the two-state Markov process of a single gate is sketched in Fig.3.5, where α and β are the opening and closing rates of the gates. If the gate is closed at time t, it will open with the probability $\alpha\delta t$ and remain closed with probability $1-\alpha\delta t$ in the time interval $(t, t+\delta t)$ for sufficiently small δt, i.e. $\delta t << 1/\alpha$. If the gate is open at time t, it will close with the probability $\beta\delta t$ and remain open with probability $1-\beta\delta t$ in the time interval $(t, t+\delta t)$ for sufficiently small δt, i.e. $\delta t << 1/\beta$. We update the state of each gate by drawing a random number r from the unit interval with a uniform distribution. If the gate is closed at time t and $r > \alpha\delta t$, the gate remains closed while it opens if $r < \alpha\delta t$(12). Similarly, if the gate is open at time t and $r > \beta\delta t$, the gate remains open while it closes if $r < \beta\delta t$(12). This method is obviously inefficient since many transitions of gates between the open and closed state do not change

the state of the channel and thus the conductance of the channel. It is, however, the most accurate method since no other assumptions than the Markov-process have been made.

3.4.2 Markov process for the occupation numbers

Instead of keeping track of the state of each gate, one can keep track only of the total populations of channels in each possible state (11). Each channel has either $0, 1, 2, 3$ or 4 gates open and can thus be in the corresponding states S_0, S_1, S_2, S_3, S_4. Thus the entire population of channels can be completely described by specifying the numbers of channels $[n_0], [n_1], [n_2], [n_3], [n_4]$ in the states S_0, S_1, S_2, S_3, S_4. Stochastic transitions are considered between the occupation numbers $[n_i]$, $i = 0, 1, 2, 3, 4$. Assuming Markov processes for these transitions, a corresponding kinetic scheme can be formalized that explicitly incorporates the stochastic behavior of the ion channels. The model requires that the potassium channels can exist in five different states, i.e(11).

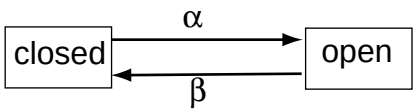

Figure 3.5: Kinetic scheme of a 2-state channel.

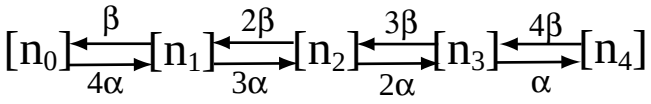

Figure 3.6: Kinetic scheme for a stochastic potassium channel.

where $[n_i]$ is the number of potassium channels with i open gates. The number of open potassium channels is given by $[n_4]$.

Similarly, sodium channels can exist in eight different states, and the corresponding kinetic scheme is given by(11)

where $[m_i h_j]$ is the number of sodium ion channels with i open activating gates of type m and j open inactivating gates of type h. Thus, $[m_3 h_1]$ denotes the number of open sodium channels. In order to update the state of the population of ion channels with time, we have to create rules in what sequence the states are updated. The simple stochastic method, described in the previous section, does not require such rules. In order to enforce positive occupation numbers we update the occupation numbers sequentially, starting with the process with the largest rate and so forth. Let, for example, the transition rate between S_1 and S_2 be $\gamma_{S_1 S_2}$ and the populations of these states be $[n_1]$ and $[n_2]$. Then, the probability p that a channel switches within the time interval $(t, t+\delta t)$ from state S_1 to S_2 is given by $p \equiv \gamma_{S_1 S_2} \delta t$. The probability that $[\delta n_{12}]$ channels switch from state S_1 to state S_2 in the same time interval satisfies the binomial distribution(11)

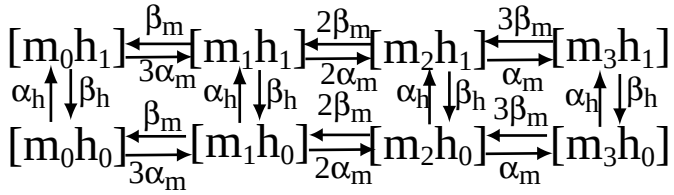

Figure 3.7: Kinetic scheme of a stochastic sodium channel

$$P([\delta n_{12}]) = \binom{[n_1]}{[\delta n_{12}]} p^{[\delta n_{12}]} (1-p)^{([n_1]-[\delta n_{12}])} . \tag{3.21}$$

Thus the number of switching channels between the states is sequentially drawn from binomial distributions. If the cluster of channels is large i.e. $[n_1]$ is large, the number of switching channels is also large on average. Thus, in the time interval δt larger channel clusters experience more transitions.

3.4.3 Gillespie's method

Similar to the Markov process for the occupation numbers, the entire population of ion channels can be described at each instant of time by the occupation numbers of all possible states(10). At any instant of time, the ion channels are distributed over the 13 states, and there are 28 possible transitions (8 transitions for potassium ion channels, 20 transitions for sodium ion channels) to all possible successive states. For each ion channel in state i at time t, the probability of the ion channel remaining in that state in the (sufficiently small) time interval δt is given by $P = e^{-\gamma_i \delta t}$(10), where γ_i is the sum of all the transition rates from state i to any possible successive state. Sufficiently small means here that during δt no other channel is switching conductance state. The probability of the cluster of ion channels remaining in the same state in time interval δt is $e^{-\lambda \delta t}$(10), where

$$\lambda = \sum_{i=0}^{3} \sum_{j=0}^{1} [m_i h_j] \gamma_{ij} + \sum_{k=0}^{4} [n_k] \gamma_k \,. \tag{3.22}$$

Here $[m_i h_j]$ denotes the number of sodium channels in state $m_i h_j$, $[n_k]$ the number of potassium channels in the state n_k, γ_{ij} the total transition rate associated with escaping from state $m_i h_j$, and γ_k the total transition rate associated with escaping from state n_k. For example, for state $m_1 h_1$, $\gamma_{11} = 2\alpha_m + \beta_m + \beta_h$. In order to pick a transition time t_{tr} for a specific ion channel state, one can draw a pseudorandom number r_1 from the uniform

distribution [0, 1] and find a transition time by $t_{tr} = \ln(r_1^{-1})/\lambda$(10). In this time step, only the state of one single gate will be changed. The next step in the stochastic algorithm is to select which of the 28 possible transitions occurs in the time interval t_{tr}. The conditional probability that a particular transition j occurs in the time interval δt is given by(10)

$$\frac{a_j \delta t}{\sum_{i=1}^{28} a_i \delta t} = \frac{a_j}{\sum_{i=1}^{28} a_i}\,, \tag{3.23}$$

where a_j is the product of the transition rate associated with transition j and the number of channels in the parent state associated with that transition. Because the sum in the denominator of 3.23 is a re-ordered version of 3.22, it also equals λ. A specific transition is selected by drawing a random variable r_2 from the uniform distribution $[0, \lambda]$, and determining μ such that(10)

$$\sum_{i=1}^{\mu-1} a_i < r_2 \leq \sum_{i=1}^{\mu} a_i. \tag{3.24}$$

Then we can update the ion channel number in each state, and can update the membrane potential consequently.

3.4.4 Langevin Approach

Fox and Liu (27; 28) have derived the following set of Ito-Langevin equations for the gating variables n, m and h for large ion channel clusters (i.e. when the number of channels in the cluster is large)

$$\begin{aligned}
\frac{d}{dt}n &= \alpha_n(1-n) - \beta_n n + \overline{g}_n(t) \\
\frac{d}{dt}h &= \alpha_h(1-h) - \beta_h h + \overline{g}_h(t) \\
\frac{d}{dt}m &= \alpha_m(1-m) - \beta_m m + \overline{g}_m(t)\,,
\end{aligned} \tag{3.25}$$

where the variables $\overline{g}_n(t), \overline{g}_h(t), \overline{g}_m(t)$ denote Gaussian, zero-mean white noise with

$$\begin{aligned} < \overline{g}_n(t)\overline{g}_n(t') > &= \frac{2}{N_K}\frac{\alpha_n(1-n)+\beta_n n}{2}\delta(t-t') \\ < \overline{g}_m(t)\overline{g}_m(t') > &= \frac{2}{N_{Na}}\frac{\alpha_m(1-m)+\beta_m m}{2}\delta(t-t') \\ < \overline{g}_h(t)\overline{g}_h(t') > &= \frac{2}{N_{Na}}\frac{\alpha_h(1-h)+\beta_h h}{2}\delta(t-t')\,. \end{aligned} \tag{3.26}$$

Here N_K and N_{Na} denote the total number of potassium and sodium channels. It is necessary to include restrictions to guarantee that m, n and h do not leave the unit interval [0, 1]. The differential equations for the membrane potential are the classic Hodgkin-Huxley equations where m^3h determines the fraction of open sodium channels and n^4 the fraction of open potassium channels, i.e.

$$C_m\dot{v} = -\left(\frac{1}{\tau_K}n^4\,(v-v_K^{rev}) + \frac{1}{\tau_{Na}}m^3h\,(v-v_{Na}^{rev}) + \frac{1}{\tau_L}\,(v-v_l)\right) + \xi_s(t)\,. \tag{3.27}$$

where C_m is the specific membrane capacitance and $\xi_s(t)$ is the synaptic noise. Equations (3.25,3.26,3.27) have to be integrated numerically in order to predict a neuronal spike train.

Chapter 4

Cable equation and compartmental model

Dendritic trees receive synaptic signals, and propagate the signals to the soma. The spike is generated at the axon hillock, and propagates to the presynaptic terminals through the axon. We therefore need to consider the extended system with cable-like structure. The cable equation determines the dynamics of the membrane potential along thin tube-like structures, such as axons and dendrites. This equation was introduced by Lord Kelvin in the middle of nineteen century to describe the propagation of potentials along the submarine telegraph cable linking America and Britain. A half century later, Hermann formulated the core conductor model to describe the flow of current along nerve axons. Two classical papers, which derived the cable equation for neurons and provided transient solutions, are written by Hodgkin & Rushton(63) and Davis & Lorente de No(65).

Cable theory studies the partial differential equations describing the propagation of the electrical potential along tube-like structures. In the 1930s and 1940s, the concept of cable theory was applied to the nervous system, especially in the squid giant axon. The work

of Rall(66) expanded the application of cable theory to passive dendrites, which began in the late 1950s, and blossomed in the 1960s and 1970s. In this chapter, we will restrict our discussion to linear cable theory. The membrane is considered to be passive, and can be described as a combination of resistances and capacitances. It is true that there are widespread dendritic nonlinearities, but the passive membrane is a valid and efficient first approximation of the active membrane.

4.1 Introduction of the cable equation

The equivalent electrical circuit of a neuronal fiber with a passive membrane is shown in Fig.4.1, where the neuronal tissue is represented by a series of discrete electrical circuits. The current per unit length flowing through the membrane at location x is $i_m(x,t)$, without making any specific assumptions and losing any generality. We can write down the following equation for the discrete circuit demonstrated in Fig.4.1 by Ohm's law

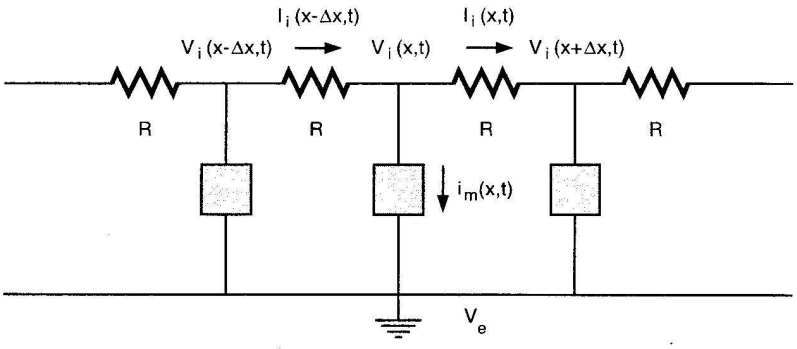

Figure 4.1: Equivalent electrical structure of an arbitrary neuronal process. Reprinted from (13).

$$V_i(x,t) - V_i(x+\delta x,t) = RI_i(x,t)[13], \tag{4.1}$$

or if we transfer the infinitesimal small interval δx into the differential ∂x, and with $V_m = V_i$, we can get the following equation:

$$\frac{\partial V_m}{\partial x}(x,t) = -r_i I_i(x,t)[13], \tag{4.2}$$

where $r_i = \delta R/\delta x$ is the unit intracellular resistance with the dimensions of ohms per centimeter. I_i is the intracellular core current along the axon, and assumed to be positive when the current flows to the right. Applying Kirchhoff's law to the node at x in Fig.4.1 , we have

$$i_m(x,t)\delta x + I_i(x,t) - I_i(x-\delta x,t) = 0(13). \tag{4.3}$$

If δx approaches zero, we obtain

$$i_m(x,t) = -\frac{\partial I_i}{\partial x}(x,t)(13). \tag{4.4}$$

Differentiating Eq.4.2 and combining Eq.4.4, we find

$$\frac{1}{r_i}\frac{\partial^2 V_m}{\partial x^2}(x,t) = i_m(x,t)(13). \tag{4.5}$$

We found the relationship between the membrane potential's spatial derivative with the unit current flowing through the membrane. We can express the unit current flowing through

the membrane $i_m(x,t)$ by the following formula:

$$i_m(x,t) = \frac{V_m(x,t) - V_{rest}}{r_m} + c_m \frac{\partial V_m(x,t)}{\partial t} - I_{inj}(x,t)(13), \tag{4.6}$$

where r_m is the unit membrane resistance with the dimension of ohms-centimeter. If the nerve fiber is homogeneous, we can put the right side of Eq.4.6 equal to the right side of Eq.4.5, multiply both sides by r_m, and get the following equation:

$$\lambda^2 \frac{\partial^2 V_m(x,t)}{\partial x^2} = \tau_m \frac{\partial V_m(x,t)}{\partial t} + (V_m(x,t) - V_{rest}) - r_m I_{inj}(x,t)(13), \tag{4.7}$$

where the time constant τ_m equals $r_m c_m$ and the space constant λ is $(r_m/r_i)^{\frac{1}{2}}$.

The above parabolic equation is very similar to the heat and diffusion equations being a first order partial differential equation in time and second order partial differential equation in space. The character of this kind of parabolic equation is dissipation and without constant wavelike solution. The cable equation is the fundamental equation to understand the evolution of membrane potential along the nerve fiber.

Now, we have to deal with the vexing unit problem. The three fundamental parameters of the nerve fibers can be expressed in two ways. If they are expressed per unit length, they are formalized as the following:

$$r_i = \frac{4R_i}{\pi d^2}(13), \tag{4.8}$$

where the unit of r_i is Ω/cm.

$$r_m = \frac{R_m}{\pi d}(13), \tag{4.9}$$

where the unit of r_m is Ωcm.

$$c_m = \pi d C_m (13), \tag{4.10}$$

where the unit of c_m is F/cm. The advantage of this set of parameters is that the cable equation has no explicit terms depending on the axonal diameter d.

The more common way is to formalize these parameters independent of the axonal diameter d. The set of parameters used are the intracellular resistance R_i with the dimensions of Ωcm, the specific membrane resistance R_m with the dimensions of Ωcm^2 and the specific membrane capacitance C_m with the dimensions of F/cm^2. Putting Eq.4.8, Eq.4.9 and Eq.4.10 into Eq.4.7, we can get the following equation,

$$C_m \frac{\partial V}{\partial t} - \frac{I_{inj}}{\pi d} + \frac{V_{rest} - V}{R_m} = \frac{d}{4R_i} \frac{\partial^2 V}{\partial x^2} (13). \tag{4.11}$$

4.2 steady-state solution

At first, we consider the steady-state solution of the cable equation. In order to evaluate the steady-state solution, we set $\partial V/\partial t$ and V_{rest} to be zero, and rewrite the cable equation, to get the following equation:

$$\lambda^2 \frac{d^2 V(x)}{dx^2} = V(x) - r_m I_{inj}(x) (13). \tag{4.12}$$

This simplification reduces the original cable equation to an ordinary second-order differential equation.

4.2.1 Infinite cable

We assume the external current I_{inj} is injected at location x = 0, and we can express the external current as $I_0\delta(x)$, where $\delta(x)$ is the dirac delta function. Considering the boundary condition, we can assume the membrane potential to be 0 when $|x| \to \infty$. Then we can get the steady-state solution of an infinite cable as follows:

$$V(x) = V_0 e^{-|x|/\lambda}(13), \tag{4.13}$$

where V_0 is equal to $I_0 r_m/(2\lambda)$. It is obvious that the membrane potential decays with the distance, and the parameter controlling the decay is the space constant λ. When x is equal to λ, the membrane potential decays to e^{-1} of the original value, or approximately 37% of the original value. When x is equal to 2λ, the membrane potential decays to e^{-2} of the original value, or approximately 13%. In Eq.4.13, the steady-state space constant is defined as

$$\lambda = (\frac{r_m}{r_i})^{1/2} = (\frac{R_m}{R_i}.\frac{d}{4})^{1/2}(13). \tag{4.14}$$

Because of the importance of the steady-state constant λ, we often normalize the space distance x with respect to λ in the dimensionless form $X = x/\lambda$, which is called the electrotonic distance. What then is the input resistance of the infinite cable? It is calculated by inserting an electrode to measure the membrane potential and the corresponding current flow. The value of the input resistance can be expressed as

$$R_{in} = \frac{V(x)}{I_i(x)} = \frac{V(x=0)}{I_0}(13). \tag{4.15}$$

If we set x to be zero in Eq.4.13, we get the following equation,

$$V(0) = V_0 = I_0 r_m/(2\lambda)(13). \tag{4.16}$$

We can get the input resistance,

$$R_{in} = \frac{r_m}{2\lambda} = \frac{r_i \lambda}{2} = \frac{(r_i r_m)^{1/2}}{2}(13). \tag{4.17}$$

In case of an infinite cable, we consider the infinite cable as two semi-infinite cables, one on the left side, the other on the right side. Then the input resistance of the semi-infinite cable is twice that of the corresponding infinite cable, because current can flow in two directions. So the input resistance of the semi-infinite cable is:

$$R_{in} = (r_i * r_m)^{1/2} = \frac{r_m}{\lambda} = (R_m R_i)^{1/2} \frac{2}{\pi d^{3/2}}(13). \tag{4.18}$$

4.2.2 Finite cable

In real neurons, the length of a neuronal fiber is limited, so we need to consider a finite cable measured by the electrotonic length $L = l/\lambda$. The general solution of the finite cable with the electrotonic length is the following,

$$V(X) = \alpha \cosh(L - X) + \beta \sinh(L - X)(13). \tag{4.19}$$

Where $X = x/\lambda$, the values of α and β are determined by the specific boundary condition.

Sealed-End boundary condition

This is the most general case of real neurons embedded in living tissue. If the terminating resistance is infinite, then the outgoing axial current at position $X = L$ is zero. Because the axial current is determined by the derivative of the voltage along the cable, then we have the following formula,

$$\frac{dV(x)}{dX}|_{X=L} = 0(13). \tag{4.20}$$

This condition is called a *Neumann* boundary condition. Applying Eq.4.20 to Eq.4.19, we get

$$V(X) = V_0 \frac{\cosh(L-X)}{\cosh(L)}(13). \tag{4.21}$$

Fig.4.2 shows the voltage profile in cables with two different electrontonic lengths with a sealed-end boundary condition.

Now, we calculate the input resistance with the same strategy as in the previous section, and obtain

$$R_{in} = R_\infty \coth(L)(13), \tag{4.22}$$

where $\coth(x) = \cosh(x)/\sinh(x)$ and R_∞ is the input resistance of the semi-infinite cable. This is plotted in Fig.4.3, which shows that the input resistance is higher in a finite length cable than that of the semi-infinite cable.

Cut-End boundary condition

Another boundary condition is the cut-end boundary condition, when the nervous fiber is physically cut open. The intracellular potential at the terminal is equal to the extracellular

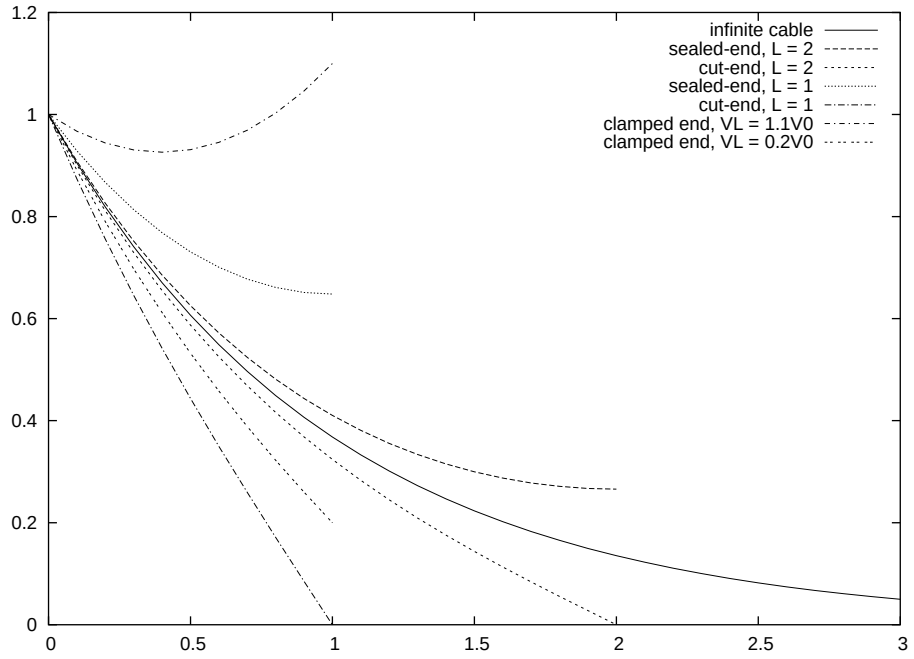

Figure 4.2: Steady-state potential attenuation

Steady-state potential attenuation with the normalized electrotonic length $X = x/\lambda$. Adapted from ref(13).

potential. The transmembrane potential at the terminal can be set to zero,

$$V(X)|_{X=L} = V_L = 0, \tag{4.23}$$

This type of boundary condition is called a *Dirichlet* boundary condition. Putting Eq.4.23 into Eq.4.19, we can get the membrane potential solution as,

$$V(X) = \frac{V_0 \sinh(L - X)}{\sinh(L)}(13), \tag{4.24}$$

and the corresponding input resistance is

$$R_{in} = R_\infty \tanh(L)(13), \tag{4.25}$$

The voltage profiles along the axon with the cut-end boundary condition for the electrotonic lengths L = 1 and 2 are plotted in Fig.4.2. This value is less than that of the semi-infinite cable, and the input resistance is also less than that of the semi-infinite cable (Fig.4.3).

Arbitrary boundary condition

However, in the general case, the boundary condition of real nervous fibers is neither sealed-end or cut-end. The terminal resistance has some finite value R_L corresponding to a junction to another cable. If we know the value R_L of the terminal resistance, then we can get the general solution as follows,

$$V(X) = \frac{V_0 \sinh(L - X) + V_L \sinh(X)}{\sinh(L)}(13). \tag{4.26}$$

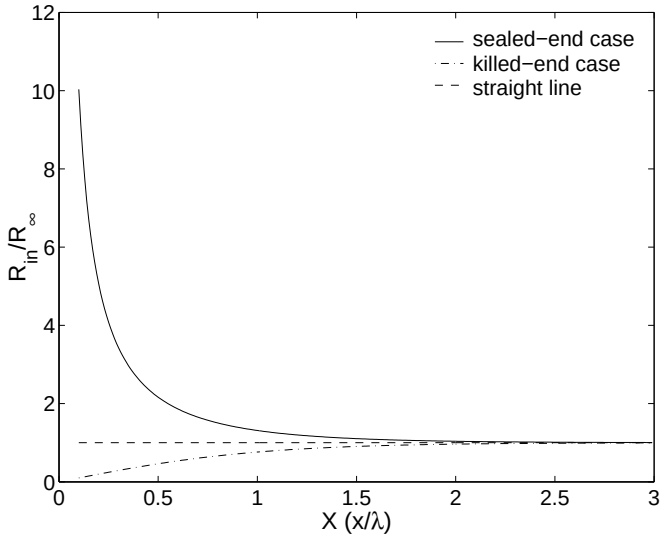

Figure 4.3: Input resistance with normalized electrotonic length $X = x/\lambda$.

The voltage profiles along the axon with $V_L = 0.2V_0$ and $V_L = 1.1V_0$ are plotted in Fig.4.2. We also can rewrite Eq.4.26 in the following form,

$$V(X) = V_0 \frac{\cosh(L - X) + (R_\infty / R_L)\sinh(L - X)}{\cosh(L) + (R_\infty / R_L)\sinh(L)}(13). \tag{4.27}$$

Combining the above equation and Eq.4.3, we can relate the input resistance with the terminating resistance R_L,

$$R_{in} = R_\infty \frac{R_L + R_\infty \tanh(L)}{R_\infty + R_L \tanh(L)}(13). \tag{4.28}$$

If we set R_L to zero or ∞, we can obtain the input resistances for sealed-end and killed-end boundary conditions from Eq.4.28.

4.3 Time-dependent solutions

Until now, we have only considered the membrane potential profile of a constant injected current. In most cases, we need to consider the voltage profile responding to the various injected currents. Because this case is more complicated, we just discuss two special cases. If we introduce the dimensionless variables for both time $T = t/\tau_m$ and space $X = x/\lambda$, and set $V_{rest} = 0$, we can rewrite Eq.4.7 as the following equation,

$$\frac{\partial^2 V(X,T)}{\partial X^2} = \frac{\partial V(X,T)}{\partial T} + V(X,T)(66). \tag{4.29}$$

The above equation has many solutions, and we need to find a solution to satisfy the boundary condition and the initial condition. There are two basic solutions for this kind of PDE.

One kind of solution is based on the method called separation of variables. Using this method, the general solution of this kind of PDE can be expressed as,

$$V(X,T) = (A\sin(\alpha X) + B\cos(\alpha X))e^{-(1+\alpha^2)T}(66). \tag{4.30}$$

where A and B are arbitrary constants determined by the initial condition, and α^2 is called the separation constant. It is easy to verify that this solution satisfies the dimensionless Eq.4.29.

The other class of solution is based on the Green's function. This solution is

$$V(X,T) = C_0(\pi T)^{-1/2}e^{-(T+X^2/4T)}(66). \tag{4.31}$$

where X can range from $-\infty$ to $+\infty$, and the point charge is located at X = 0 when T = 0. If the amount of the charge is Q coulombs, then for a semi-infinite cable, C_0 is equal to $Q/(\lambda c_m)$. For the doubly infinite case, the charge moves in two directions, then C_0 has half the value.

4.3.1 Finite length cable with sealed ends

For a uniform cable, with two sealed-end boundary conditions, it is found that the value of A in Eq.4.30 is zero, and the coefficients α have an infinite number of values, $\alpha_n = n\pi/L$, where n is an integer from zero to infinity. Then we can express the solution of the cable equation with two sealed-end boundary conditions by the following equation,

$$V(X,T) = \sum_{n=0}^{\infty} B_n cos(n\pi X/L)e^{-[1+(n\pi/L)^2]T}(66), \tag{4.32}$$

where the coefficients B_n are called Fourier coefficients, and are determined by the initial condition,

$$B_0 = (1/L) \int_0^L V(X,0) dX (66), \tag{4.33}$$

$$B_{(n>0)} = (2/L) \int_0^L V(X,0) cos(n\pi X/L) dX (66). \tag{4.34}$$

There is an alternative expression for Eq.4.31,

$$V(X,T) = C_0 e^{-t/\tau_0} + C_1 e^{-t/\tau_1} + C_2 e^{-t/\tau_2} + ...(66) \tag{4.35}$$

where $C_0 = B_0$ and τ_0 equals the positive membrane time constant, and

$$C_n = B_n cos(n\pi X/L)(66). \tag{4.36}$$

And for τ_n

$$\tau_0/\tau_n = 1 + \alpha_n^2 = 1 + (n\pi/L)^2 (66). \tag{4.37}$$

where $n = 0$ is associated with the slowest decay time constant.

It is important to note that the time constants depend on the electrotonic length L, but are independent of the initial condition. The electrotonic length L can be calculated as

$$L = \frac{n\pi}{\sqrt{\tau_0/\tau_n - 1}} (66). \tag{4.38}$$

The coefficients C_n depend on the initial condition and the measured position.

4.4 Compartmental model

In order to describe the spatial and temporal evolution of the action potential along the heterogeneous axon, a spatially explicit model of the axon is needed. If we set the injected current to be 0, and rewrite the third term of left side of Eq.4.11 as $i_{\text{ion}}(V)$, the cable equation for a one-dimensional axon is given by (see e.g. in (32)),

$$C_m \frac{\partial V(x,t)}{dt} + i_{\text{ion}}(V) = \frac{d}{4R_i}\frac{\partial^2 V}{\partial x^2}(67). \tag{4.39}$$

where R_i denotes the axoplasmic resistivity, d the diameter of the axon, and C_m the membrane capacity per area. The ionic current sources

$$i_{\text{ion}} = g_{Na}(V - V_{Na}) + g_K(V - V_K) + g_{leak}(V - V_{leak})(66). \tag{4.40}$$

are given by the Hodgkin-Huxley model described in the previous section.

The compartmental model replaces the continuous partial differential equation of the cable model 4.39 by a set of N ordinary differential equations(67). There are two key advantages of this model. First, the flexibility of the compartmental model ensures that this model can embody the structure and physiological differences of specific dendrites. Second, the compartmental model can be implemented directly on a computer. In the compartmental model, an unbranched region of an axon is divided into a number of contiguous compartments (68).Each compartment is small enough to be considered as being at a constant potential. Then the differences in physical properties and potential only occur between two nearby compartments rather than in one compartment(70; 71).

We consider an unbranched, cylindrical region of a passive axon, divided into three

linked compartments. A linked chain of equivalent electrical circuits illustrating this region is shown in Fig.4.4a. These compartments are represented by the equivalent circuit of Fig.4.4b. As shown in Fig.Fig4.4b, the circuit of each compartment consists of a capacitor in parallel with a resistor. Each compartment α is joined to its immediate neighbors by junctional resistors $r_{\alpha-1,\alpha}$ and $r_{\alpha,\alpha+1}$. If the cylindrical compartment α has uniform diameter d and length l_α, the membrane capacitance parameters have the following formulas

$$\begin{aligned} c_{m_\alpha} &= C_{m_\alpha} l_\alpha \pi d \\ r_{\alpha,\alpha} &= \frac{r_\alpha}{2} + \frac{r_\alpha}{2} = \frac{2R_{i_\alpha} l_\alpha + 2R_{i_\alpha} l_\alpha}{\pi d^2}, \end{aligned} \tag{4.41}$$

where C_{m_α} is the membrane capacitance per unit area.

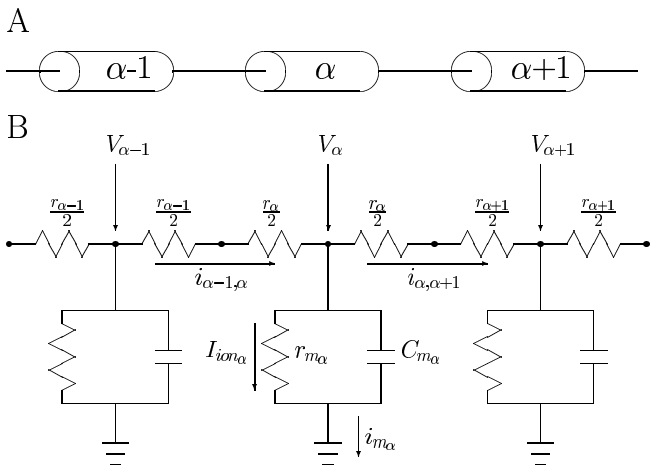

Figure 4.4: Schematic graph of compartmental chain
(A) A chain of three cylindrical compartments that are sufficiently short to be considered isopotential. (B) Equivalent circuit for a compartmental model of a chain of three successive small cylindrical compartments of passive axonal membrane. Adapted from ref(67).

The compartmental model is represented by a set of ordinary differential equations. Each equation is derived from Kirchhoff's laws. In each compartment, α, the net current through the membrane, i_α, must equal the longitudinal current that enters that compartment minus the longitudinal current that leaves it. If the αth compartment lies between the $(\alpha-1)$th compartment and the $(\alpha+1)$th compartment, the membrane current of the αth compartment is given by

$$i_{m_\alpha} = i_{\alpha-1,\alpha} - i_{\alpha,\alpha+1}(67), \tag{4.42}$$

where $i_{\alpha-1,\alpha}$ is the current that flows from the $(\alpha-1)$th compartment to the αth compartment and $i_{\alpha,\alpha+1}$ is the current that flows from the αth compartment to the $(\alpha+1)$th compartment. The membrane current is the sum of the capacitance (charging) current and the net ionic current (i_{ion}) that flows through the transmembrane resistance. For the compartment α, the membrane current can be expressed as

$$i_{m_\alpha} = c_{m_\alpha}\frac{dV_\alpha}{dt} + i_{ion_\alpha}(67), \tag{4.43}$$

where V_α is the membrane potential measured with respect to the resting potential. The longitudinal current is the voltage gradient between two nearby compartments divided by the axial resistance between the two compartments. Combining Eq.4.42 and Eq.4.43 , we can get the following equations

$$c_{m_\alpha}\frac{dV_\alpha}{dt} + i_{ion_\alpha} = \frac{V_{\alpha-1}-V_\alpha}{r_{\alpha-1,\alpha}} - \frac{V_\alpha - V_{\alpha+1}}{r_{\alpha,\alpha+1}}(67), \tag{4.44}$$

or

$$c_{m_\alpha}\frac{dV_\alpha}{dt} + i_{ion_\alpha} = (V_{\alpha-1} - V_\alpha)g_{\alpha-1,\alpha} - (V_\alpha - V_{\alpha+1})g_{\alpha,\alpha+1}(67), \tag{4.45}$$

where $g_{\alpha-1,\alpha} = 1/r_{\alpha-1,\alpha}$ is the axial conductance between the $(\alpha-1)$th compartment and the αth compartment. For the first compartment in a chain, only the second term for the longitudinal current appears on the right-hand side of the equations; for the last compartment in a chain, only the first term for the longitudinal current appears on the right-hand side of the equations.

Inserting the explicit expression for the ionic transmembrane currents (for all compartments α)

$$i_{m_\alpha} = c_{m_\alpha}\frac{dV_\alpha}{dt} + g_{leak,\alpha}(V - V_{leak}) + g_{Na,\alpha}(V - V_{Na}) + g_{K,\alpha}(V - V_\alpha)(67). \tag{4.46}$$

into Eq.4.45, one finds

$$c_{m_\alpha}\frac{dV_\alpha}{dt} = g_{\alpha-1,\alpha}V_{\alpha-1} + g_{\alpha,\alpha+1}V_{\alpha+1} - \left(g_{\text{leak},\alpha} + g_{Na,\alpha} + g_{K,\alpha} + g_{\alpha-1,\alpha} + g_{\alpha,\alpha+1}\right)V_\alpha + g_{\text{leak},\alpha}V_{\text{leak},\alpha} + g_{Na,\alpha}V_{Na,\alpha} + g_{K,\alpha}V_{K,\alpha}(67). \tag{4.47}$$

For a homogeneous axon, if we insert Eq.4.41 into Eq.4.45, and combine the two terms in right side of Eq.4.45 , we can get the following equation,

$$\frac{dV_\alpha}{dt} + \frac{i_{ion_\alpha}}{C_m l_\alpha \pi d} = \frac{d}{4R_i C_m l^2}(V_{\alpha-1} - 2V_\alpha + V_{\alpha+1}). \tag{4.48}$$

Chapter 5

Mechanism for neuronal spike generation by small and large ion channel clusters

5.1 Introduction

Conductance-based models for the trans-membrane voltage of neurons - pioneered in the seminal paper by Hodgkin and Huxley(23) - are the cornerstone of modern computational neuroscience. The essential idea is that the conductance of the membrane is determined by the conductance of the potassium and sodium systems which in turn is determined by the membrane potential. The nonlinear dependence of the sodium and potassium conductances on the membrane potentials generates action potentials that travel down the axon to contact other neurons. The conductance of sodium and potassium through the membrane is facilitated by specific ion channels that individually switch stochastically between

the open and the closed states - as demonstrated by Neher and Sakman(2). Experiments show that individual ion channels open and close randomly with membrane voltage dependent opening and closing rates(2; 3). The deterministic Hodgkin-Huxley equations (23) describe the dynamics of the membrane potential if the number of ion channels is very large, i.e. when conductance fluctuations are negligible. If the action potentials are generated by a cluster of sodium and potassium channels that comprises only a few channels, stochastic effects become important, giving rise to spontaneous spiking (24; 25). In such situations, stochastic Hodgkin-Huxley equations have to be employed to describe the transmembrane potential(10; 11; 26; 27; 28; 72). When the ion channel number is large, the stochastic Hodgkin-Huxley equation results will approach the conventional Hodgkin-Huxley equation results(27; 28). The effects of channel noise (as a function of the size of the ion channel cluster) have been studied recently in the context of the coherence of the generated neuronal spike train(12; 74). Besides channel noise, other sources of noise are important. Synaptic noise is generated by stochastic effects in the diffusion of neurotransmitter through the synaptic cleft as well as by the relatively small number of postsynaptic receptors. Furthermore, a neuron is often contacted by a large number of other neurons whose signals can act like a noise source(30). Other sources of noise are ligand-gated ion channels(29). In this chapter we report on the differences of the mechanisms of action-potential generation by small and large ion channel clusters and how these differences are expressed in the statistical properties of the neuronal spike train. We further explore the role of synaptic noise on the generation of action potentials by small and large clusters of ion channels in the neuronal membrane. Since synaptic noise is extrinsic to the ion channel processes that generate the action potentials, it appears as noise terms in the equation for the membrane voltage. Intrinsic channel noise appears in the equations for the gating

variables(27; 28). In Section 5.2, we describe the Hodgkin-Huxley model in the presence of channel noise and synaptic noise. In Section 5.3 we describe results for the spiking rates, variability of the spiking and temporal coherence of the generated spike trains. In section 5.4 our results are summarized. The results of this chapter have been published in Physics Review E(69).

5.2 Model

We adapt the classic model for the ion channels introduced by Hodgkin and Huxley that models the potassium channel by four identical gates that stochastically switch between an open state and a closed state. The open probabilities p_n for the four gates $n = 1, 2, 3, 4$ are described by the rate equations

$$\dot{p_n}(t) = -\left(\alpha_K(v) + \beta_K(v)\right) p_n(t) + \alpha_K(v)\,, \tag{5.1}$$

where $\alpha_K(v)$ and $\beta_K(v)$ are the membrane-voltage v dependent opening and closing rates, and the unit is 1/msec.

$$\alpha_K(v) = \frac{0.01(10-v)}{\exp\left((10-v)/10\right)-1} \quad , \quad \beta_K(v) = 0.125\exp\left(-\frac{v}{80}\right). \tag{5.2}$$

The trans-membrane voltage v is measured here and in all equations below in mV with respect to the physiological cellular resting potential of $-65mV$. The potassium channel is open only when all four gates are open, i.e. with probability $p_1p_2p_3p_4$.

The sodium channel consists of four gates. Three identical fast gates increase their opening probability q_1, q_2, q_3 when the voltage v becomes larger than the resting potential.

The slower fourth inactivation gate decreases its open probability q_4 when the membrane potential increases. The gate variables obey the following rate equations:

$$\begin{aligned} \dot{q}_n(t) &= -\left(\alpha^f_{Na}(v) + \beta^f_{Na}(v)\right) q_n(t) + \alpha^f_{Na}(v), \\ \dot{q}_4(t) &= -\left(\alpha^s_{Na}(v) + \beta^s_{Na}(v)\right) q_4(t) + \alpha^s_{Na}(v), \end{aligned} \tag{5.3}$$

with the opening and closing rates

$$\begin{aligned} \alpha^f_{Na}(v) &= \frac{0.1(25-v)}{\exp\left((25-v)/10\right)-1} \quad , \quad \beta^f_{Na}(v) = 4.0\exp\left(-\frac{v}{18}\right), \\ \alpha^s_{Na}(v) &= 0.07\exp\left(-\frac{v}{20}\right), \qquad \beta^s_{Na}(v) = \frac{1}{\exp\left((30-v)/10\right)+1}. \end{aligned} \tag{5.4}$$

Although each individual ion channel opens and closes independently, the opening and closing rates are regulated by the same membrane potential. As a consequence all ion channels are globally coupled through the membrane potential. For the density of the sodium and potassium channels (number of channels per unit area) we use $\rho_{Na} = 60/\mu m^2$ and $\rho_K = 20/\mu m^2$, respectively. The single-channel conductances of the sodium and potassium channels are given by $\gamma_{Na} = \gamma_K = 20pS$. Except for $\rho_K = 20/\mu m^2$ these values have been reported for the squid giant axon (23). Using a membrane capacitance of $1\mu F/cm^2$ we end up with the following equation for the membrane potential

$$\dot{v} = -\left(\frac{N^{open}_K}{\tau_K N_K}\left(v - v^{rev}_K\right) + \frac{N^{open}_{Na}}{\tau_{Na} N_{Na}}\left(v - v^{rev}_{Na}\right) + \frac{1}{\tau_L}\left(v - v_l\right)\right), \tag{5.5}$$

where $v^{rev}_K = -12mV, v^{rev}_{Na} = 115mV, v_l = 10.6mV, N^{open}_{Na}, N^{open}_K, N_{Na}, N_K$ denote reversal potentials of the potassium system, sodium system and leakage system, open sodium channel number, open potassium channel number, sodium channel number, and potassium

channel number, respectively. The minimal time constants are given by

$$\begin{aligned} \tau_K &= \frac{1}{36} ms \\ \tau_{Na} &= \frac{1}{120} ms \\ \tau_L &= 3.3 ms. \end{aligned} \tag{5.6}$$

The numbers of open K^+ and Na^+ channels, N_K^{open} and N_{Na}^{open}, respectively, have to be determined as a function of time by stochastic simulations with methods described in Chapter 3.

The time scale of synaptic noise is about one order of magnitude smaller than channel noise (see e.g. in (75)). Thus we can consider synaptic noise as Gaussian white noise $\xi_s(t)$ with

$$\begin{aligned} < \xi_s(t) > &= 0 \\ < \xi_s(t)\xi_s(t') > &= \sigma_s^2 \delta(t - t') \end{aligned} \tag{5.7}$$

where σ_s describes the strength of the synaptic noise. Since synaptic noise leads to events that are integrated, it has to be added to the right hand side of Eq.5.5, i.e.

$$\dot{v} = -\left(\frac{N_K^{open}}{\tau_K N_K} (v - v_K^{rev}) + \frac{N_{Na}^{open}}{\tau_{Na} N_{Na}} (v - v_{Na}^{rev}) + \frac{1}{\tau_L} (v - v_l) \right) + \xi_s(t), \tag{5.8}$$

5.3 Results

We have compared the average time-interval between two subsequent action potentials and the variance obtained from spike trains of 5000 action potentials that have been gener-

ated by the methods described earlier. The simple stochastic scheme, the Markov process method for the occupation number and the Gillespie method yield results that agree within a 5% error. The Langevin method does not reproduce accurate results either for small or large cluster sizes (see Figs.5.1 and 5.2). The disagreement is particularly large in the absence of synaptic noise when the average time interval between subsequent spikes diverges for large cluster sizes.

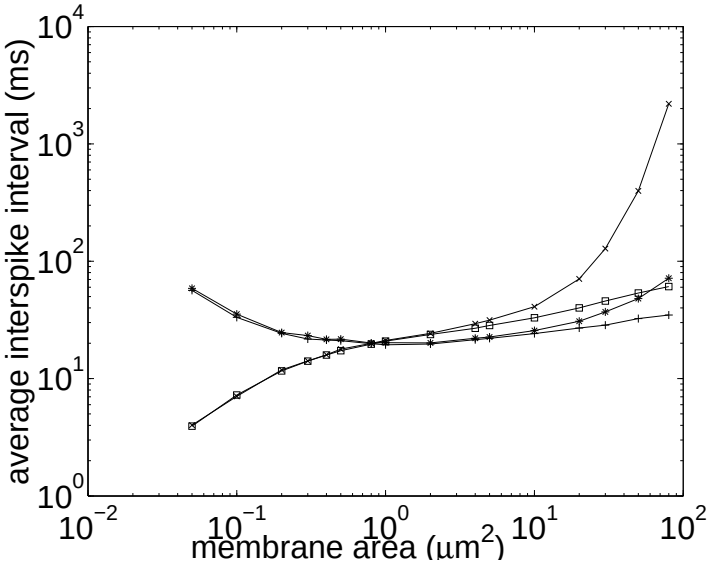

Figure 5.1: Average time intervals between subsequent action potentials
Comparison of the average time intervals between subsequent action potentials obtained from spike trains of 5000 action potentials for $\sigma_s = 0$ and $\sigma_s = 2\mu A/cm^2$. (x): Langevin method at $\sigma_s = 0$, (*): occupation number method at $\sigma_s = 0$, (+): occupation number method at $\sigma_s = 2\mu A/cm^2$, (square):Langevin method at $\sigma_s = 2\mu A/cm^2$.

The computation times for the different algorithms are compared in Fig.5.3. For the simple stochastic method, the simulation times increase linearly with the number of the channels in the cluster. The computing time for the Gillespie method also increases lin-

early in cluster size since the time-steps - drawn from an exponential distribution with a linearly decreasing decay time - become smaller as the cluster size increases. The Gillespie method is, however, much more efficient than the simple stochastic method. The occupation number method appears to us as the most efficient method. It leads to faster code with no cost in accuracy since 1) several channels are updated at each time step and 2) the time interval is fixed independent of the cluster size.

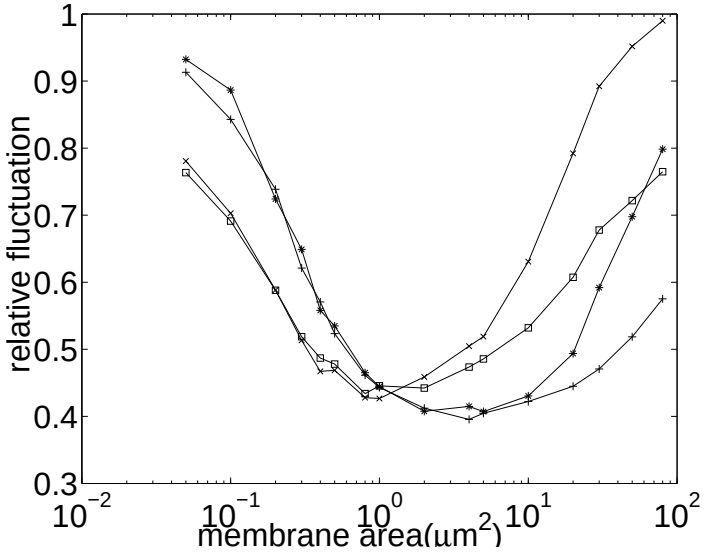

Figure 5.2: Comparison of the relative fluctuations $\frac{\sqrt{<(T-<T>)^2>}}{<T>}$ (Eq.5.14)

Comparison of the relative fluctuations $\frac{\sqrt{<(T-<T>)^2>}}{<T>}$ (Eq.5.14) of the intervals between subsequent action potentials obtained from spike trains of 5000 action potentials for $\sigma_s = 0$ and $\sigma_s = 2\mu A/cm^2$. (x): Langevin method at $\sigma_s = 0$, (*): occupation number method at $\sigma_s = 0$, (+): occupation number method at $\sigma_s = 2\mu A/cm^2$, (square):Langevin method at $\sigma_s = 2\mu A/cm^2$.

In order to further verify the accuracy of our simulations, we have verified 1) that the results obtained with the stochastic schemes approach the deterministic Hodgkin-Huxley

equations when the ion channel number is large, and 2) that our results agree with those in Ref.(11).

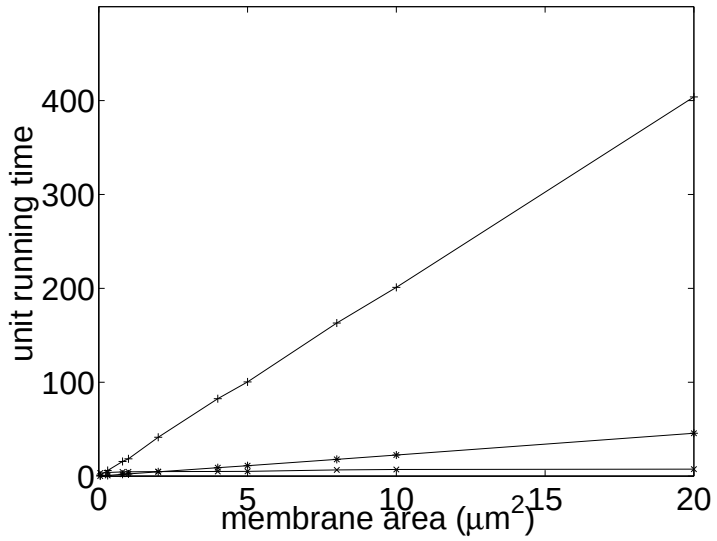

Figure 5.3: Comparison of the compute times
Comparison of the compute times for clusters of Na^+ and K^+ channels to generate a train of 5000 action potentials using the simple stochastic method (+), the Markov process for the occupation number (x) and the Gillespie method (*).

The Langevin method does not reproduce accurate results for small and large cluster sizes and therefore we did not compare the compute times of this method.

5.3.1 Average interspike interval of the ion channel cluster

We consider the combined effect of channel noise and synaptic noise on the average interspike interval $< T >$ as shown in Fig.5.4 as a function of the cluster size in the absence of an external stimulus. The fraction and density of sodium versus potassium channels is kept constant while the cluster size is increased. In the case of vanishing synaptic noise,

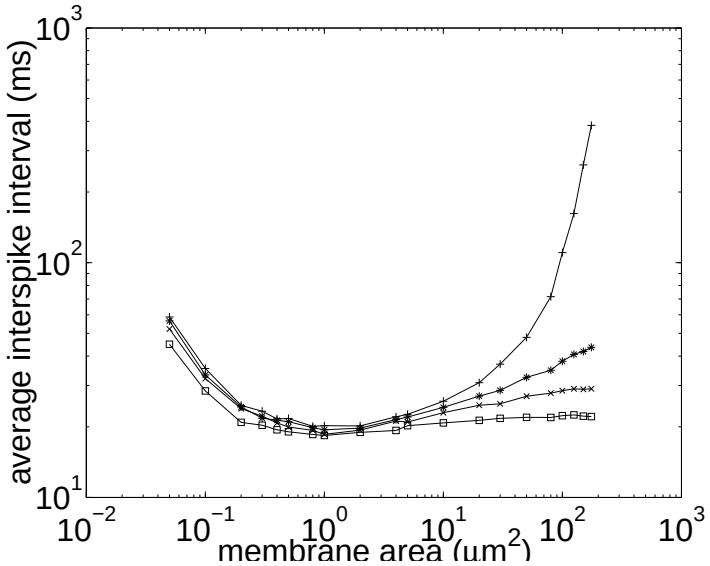

Figure 5.4: The average time interval between two subsequent action potentials
The average time interval between two subsequent action potentials (in ms) versus membrane area (in μm^2) at $\sigma_s = 0$ (+), $\sigma_s = 2\mu A/cm^2$ (*), $\sigma_s = 3\mu A/cm^2$ (x) and $\sigma_s = 5\mu A/cm^2$ (square). These results were obtained with the occupation number method.

the average interspike interval $< T >$ first decreases with increasing area of cluster, but then increases again since for infinitely many channels the deterministic Hodgkin-Huxley model is approached. In the presence of synaptic noise, the spiking rate does not decrease to zero as the size of the cluster increases. The average time-interval between two subsequent spikes is thus only determined by the synaptic noise as the number of channels becomes very large. We therefore encounter the paradoxical situation that channel noise *in addition* to synaptic noise *decreases* the spontaneous firing rate for small clusters. To understand this phenomenon it is useful to consider the two extreme situations of an infinitely large cluster of sodium and potassium channels with synaptic noise and a cluster

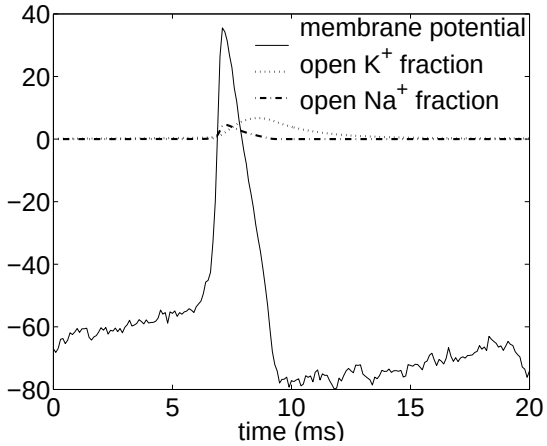

Figure 5.5: Membrane potential, fraction of open sodium and potassium channels. The membrane potential in mV, the fraction of open sodium and potassium channels are shown as a function of time for an ion channel cluster with infinitely many channels. The variance of the external noise is $5\mu A/cm^2$. For better visibility, the fraction of open channels is multiplied by 20.

of three sodium channels and one potassium channel. The membrane area of the second extreme situation is $0.05\mu m^2$. We set the magnitude of the variance σ_s of the synaptic noise as 5 $\mu A/cm^2$. The membrane potential, the fraction of open sodium ion channels and the fraction of open potassium ion channels in the case of an infinite cluster size are plotted in Fig.5.5. Here the membrane potential fluctuates about its rest state due to the synaptic noise. An action potential is fired when the membrane potential exceeds a threshold (of about $-55mV$) which is determined by the deterministic Hodgkin-Huxley equations. The average time interval between two successive spikes is determined by the probability for the membrane potential to cross the threshold.

In the other extreme case, a small cluster of three sodium channels and one potassium channel is considered. The time course of the membrane potential, the number of

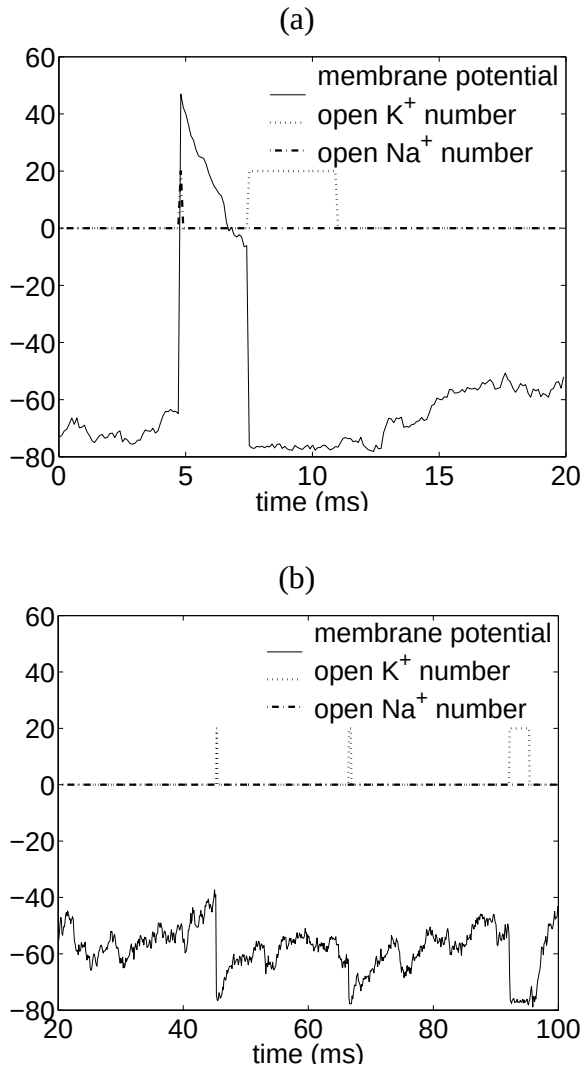

Figure 5.6: Membrane potential, open Na^+ number, open K^+ number.
The membrane potential (in mV), the number of open sodium ion channels and the number of open potassium channels is shown as a function of time for the membrane with one potassium channel and three sodium channels. The variance of external noise is 5 $\mu A/cm^2$. The number of open channels has been multiplied by a factor of 20. (a) When one sodium channel is open, an action potential is evoked. (b) Even if the membrane potential is greater than the threshold value of infinite large ion channel cluster, if there is no open sodium channel, no action potential is evoked.

open sodium channels, and the number of open potassium channels is shown in Fig.5.6. As can be seen in Fig.5.6a, an action potential is fired exactly when one sodium channel opens, although the membrane potential is well below the firing threshold of the deterministic Hodgkin-Huxley equations (about $-55mV$). In Fig.5.6b, we show a trace of the membrane potential in comparison with the number of open channels where the membrane potential is well *above* threshold but no action potential is fired. In contrast to the mechanism of action potential generation by large clusters, the mechanism for small clusters is not determined by the firing threshold of the membrane potential, but rather by the single channel kinetics. To see this we show in the following that the average time for any (of the three) sodium channels of the cluster to open after they all have been reset (after action potential) to a state where all gates are closed agrees well with the average time interval between two successive spikes. In other words, we show that the average interspike interval is determined by the activation time of the sodium channels. A single sodium channel is described by the following set of kinetic equations in which the rates out of the open-state m_3h_1 are discarded, i.e. thus generating the cumulative probability $P_o(t) = [m_3h_1]$ for the

probability that the channel has opened in the time interval $[0:t]$

$$\begin{aligned}
\frac{d}{dt}[m_0h_1] &= \alpha_h[m_0h_0] + \beta_m[m_1h_1] - (\beta_h + 3\alpha_m)\,[m_0h_1] \\
\frac{d}{dt}[m_0h_0] &= \beta_h[m_0h_1] + \beta_m[m_1h_0] - (\alpha_h + 3\alpha_m)\,[m_0h_0] \\
\frac{d}{dt}[m_1h_1] &= \alpha_h[m_1h_0] + 3\alpha_m[m_0h_1] + 2\beta_m[m_2h_1] - (\beta_m + 2\alpha_m + \beta_h)\,[m_1h_1] \\
\frac{d}{dt}[m_1h_0] &= \beta_h[m_1h_1] + 3\alpha_m[m_0h_0] + 2\beta_m[m_2h_0] - (\beta_m + 2\alpha_m + \alpha_h)\,[m_1h_0] \\
\frac{d}{dt}[m_2h_1] &= \alpha_h[m_2h_0] + 2\alpha_m[m_1h_1] - (2\beta_m + \alpha_m + \beta_h)\,[m_ih_1] \\
\frac{d}{dt}[m_2h_0] &= \beta_h[m_2h_1] + 2\alpha_m[m_1h_0] + 3\beta_m[m_3h_0] - (2\beta_m + \alpha_m + \alpha_h)\,[m_ih_1] \\
\frac{d}{dt}[m_3h_1] &= \alpha_h[m_3h_0] + \alpha_m[m_2h_1] \\
\frac{d}{dt}[m_3h_0] &= \alpha_m[m_2h_0] - (\alpha_h + 3\beta_m)[m_3h_0])\ , \qquad (5.9)
\end{aligned}$$

with the initial conditions

$$[m_ih_j] = \begin{cases} 1 & \text{for } \ i = j = 0 \\ 0 & \text{otherwise} \end{cases} \ . \qquad (5.10)$$

Assuming for now that the voltage is clamped, the solution for this set of equations for one single sodium channel is independent of the potassium conductance and can be solved easily for the cumulative probability $P_o(t)$. Since the sodium channels are independent, the cumulative probability that any of the three sodium channels has opened within the time interval $[0:t]$ is given by

$$P_3(t) = 1 - (1 - P_o(t))^3\ , \qquad (5.11)$$

and thus the probability density of re-open times of any channel within the cluster of three sodium channels reads

$$\rho_3(t) = \frac{d}{dt}P_3(t) = 3\dot{P}_o(t)\left(1 - P_o(t)\right)^2 \ , \tag{5.12}$$

where the dot indicates a derivative with respect to time t. The average opening time can then be obtained from

$$< t_3 >= \int_0^\infty t\rho_3(t)dt \ . \tag{5.13}$$

Since the voltage is fluctuating for a cluster of three sodium and one potassium channel (see Fig.5.6), the clamped voltage in the rate equations (Eq.5.9) is replaced by the average voltage of $-55.49mV$. Plugging the solution of Eq.5.9 into Eqs.5.10-5.13 one finds an average opening time of $58.18ms$. This number compares favorably with the average inter-spike interval of $58.71ms$ for a cluster of three sodium channels and one potassium channel obtained by stochastic simulations. This agreement supports the above stated hypothesis that the firing of action potentials in small channel clusters is determined by single channel kinetics and not by a threshold of the membrane potential.

As the cluster size is increased, the probability of opening just one sodium ion channel will increase since more sodium channels are available. Thus, the spontaneous firing rate increases with increasing cluster size and the average time interval between subsequent spikes decreases - as can be observed in Fig.5.4. When the cluster size increases further, opening of single sodium channels will not always trigger an action potential, a critical fraction of all available sodium channels is required to be open - consistent with the membrane potential crossing a threshold.

Thus the observed reduction of the spontaneous firing rate in spite of additional channel

noise reflects a change in the mechanism by which spikes are generated as the ion channel clusters become smaller.

As already mentioned earlier the Langevin approximation does not accurately reproduce these results. It fails at small and large cluster sizes (see Fig.5.1).

5.3.2 The relative fluctuation of the average interspike interval

The variability of the interspike intervals T is described by the relative fluctuations

$$\eta = \frac{\sqrt{< (T - < T >)^2 >}}{< T >} . \tag{5.14}$$

The relative fluctuations of the interspike intervals are plotted versus the cluster size for various values of the strength of the synaptic noise in Fig.5.7. In the absence of synaptic noise, the fluctuations of the intervals decrease with increasing cluster size until they reach a minimum. For further increasing cluster sizes, the fluctuations of the intervals increase again (see also (12; 74)). The power spectra of the spike trains shown in Fig.5.8 confirm that the spike train exhibits a maximum temporal periodicity at the cluster size where the relative fluctuations are at minimum.

The power spectrum of the spike train generated by a membrane with area 0.1 μm^2 is relatively flat. At a membrane area of $5\mu m^2$ (near the point with minimal relative fluctuation) the power spectrum exhibits a peak close to the angular frequency of $0.37/ms$, which corresponds to an average interspike interval of about $17ms$, consistent with the minimum average interspike interval (see Fig.5.4). The power spectrum confirms the maximal temporal coherence of the spike train at the same cluster size where the cluster fires action potentials at its highest rate.

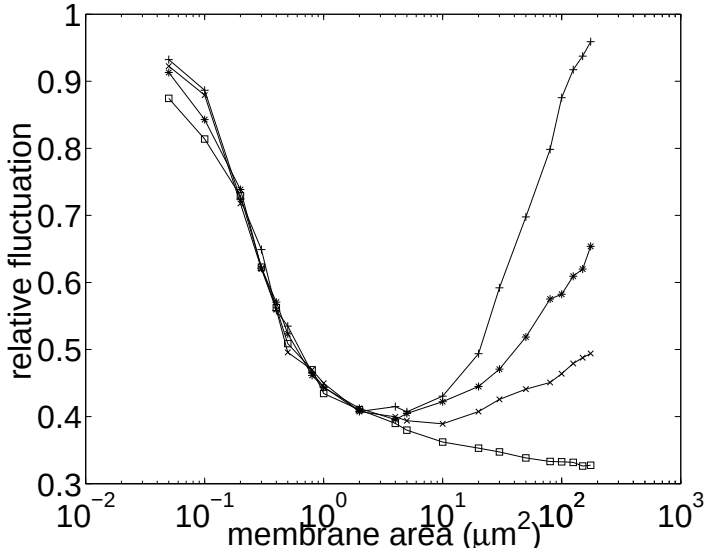

Figure 5.7: The relative fluctuations (5.14) versus membrane area (in μm^2).
The relative fluctuations (5.14) versus membrane area (in μm^2). at $\sigma_s = 0$ (+), $\sigma_s = 2\mu A/cm^2$ (*), $\sigma_s = 3\mu A/cm^2$ (x) and $\sigma_s = 5\mu A/cm^2$ (square). These results were obtained with the occupation number method.

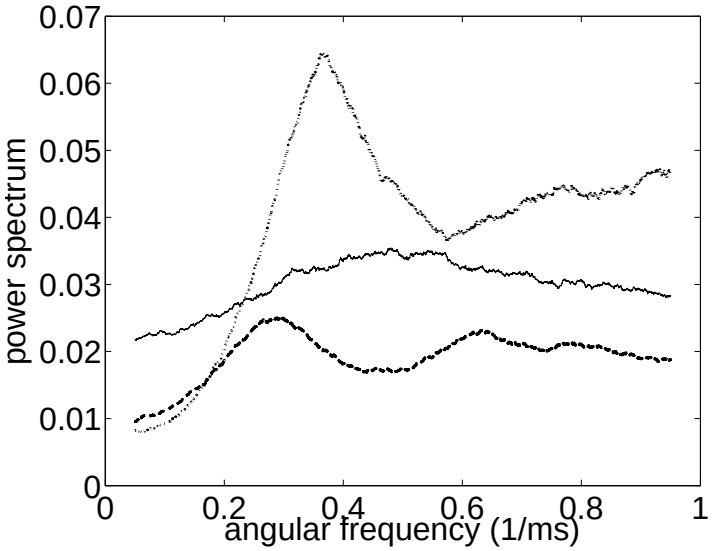

Figure 5.8: The power spectrum curves of spike trains

The power spectrum curves of spike trains generated by membranes with area=$0.1\mu m^2$(solid line), area=$5\mu m^2$ (dotted line) and area=$50\mu m^2$ (dashed line) in the absence of synaptic noise.

As shown in Fig.5.7, synaptic noise alters the relative fluctuations mostly at larger membrane areas, where the channel noise induced spikes are infrequent. On the other hand, when the area of membrane is small, the statistical features of the neuronal spike train are mainly determined by channel noise.

5.4 Discussion

We have compared the average interspike interval and the relative fluctuations of trains of action potentials generated by small and large clusters of ion channels. For large ion-channel clusters, action potentials are elicited by synaptic noise when the membrane potential exceeds an excitation threshold. For small ion channel clusters, channel noise dominates over synaptic noise. Action potentials are generated at a frequency that is determined by the single channel kinetics and is only dependent very weakly on the synaptic noise strength. We have further shown that at the size of the ion channel cluster at which a maximum spontaneous spiking rate is observed, the spike trains exhibits maximum temporal periodicity. Different stochastic algorithms have been compared. Because the simple stochastic method requires the least number of assumptions it is a priori the most accurate method. For spike trains of 5000 spikes the occupation number method and the Gillespie method reproduce the results obtained with the simple stochastic method within 5% error. If the membrane comprises N ion channels, $4N$ random numbers are required for the simple stochastic method. Thus, the simulation time of the simple stochastic method increases linearly with the number of ion channels. In Gillespie's method, the step time is inversely proportional to λ (3.22). Since the value of λ is linearly proportional to the number of ion channels, the simulation step time is inversely proportional to the ion channel number. Thus, the simulation time of the Gillespie's method is also linearly proportional to the

number of ion channels - though with a smaller slope than the simple stochastic method. In each simulation step, the occupation number method needs to generate a fixed number of 28 random numbers regardless of the number of ion channels. Thus, the simulation time is approximately independent of the number of the ion channels; in our tests it was the fastest method for a given accuracy. The Langevin method - although designed for large ion channel clusters - generates accurate results only for intermediate cluster sizes.

Chapter 6

Synchronization of ion-channel clusters on axon

6.1 Introduction

Synchronization is a basic phenomenon in science, discovered by Huygens three centuries ago(77). During the past decade, the concept of synchronization has been used to describe the interaction of chaotic oscillators. Periodic self-sustained oscillators adjust the oscillating frequencies through synchronization due to weak interactions(78; 79). Recently, the concept of phase synchronization of chaotic systems has been introduced(80). Phase synchronization is the appearance of a certain relationship between the phases of interacting systems. In the synchronization of chaotic systems, phase locking is important, while there are no restrictions on the amplitudes of chaotic oscillations. The properties of phase synchronization in chaotic systems are similar to those of synchronization in noisy oscillators and periodic oscillators(64).

Synchronization phenomena are often encountered in living systems. In living systems, the notion of synchronization is used widely to describe the interaction between different physiological systems demonstrating oscillating behavior. There are many synchronization phenomena in living systems, such as: phase locking of respiration with locomotory rhythms(76), coordinated movement(81), synchronization of oscillations of human insulin secretion(82), and synchronization of the noisy electrosensitive cells in the paddlefish(83). The notion of synchronization is also related to several important issues of neuroscience(84). Synchronization is the essential mechanism for information processing in brain areas, and responsible for the information communication between different brain areas. Synchronization of neuronal activity in the visual cotex is also responsible for combining several related visual features into a whole and integrated one(84; 85).

In neurons, the spiking frequency and time of action potential generation can be synchronized by weak interactions. The generation of action potentials is due to the movement of ions across the membrane through ion channels. Ion channels are usually uniformly distributed along the unmyelinated axon to support action potential propagation, but in some cases, ion channels are also distributed in clusters in giant squid axons(5) and in the rat retinal nerve fiber layer(86). The ion channel clusters along unmyelinated axons generate spontaneous spiking due to ion-channel noise(10; 27). The ion-channel clusters are coupled by an axonal cable, and the spontaneous spiking of each ion channel cluster is synchronized. Here we consider the synchronization of two ion channel clusters coupled by the axon. First, we calculate the effect of axonal parameters on the synchronization of ion channel clusters along the axon, then we consider the effect of ion channel cluster size on the synchronization. It is reported that there is an optimal size of the ion channel cluster for which the effect of synchronization is maximal.

Table 6.1: Axonal parameters of unmyelinated axon

Axon diameter (d)	$2\mu m$
Membrane capacitance (C_m)	$1\mu F/cm^2$
Axoplasmic resistivity (R_i)	$80\Omega - cm$
Length of each compartment	$2\mu m$
Length between two ion channel clusters	$20\mu m$
Na^+ density in the ion channel cluster (ρ_{Na})	$60/\mu m^2$
K^+ density in the ion channel cluster (ρ_K)	$20/\mu m^2$
Conductance of each ion channel (γ_{Na}, γ_K)	20pS
Na^+ reversal potential (V_{Na})	50 mV
K^+ reversal potential (V_K)	-77 mV
Leakage reversal potential (V_L)	-54.4 mV
Leakage current conductance (g_L)	0.3 mS/cm^2
Transition rate (α_n)	$\alpha_n = \frac{0.01(V+55)}{1-e^{-(V+55)/10}}$
Transition rate (β_n)	$\beta_n = 0.125e^{-(V+65)/80}$
Transition rate (α_m)	$\alpha_m = \frac{0.1(V+40)}{1-e^{-(V+40)/10}}$
Transition rate (β_m)	$\beta_m = 4e^{-(V+65)/18}$
Transition rate (α_h)	$\alpha_h = 0.07e^{-(V+65)/20}$
Transition rate (β_h)	$\beta_h = \frac{1}{1+e^{-(V+35)/10}}$

6.2 Results

We use the occupation number method to compute results from the stochastic HH equations, and analyse a spike train with 10000 spikes. In order to verify the accuracy of our simulation, we have 1) verified that when the ion channel number is large, the simulation result with stochastic HH equations approaches the result of the deterministic HH equations, 2)verified that the results agree with that of (11). We consider two ion-channel clusters connected by an unmyelinated axon. The unmyelinated axon is divided into 10 compartments. The parameters of the cable system are given in Table.1.

If there is no coupling between two ion channel clusters, the two clusters will spike independently. If we choose a large distance between two ion channel clusters, they can be considered as two independent clusters. Fig.6.1 illustrates the spontaneous spiking of two approximately independent ion channel clusters. As the figure shows, the spontaneous spiking times of two approximately independent ion channel clusters are independent and not correlated. If we set the distance between two clusters to $20\mu m$, then the two ion channel clusters are coupled. Fig.6.2 illustrates the spontaneous spiking of two coupled ion channel clusters. As Fig.Fig6.2 shows, the spontaneous spiking time of two coupled ion channel clusters are synchronized.

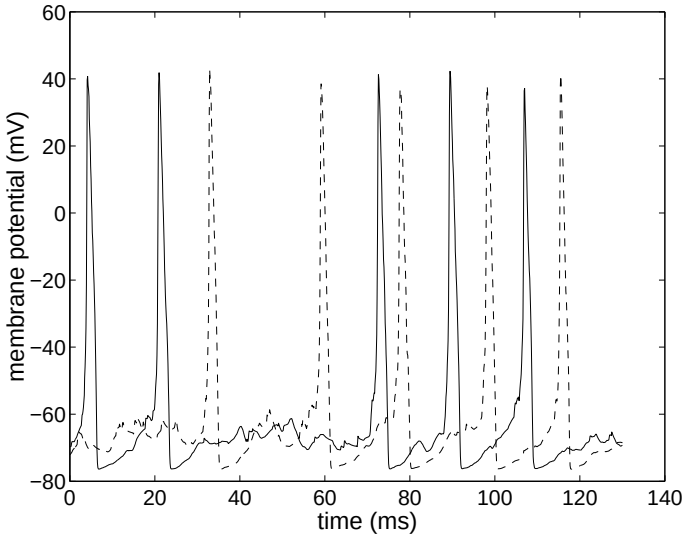

Figure 6.1: The spontaneous spikes of two independent ion channel clusters.

From Fig.6.2, we find that the spike time of two synchronized spikes is not exactly the same. The time difference of two synchronized spikes is the action potential propagation time between the two ion channel clusters. The average spiking time difference between

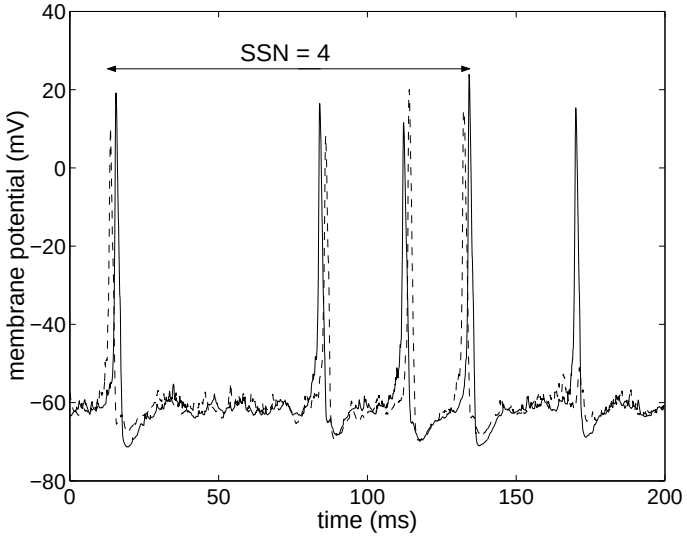

Figure 6.2: The spontaneous spikes of two coupled ion channel clusters.

200 pairs of synchronized spikes is 1.9 ms. The maximal time difference of the 200 pairs of spikes is 2.9 ms. If the time difference of two spikes is less than 3 ms, we consider the two spikes to be synchronized. In order to consider the synchronization strength, we calculate the average consecutive synchronized spiking number (SSN), which is shown in Fig.6.2. In our simulation, we first calculate 10000 spikes for one cluster, then calculate the average consecutive synchronized spiking number.

6.2.1 Effects of axonal parameters

We first consider the effects of cable parameters on the synchronized spiking number. We consider the effects of the specific membrane capacitance, the specific electrical resistivity of the cytoplasmic core, the axon diameter and the cable length on the synchronized spiking number, respectively. When we consider the effect of one parameter listed above, we fix the other parameters at the values shown in Table6.1. The effect of cable parameters is shown in Fig.6.3.

As shown in Fig.6.3, the synchronized spiking number will decrease if the specific membrane capacitance, electrical resistivity and the cable length are increased; if the axon diameter is increased, the synchronized spiking number will increase. The effect is dramatic and approximately exponential. We can consider the coefficient $\frac{d}{4R_iC_ml^2}$ of the term on the right side of Eq.4.48 as the coupling strength. It is clear that if R_i, C_m and l are increased, the coupling strength will decrease. If d is increased, the coupling strength will increase. Increasing the coupling strength, increases the synchronized spiking number, and vice versa.

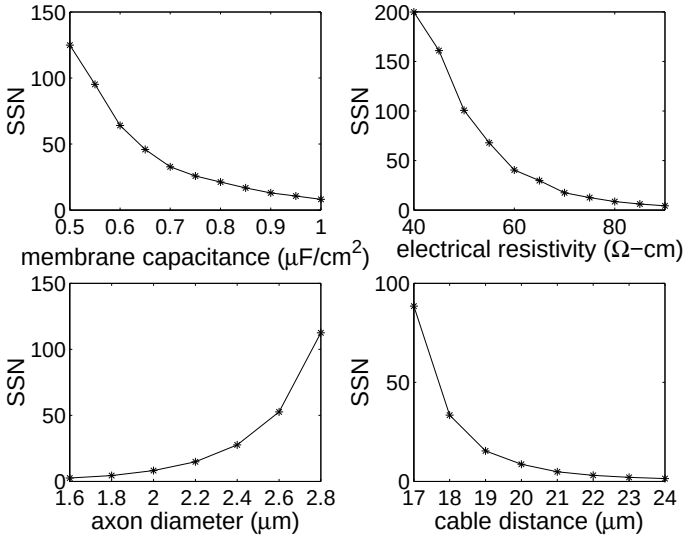

Figure 6.3: Effects of axonal parameters on the synchronized spiking number.
The effects of the specific membrane capacitance, the specific electrical resistivity of the cytoplasmic core, the axon diameter and the cable length on the synchronized spiking number, respectively.

6.2.2 Effect of cluster length distribution

Now we fix the total length of two ion-channel clusters at $4\mu m$, fix the parameters at the values shown in Table.6.1, and change the length of one cluster. The synchronized spiking number versus the length of ion-channel cluster is shown in Fig.6.4. Because the system is symmetric about the middle point, where the length of each ion channel cluster is 2 μm, we first calculate the synchronized spiking number with the length of cluster one ranging from $0.6\mu m$ to $3.4\mu m$, then calculate the average value about the middle point. As Fig.6.4 shows, when the two ion channel clusters have the same area, the synchronized spiking number has the maximal value, and the synchronization effect is most dramatic. It agrees with the real biological myelinated axon, where nodes are distributed homogeneously, and each node has approximately the same area.

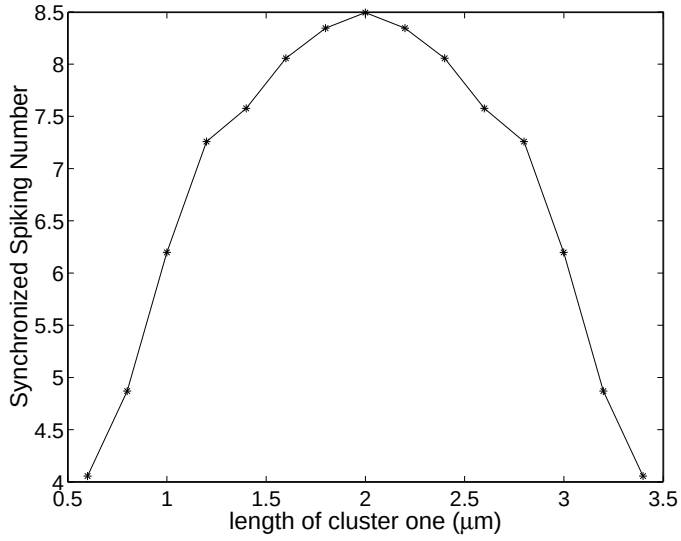

Figure 6.4: Synchronized spiking number versus the length of ion channel cluster one. The total length of two ion channel clusters is fixed at $4\mu m$.

6.2.3 Effect of cluster length

Now we fix the parameters to the values shown in Table.6.1, and change the length of each ion channel cluster simultaneously. The synchronized spiking number versus the length of each ion channel cluster is shown in Fig.6.5. As we increase the length of each ion channel cluster, the synchronized spiking number first increases, and after reaching a maximal value, it then decreases. The synchronization of spiking is due to the charge propagation between two clusters. When there is a spike in cluster one, then the charge will propagate from cluster one to cluster two. If the charge is big enough, the potential of cluster two will reach the threshold value, and a spike will be evoked. There is then a pair of synchronized spikes between the two clusters. If the charge is not big enough, cluster two will not evoke a spike, and there will not be a pair of synchronized spikes between the two clusters. So whether the quantity of charge propagating between two clusters is above a threshold value is the main factor that determines the synchronization of two clusters.

When the parameters of the axon are fixed, the charge carried by one spike is approximately fixed. Then the threshold value of charge to evoke a spike is the main factor to determine the synchronization of two clusters. At first glance, one would expect that the smaller the area of the cluster, the smaller the threshold value of charge to evoke a spike. Thus the smaller the area of the cluster, the bigger the synchronized spiking number. But the simulation results in Fig.6.5 show the opposite picture. The synchronized spiking number first increases with increasing cluster size. After reaching a maximal value, SSN decreases with increasing cluster size. We inject a current pulse in the ion channel cluster to calculate the threshold value to evoke a spike. The duration of the current pulse is fixed at 0.1 ms. We calculate the threshold value of the injected current in two cases. In one case, the ion channel cluster is connected with the axon; in the other case, the ion channel cluster

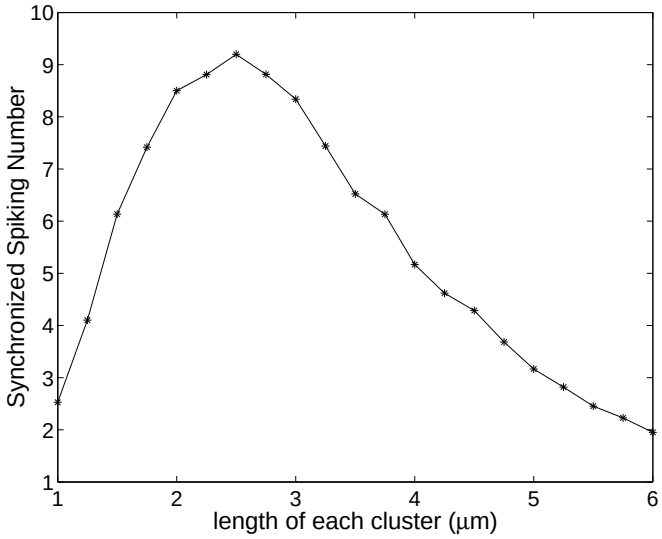

Figure 6.5: Synchronized spiking number versus the length of each ion channel cluster. The length of each ion channel cluster changes simultaneously.

is isolated, and is not connected with the axon. The threshold values of the injected current in the two cases are plotted in Fig.6.6.

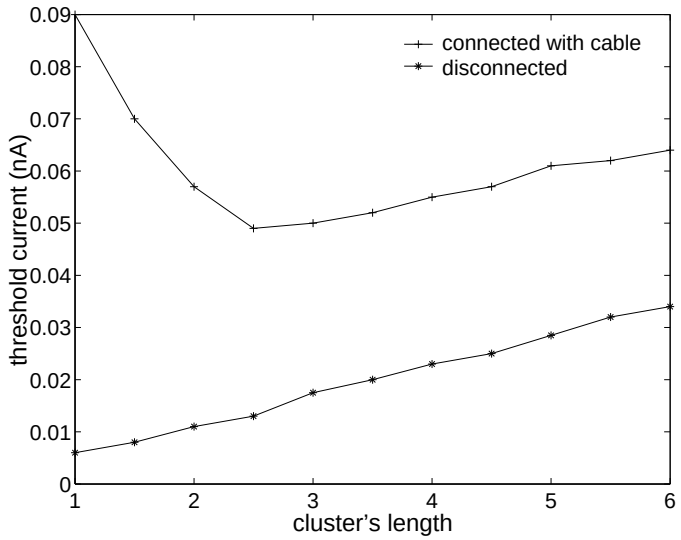

Figure 6.6: The threshold value of the injected current for the ion channel cluster. The duration of the current pulse is fixed as 0.1 ms. In one case, the ion channel cluster is connected with the axon; in the other case, the ion channel cluster is isolated, and is not connected with the cable.

As Fig.6.6 shows, in the case where the ion channel cluster is isolated, the threshold value of the injected current increases linearly with the length of the ion channel cluster. It is reasonable that the larger the area of the ion channel cluster is, more charge is needed to evoke a spike. In the other case where the ion channel cluster is connected with the axon, the threshold value of the injected current first decreases as the size of the ion channel cluster is increased, and after reaching the minimal value, it then increases with increasing cluster size. This phenomenon can explain why the synchronized spiking number first increases, reaches a maximal value, and then decreases.

When the action potential propagates from one ion channel cluster to the second ion channel cluster, charge moves in two directions in two different periods. During the first period, the voltage of the connected axon is higher than that of the second ion channel cluster. Charge moves from the connected axon to the second ion channel cluster, and the voltage of the second ion channel cluster will increase. When the voltage of the second ion channel cluster is higher than that of the connected axon, the second period is entered. In the second period, charge moves from the second ion channel cluster to the connected axon, and will affect the voltage increase of the second ion channel cluster. The dissipation of charge by the connected axon will decrease the spiking of the second ion channel cluster. In order to measure the effect of charge dissipation from the cluster to the axon on the spiking of the ion channel cluster, we calculate the spontaneous spiking frequencies in two cases. In one case, the ion channel cluster is connected with the axon; in the other case, the ion channel cluster is isolated, and is not connected with the axon. We calculate the ratio of spontaneous spiking frequencies in the two cases versus the length of ion channel cluster, and plot it in Fig.6.7.

As shown in Fig.6.7, the ratio of spontaneous spiking frequency increases with increasing length of the ion channel cluster. When the length of the ion channel cluster is small, the ratio is as small as 10%; when the length of the ion channel cluster is large, the ratio reaches 60%. When the size of the ion channel cluster is small, the effect of charge dissipation by the axon is dramatic, and the firing threshold is large. When the size of the ion channel cluster is increased, the ratio of the spontaneous spiking frequency increases. This mechanism will cause the threshold value of the ion channel cluster connected with the axon to decrease. On the other hand, the threshold value of the isolated ion channel cluster will increase due to increasing membrane area. This mechanism will cause the threshold

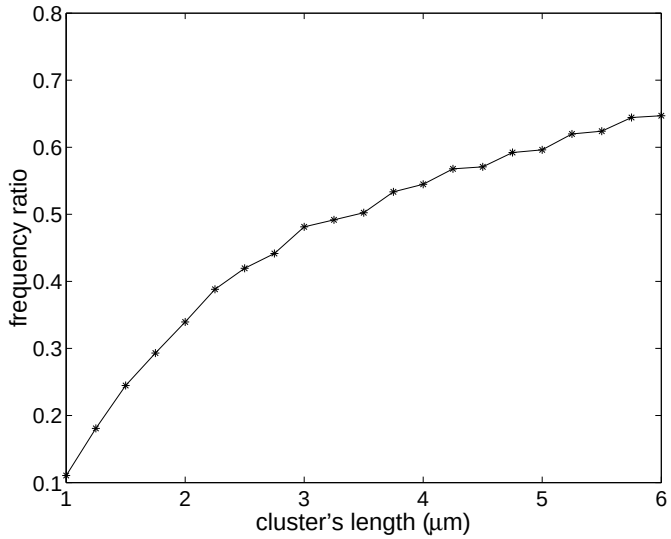

Figure 6.7: The frequency ratio in two cases.
In case one, the ion channel cluster is connected with the axon; in case two, the ion channel cluster is isolated, and is not connected with the axon. The numerator is the spontaneous spiking frequency of case one, the denominator is the spontaneous spiking frequency of case two.

value of the ion channel cluster connected with the axon to increase. There is a competition between the two mechanisms. When the length of the ion channel cluster is approximately 2.5 μm, the competition induces an optimal value. The threshold value of injected current reaches a minimum, when the synchronized spiking number has a maximum.

6.3 Discussion

We consider synchronization of two coupled ion channel clusters on an axon. We use the synchronized spiking number to describe the synchronization strength. The axonal parameters, such as the specific membrane capacitance, the specific axial electrical resistivity, and the axon diameter, affect the synchronized spiking number exponentially. The coefficient $\frac{d}{R_i C_m}$ is used to describe the coupling strength. Increasing the axonal diameter (d), decreasing the specific membrane capacitance (C_m) and the specific electrical resistivity (R_i) will increase the synchronized spiking number dramatically. It is known that the velocity of spike propagation will be proportional to the axonal diameter(88). On the other hand, increasing the axonal diameter will also be beneficial for the spiking synchronization. In myelinated axons, myelin isolates the membrane, and decreases the membrane capacitance. Decreasing the membrane capacitance can decrease the time constant of the axon, and increase the spike propagation speed(13). On the other hand, it is also shown here that decreasing the membrane capacitance can increase the synchronization.

It is shown that two ion channel clusters exhibit maximal synchrony when they have the same size. Correspondingly, in the biological system the length of nodes of Ranvier in myelinated axon is uniform. It is also shown that there is an optimal size of ion channel clusters with maximal synchronized spiking number. The length of ion channel clusters with the maximal synchronized spiking number is approximately 2.5 μm. This value ac-

cords with the length of the node of Ranvier in the myelinated axon(89). In order to explain the optimal phenomenon of the synchronized spiking number, we calculate the threshold value of the injected current of the ion channel cluster connected with the axon. Correspondingly, the threshold value of the injected current has a minimal value when the length of the ion channel cluster is approximately 2.5 μm. There are two mechanisms that affect the threshold value of the injected current. First, when increasing the area of the ion channel cluster, the threshold value of the injected current of an isolated ion channel cluster will increase. Second, when increasing the area of the ion channel cluster, the effect of charge dissipation by the axon will cause the threshold decrease. The competition between the two mechanisms generates an optimal threshold value of injected current, and produces an optimal ion channel cluster length with the maximal synchronization.

Chapter 7

Axonal Oscillations in Developing Mammalian Nerve Axons

7.1 Introduction

An important requirement for the successful evolution to large body sizes of organisms is the stable, efficient, and fast propagation of action potentials across the long axons of the peripheral nervous system. An elegant solution of this problem is the development of the myelinated axon, where the sodium channels are concentrated at the nodes of Ranvier, separated by segments sheathed with myelin. The myelin sheath is a high resistance, low capacitance barrier for the axonal membrane and provides the basis for fast propagation of action potentials. The nodes of Ranvier are distributed along the axon where the myelin is interrupted at distances ranging from $50\mu m$ to $1000\mu m$ for different nerves. These spatial axonal domains differ dramatically from internodal axonal regions. Voltage-dependent sodium channels can be found in the nodes of Ranvier at a much larger density

(approximately $2000/\mu m^2$(3)) than in the internodal region(41; 42; 43; 45) (of the order $10/\mu m^2$). Furthermore, the capacitance of the nodes of Ranvier is higher than that of the internodal region. Voltage-dependent potassium channels are excluded from nodes of Ranvier(44); they are clustered beneath the myelin sheaths in regions adjacent to paranodes, called juxtaparanodes(45; 46).

Potassium ion channels play an important role in the modulation of excitability(3). In their pioneering work on neuronal excitability, Hodgkin and Huxley(23) demonstrated that potassium ion channels play an important role in the repolarization of the action potential in the squid giant axon. Blockage of internodal potassium ion channels in young dorsal roots(90) and regenerating rat nerve fibers (91) results in a bursting activity triggered by a single impulse. Vabnick et al.(92) demonstrated that internodal potassium ion channels prevent bursting activity in the developing sciatic nerve of rat. In contrast, blockage of internodal potassium ion channels does not affect the spike waveform and firing properties of normal mature sciatic nerve fibers(91).

Although sodium ion channels clustered in nodes of Ranvier provide the physiological basis for saltatory conduction, the function of internodal potassium ion channels remains unclear. There are two suggestions about the function of internodal potassium ion channels. One suggestion is that they stabilize the paranodal axolemma against nodal back-firing after a single impulse(45). The other suggestion is that the function of internodal potassium ion channels is to maintain a resting potential under the myelin(47; 48). In this chapter, we use a computational model for a developing mammalian axon to explore the role of the spatial distribution of potassium channels with regard to reliability and speed of action potential propagation. Our main result is that the observed configuration of juxtaparanodal concentrations of potassium channels optimizes speed and reliability of action potential

propagation during the development of the axon. The results of this chapter are accepted by Physical Review E.

7.2 Model

We consider two nodes of Ranvier connected by an axon. There are 10 compartments between two successive nodes(93). The present model provides an explicit representation of the node of Ranvier, the myelin attachment compartment (MYSA), the paranode main compartment (FLUT) and the internode compartments (STIN). The geometric structure of the cable model is shown in Fig.7.1. Sodium ion channels exist in a high density in the node of Ranvier, and a very low density in the internodal region. Potassium ion channels only exist in the juxtaparanodal region. The nodes consist of a parallel combination of the nonlinear sodium conductance, the leakage conductance and the membrane capacitance. The internodal region consists of a parallel combination of the nonlinear sodium conductance, nonlinear potassium conductance, the leakage conductance, and the membrane capacitance. The parameters of the cable model are listed in the Table7.1.

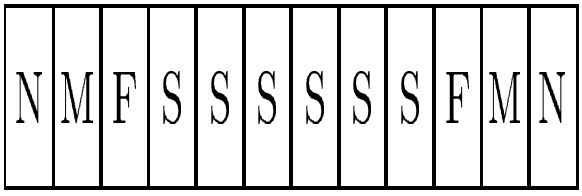

Figure 7.1: The cable model with 10 internodal compartments.
Each internodal section of the model consists of 2 myelin attachment compartments (MYSA), 2 paranode main compartments (FLUT) and 6 internodal compartments (STIN). FLUT is the juxtaparanode.

Table 7.1: Axonal parameters

Axon diameter	$5\mu m$
Nodal membrane capacitance	$2\mu F/cm^2$
Axoplasmic resistivity	$70\Omega - cm$
Na^+ conductance in nodal region	$800mS/cm^2$
Na^+ reversal potential	50 mV
K^+ reversal potential	-90 mV
Leakage reversal potential	-80 mV
Nodal leakage current conductance	8 mS/cm^2
Nodal length	1 μm
MYSA length	3 μm
FLUT length	20 μm
STIN length	50 μm

7.3 Results

7.3.1 Oscillation activity of myelinated axon in development

Myelin isolates the cytoplasmic core of the axon from the extracellular environment, and provides low internodal capacitance and high transverse resistance for the membrane(13). During the development of the axon, the thickness of the myelin increases and thus, the internodal capacitance and leakage currents decrease(14). Due to the segregation of sodium ion channels and the isolating effect of myelin, the conductance of internodal sodium ion channels will also decrease in development(42). In order to simulate action potentials in development, we increase the internodal capacitance, leakage conductance and internodal sodium channel conductance proportionally. In order to determine the effect of juxtaparanodal potassium ion channels, we first set the potassium conductance zero everywhere.

We simulate four groups of data. Internodal parameters are listed in Table.7.2. The case

Table 7.2: Internodal parameters

Set number	Internodal Na^+ density (mS/cm^2)	Internodal leakage density (mS/cm^2)	Internodal membrane capacitance ($\mu F/cm^2$)
First	0.5	0.005	0.005
Second	1	0.01	0.01
Third	2	0.02	0.02
Fourth	3	0.03	0.03

numbers correspond to conditions for decreasing degrees of axon myelination as an animal develops. External current is injected in node one to evoke an action potential. Action potentials in the four groups of data are plotted in Figs.7.2.

In the first group, the values of g_{Na_i}, g_{leak_i} and c_{m_i} are very small, corresponding to a more mature axon. As shown in Fig.7.2(A), the action potential evoked in node one (solid line) by an external current, propagates along the axon to node two (dashed line), where it evokes another action potential. This behavior is consistent with the observation that blockage of internodal potassium ion channels does not affect the spike waveform and firing properties of normal mature axons(91). As shown in Figs.7.2(B)(C)(D), the shape of the action potentials changes gradually when the values of the internodal sodium conductance g_{Na_i}, leakage conductance g_{leak_i} and internodal capacitance c_{m_i} are increased, with increases corresponding to an axon in an earlier stage of development. Consistent with observations in developing axons (90; 91) we observe multiple spikes in nodes one and two in the absence of potassium channels, and sustained axonal oscillations can be observed in Fig.7.2D. In the following section we discuss what parameter changes can cause these oscillations.

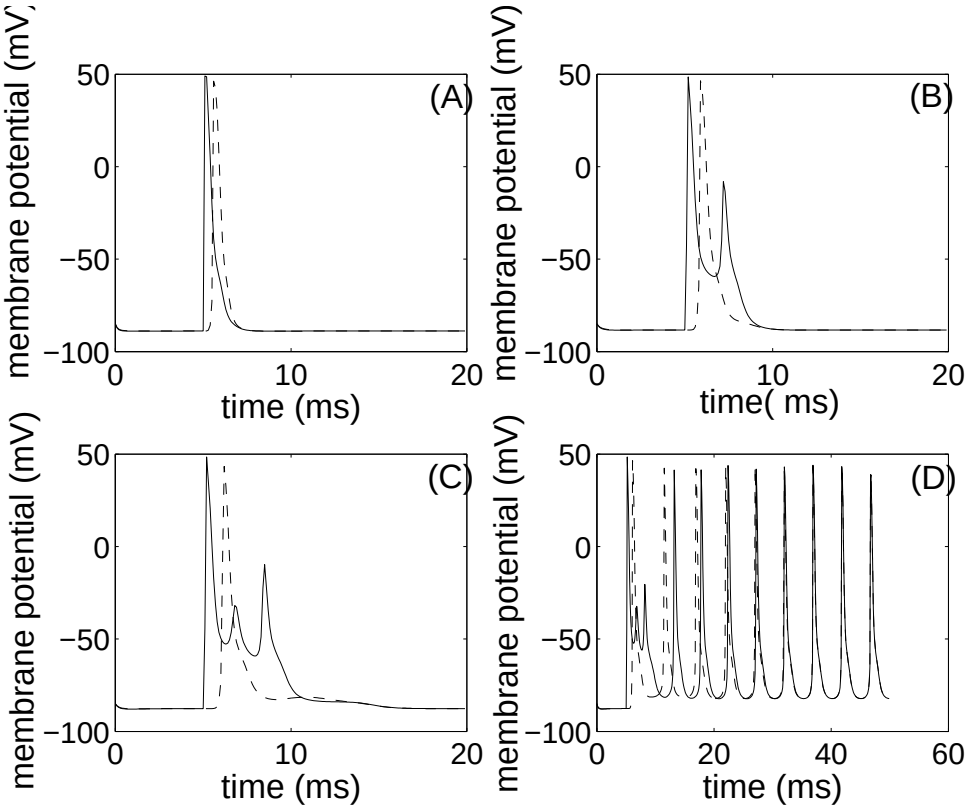

Figure 7.2: Action potentials of two connected nodes.

Action potentials of two connected nodes without juxtaparanodal and internodal potassium channels. The solid lines represent the action potential of node one and the dashed lines denote the action potentials of node two. Current is injected into node one to evoke an action potential. (A)$g_{\mathrm{Na}_i} = 0.5mS/cm^2$, $g_{\mathrm{leak}_i} = 0.005mS/cm^2$, $c_{m_i} = 0.005\mu F/cm^2$. (B)$g_{\mathrm{Na}_i} = 1mS/cm^2$, $g_{\mathrm{leak}_i} = 0.01mS/cm^2$, $c_{m_i} = 0.01\mu F/cm^2$. (C)$g_{\mathrm{Na}_i} = 2mS/cm^2$, $g_{\mathrm{leak}_i} = 0.02mS/cm^2$, $c_{m_i} = 0.02\mu F/cm^2$. (D)$g_{\mathrm{Na}_i} = 3mS/cm^2$, $g_{\mathrm{leak}_i} = 0.03mS/cm^2$, $c_{m_i} = 0.03\mu F/cm^2$.

7.3.2 Effects of parameters of internodal membrane on oscillation activity

In order to determine the effect of each parameter, we only change one parameter value, and keep the values of other parameters constant. First, we test the effect of leakage conductance. At constant values of $g_{\mathrm{Na}_i} = 0.5mS/cm^2$, and $c_{m_i} = 0.005\mu F/cm^2$, we change the value of g_{leak_i} from $0.005mS/cm^2$ to $0.03mS/cm^2$. An external current pulse is injected into node one to evoke an action potential. Simulation results (Fig.7.3) show that the leakage current does not change the shape of action potentials. Thus, the leakage current is not the source of oscillation activity.

Next we investigate the effect of the internodal membrane capacitance. At constant values of $g_{\mathrm{Na}_i} = 0.5mS/cm^2$ and $g_{\mathrm{leak}_i} = 0.005mS/cm^2$, we change the value of c_{m_i} from $0.005\mu F/cm^2$ to $0.03\mu F/cm^2$. An external current pulse is injected into node one to evoke an action potential. The subsequent membrane potentials at both nodes are plotted in Fig.7.4. As shown in Fig.7.4, the shape of the action potentials changes gradually as the internodal membrane capacitance is increased. When the capacitance increases beyond a certain value, the axon can respond with multiple spikes (at each node) to a single action potential. For large enough capacitance tonic oscillation occurs. Thus, a relatively big value of internodal membrane capacitance in development is a potential source of axonal oscillation if the internodal and juxtaparanodal potassium ion channels are blocked.

A simple theory can predict the onset of axonal oscillations. Given the refractory time of a node of about $\tau_r = 2ms$, an action potential starting out at node one and propagating to node two can back-fire to node one if the propagation speed of the action potential u is less than $2\Delta/\tau_r$ where Δ is the distance between the two nodes, i.e. for our model axon $\Delta = 350\mu m$. Thus backfiring *between two subsequent nodes* is expected to occur if

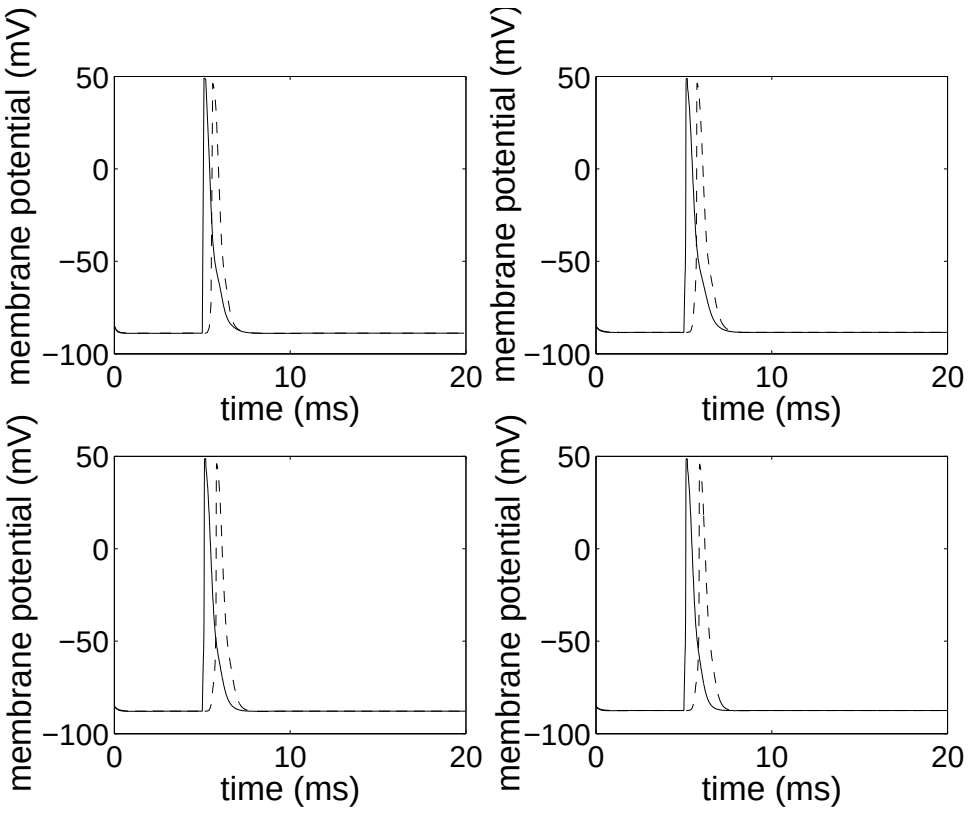

Figure 7.3: The effect of internodal leakage conductance on action potentials.
The effect of internodal leakage conductance on action potentials of two connected nodes without juxtaparanodal and internodal potassium ion channels. The solid line denotes the action potential of node one, while the dashed line represents the action potential of node two. Stimuli current is injected in node one. The parameters are $g_{\mathrm{Na}_i} = 0.5mS/cm^2, g_{\mathrm{leak}_i} = 0.005mS/cm^2, c_{m_i} = 0.005\mu F/cm^2(A), g_{\mathrm{leak}_i} = 0.01mS/cm^2(B), g_{\mathrm{leak}_i} = 0.02mS/cm^2(C), g_{\mathrm{leak}_i} = 0.03mS/cm^2(D)$.

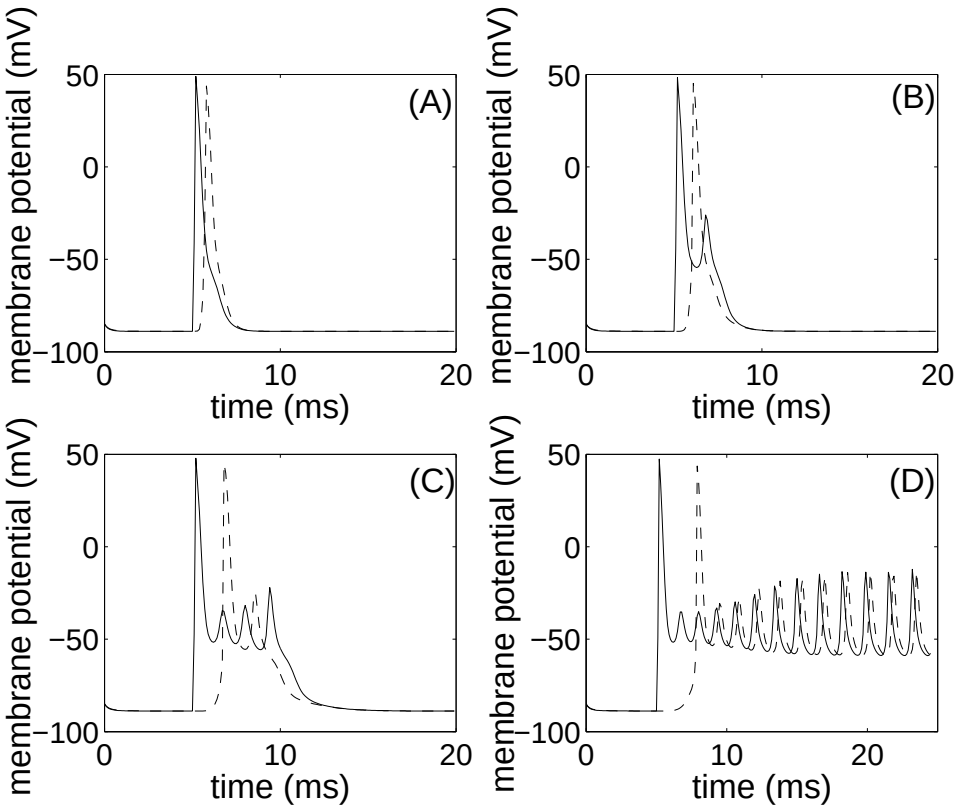

Figure 7.4: The effect of internodal membrane capacitance on action potentials.
The effect of internodal membrane capacitance on action potentials of two connected nodes without internodal and juxtaparanodal potassium ion channels. The solid line denotes the action potential of node one, while the dashed line represents the action potential of node two. Stimuli current is injected in node one. The parameters are $g_{\mathrm{Na}_i} = 0.5mS/cm^2, g_{\mathrm{leak}_i} = 0.005mS/cm^2, c_{m_i} = 0.005\mu F/cm^2(A), c_{m_i} = 0.01\mu F/cm^2(B), c_{m_i} = 0.02\mu F/cm^2(C), c_{m_i} = 0.03\mu F/cm^2(D)$.

the speed of the action potential is below $0.35m/s$. The speed of the action potential in Fig.7.4(A) is approximately $0.7m/s$ while it is only $0.35m/s$ in Fig.7.4(B) with a larger internodal capacitance. Consistent with the simple criteria developed above, backfiring is seen in Fig.7.4(B). As described below, this theory is not complete. Other effects than the competition between refractoriness and propagation time are relevant for axonal oscillations.

Next we study the effect of internodal sodium ion channels. At constant values of $g_{\mathrm{leak}_i} = 0.005mS/cm^2$, and $c_{m_i} = 0.005\mu F/cm^2$, we change the value of g_{Na_i} from $0.5mS/cm^2$ to $3mS/cm^2$. An external current pulse is injected into node one to evoke an action potential there. The subsequent action potentials of node one and node two are plotted in Fig.7.5. With an increase in the conductance of internodal sodium ion channels, the shape of the action potentials changes suddenly. Below a sodium conductance of $g_{\mathrm{Na}_i} = 2mS/cm^2$, tonic spiking can be observed, below a sodium conductance of $g_{\mathrm{Na}_i} = 3mS/cm^2$, tonic oscillation can be observed. Thus, a relatively large value of internodal sodium conductance in development can induce axonal oscillation when the internodal potassium ion channels are blocked.

Because there are no low-threshold calcium ion channels in the system, the mechanism of the oscillation activity is purely due to back-firing of the action potential. Increasing the internodal sodium conductance will enhance the excitability of the internodal membrane, enhance the back propagation of the action potential and thus can facilitate the onset of axonal oscillation.

The next question we consider is whether internodal sodium channels are *necessary* for the axonal oscillation. To this end we block all internodal sodium channels, i.e. we set the internodal sodium conductance to zero. In order to guarantee the success of action

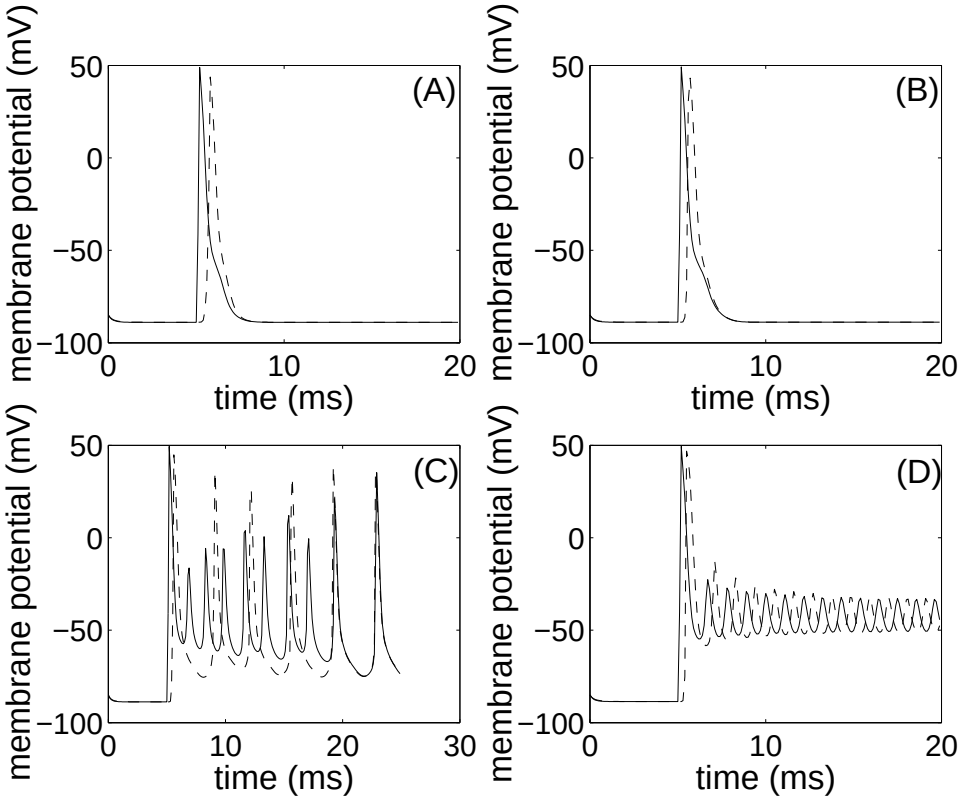

Figure 7.5: The effect of internodal sodium conductance on action potentials.
The effect of internodal sodium conductance on action potentials of two connected nodes without internodal and juxtaparanodal potassium ion channels. The solid line depicts the action potentials of node one and the dashed line represents the action potential of node two. An electrical current pulse is injected into node one to evoke an action potential. The parameter values are $g_{\text{leak}_i} = 0.005 mS/cm^2, c_{m_i} = 0.005 \mu F/cm^2, g_{\text{Na}_i} = 0.5 mS/cm^2 (A), g_{\text{Na}_i} = 1 mS/cm^2 (B), g_{\text{Na}_i} = 2 mS/cm^2 (C), g_{\text{Na}_i} = 3 mS/cm^2 (D)$

potential propagation from node one to node two, we increase the axon diameter to 10 μm, and shorten the length of the internode to 250 μm. Increasing the capacitance of the internodal membrane, i.e. reducing the speed of action potential propagation causes axonal oscillation. Thus, internodal sodium ion channels are not necessary for axonal oscillation.

By carefully inspecting the sequence of action potentials in Fig.7.4 we realize that the qualitative picture of action potentials bouncing back from node two to node one seems to be correct only at the onset of axonal oscillation. In Fig.7.4(D) node one fires the second time before node two has ever fired. Furthermore, the period of the bursts (same figure) is too short for action potential propagation delayed spikes, as can be seen by the long time interval between the first spike of node one and the first spike of node two. Thus, our hypothesis is that the backfiring can occur through sodium channels in the internode. To this end we remove node two and evoke an action potential in node one.

We delete the second node, evoke action potentials at the remaining node and perform simulations under the same conditions as in Figs.7.2-7.5. In the presence of internodal sodium channels we find - similar to the case with two nodes (Figs.7.4-7.5) - that onset of axonal oscillation occurs with increasing internodal membrane capacitance and sodium channel conductance. (see Fig.7.6 for the effect of increasing internodal sodium channels).

Thus, as hypothesized above, axonal oscillations can be facilitated through backfiring at internodal sodium channels. However, as Fig.7.7 shows, in the absence of internodal sodium channels, no oscillation can be observed in the absence of the second node regardless of increases in internodal membrane capacitance. Thus, in the absence of internodal sodium channels, only backfiring *between nodes* generates axonal oscillation.

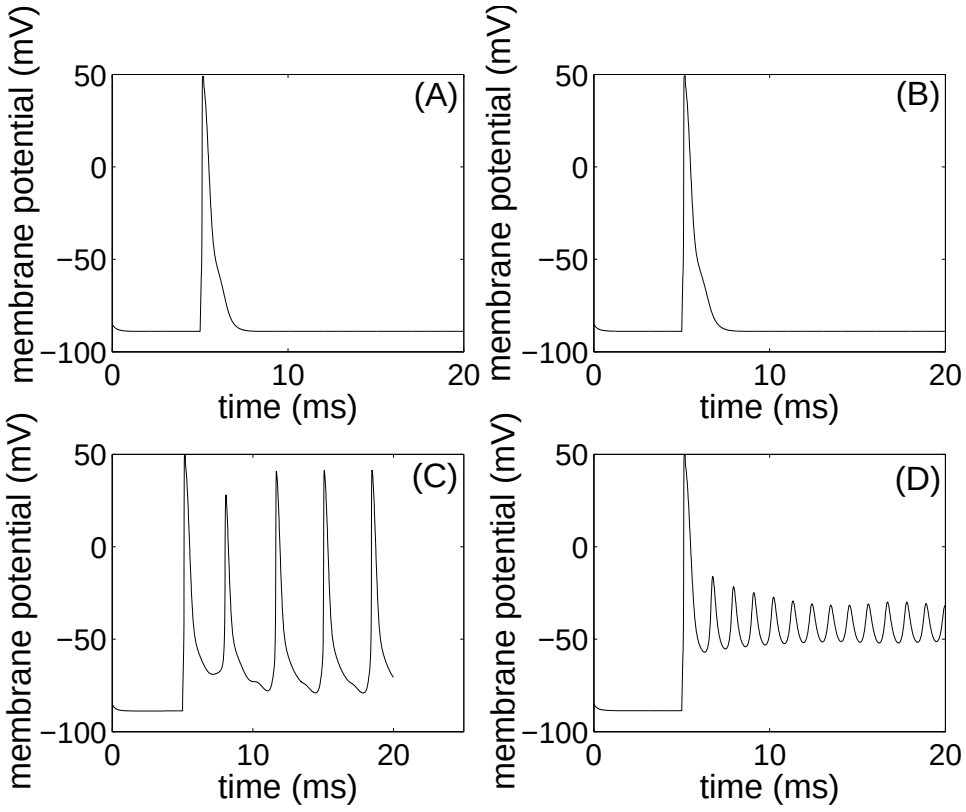

Figure 7.6: The effect of internodal sodium conductance on action potentials.
The effect of internodal sodium conductance on action potentials of a single node connected to an internode without juxtaparanodal and internodal potassium channels. The solid line depicts the action potentials at the node. An electrical current pulse is injected into the node to evoke an action potential. The parameter values are $g_{\text{leak}_i} = 0.005mS/cm^2, c_{m_i} = 0.005\mu F/cm^2, g_{\text{Na}_i} = 0.5mS/cm^2(A), g_{\text{Na}_i} = 1mS/cm^2(B), g_{\text{Na}_i} = 2mS/cm^2(C), g_{\text{Na}_i} = 3mS/cm^2(D)$

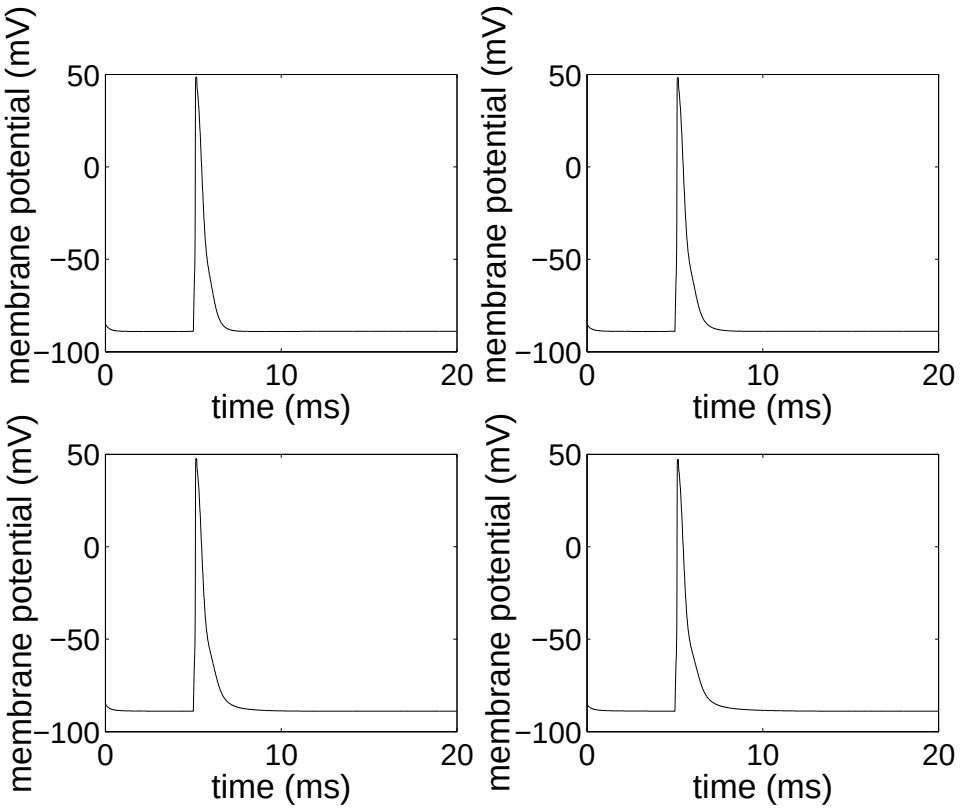

Figure 7.7: The effect of internodal membrane capacitance on action potentials.
The effect of internodal membrane capacitance on action potentials of a single node connected to an internode without juxtaparanodal and internodal potassium channels and internodal sodium ion channels. The solid line depicts the action potentials at the node. An electrical current pulse is injected into the node to evoke an action potential. The parameter values are $g_{\mathrm{leak}_i} = 0.005 mS/cm^2, c_{m_i} = 0.005 \mu F/cm^2, g_{\mathrm{Na}_i} = 0 mS/cm^2 (A), c_{m_i} = 0.01 \mu F/cm^2 (B), c_{m_i} = 0.02 \mu F/cm^2 (C), c_{m_i} = 0.03 \mu F/cm^2 (D)$

7.3.3 The role of internodal potassium ion channels

In order to test the role of internodal potassium ion channels, we set the conductance of potassium ion channels g_{K_i} in juxtaparanodes to $6mS/cm^2$ and 0 in internodes. For the conductance of the internodal sodium channels and internodal membrane capacity we pick values at which axonal oscillations are observed, i.e. $g_{\mathrm{Na}_i} = 0.5mS/cm^2, g_{\mathrm{leak}_i} = 0.005mS/cm^2$, and $c_{m_i} = 0.03\mu F/cm^2$. In the absence of internodal potassium channels, the axon exhibits oscillation as shown in Fig.7.4(D). The action potentials in the presence of internodal potassium ion channels (see Fig.7.8) do not cause axonal oscillation, consistent with the experimental observation in(92). Thus internodal potassium ion channels stabilize the internodal axolemma against oscillation.

An interesting point is that the required potassium conductance in order to prevent axonal oscillation depends on the spatial distribution of these channels. In order to inhibit the oscillation activity for the parameter sets in Fig.7.2(D), the conductance of potassium ion channels in juxtaparanodes must be larger than $200mS/cm^2$. Instead, if internodal potassium ion channels are distributed uniformly along the axon, an internodal potassium conductance of as low as $1mS/cm^2$ is sufficient to inhibit the oscillation activity. Thus, a uniform distribution of internodal potassium ion channels is more efficient to inhibit the oscillation activity than a localized juxtaparanodal distribution. On the other hand, the conduction speed is also affected by the distribution of the potassium channels. In general, internodal and juxtaparanodal potassium channels slow down the speed of the action potential of the purely passive cable. Localizing the potassium channels on the juxtaparanodes, however, leaves the internodes almost passive (except for some internodal sodium channels) and thus the reduction of the conduction speed is small in comparison to a uniform distribution at the same conductance. In Fig.7.9 the effects of internodal potassium

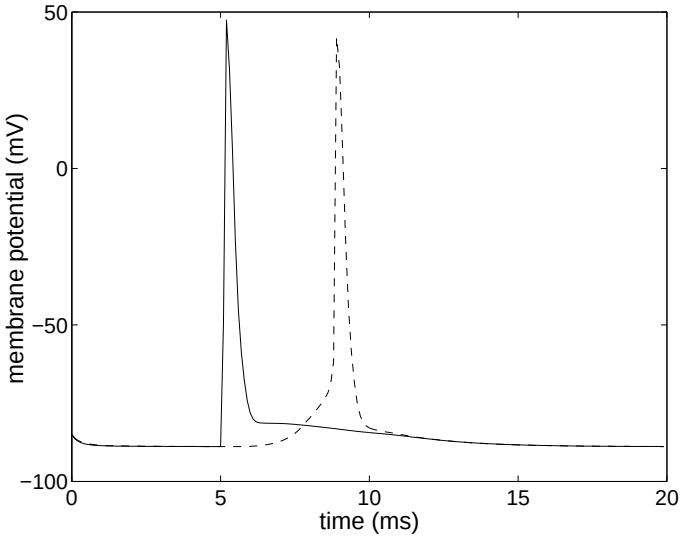

Figure 7.8: Action potentials of two connected nodes

Action potentials of two connected nodes with juxtaparanodal potassium ion channels. Solid line is the action potential of node one. Dashed line is the action potential of node two. Stimuli current is injected in node one. The parameters are $g_{\mathrm{Na}_i} = 0.5mS/cm^2$, $g_{\mathrm{leak}_i} = 0.005mS/cm^2$ and $c_{m_i} = 0.03\mu F/cm^2$.

channels on action potential propagation speed in two cases are shown. For an internodal membrane capacity of $0.02\mu F/cm^2$ and a maximum internodal sodium conductance of $2.0mS/cm^2$ the propagation speed in the absence of potassium channels is $0.366m/s$. For a maximum internodal potassium channel conductance of $10mS/cm^2$ the conduction speed is $0.249m/s$ for a uniform potassium channel distribution, but $0.348m/s$ for juxtaparanodal distribution.

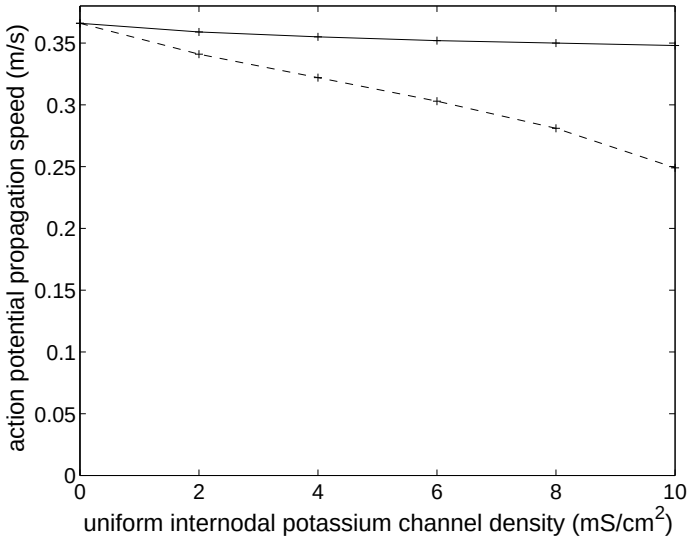

Figure 7.9: Effects of potassium channels on action potential propagation speed. The solid line depicts the effect of localized potassium channels in the juxtaparanode on action potential propagation speed. The value of x-axis for the solid line is 8.65 times that of x-axis for the dashed line. The Dashed line depicts the effect of uniformly distributed internodal potassium on action potential propagation speed. In the two cases, the total potassium numbers are the same. The parameter values are $g_{leak_i} = 0.005mS/cm^2$, $c_{m_i} = 0.02\mu F/cm^2$, $g_{Na_i} = 2mS/cm^2$.

7.4 Discussion

We simulated the action potentials of two nodes connected by an axon. Our simulation results show that blockage of internodal potassium ion channels can induce axonal oscillations in *developing* axons, but has no effect on the action potentials of normal *mature* axons. These results are consistent with the experimental results(90; 91). Our simulation results also show - consistent with experimental results(49) - that internodal potassium ion channels stabilize the internodal axolemma, and prevent axonal oscillation in developing axons. We tested the effects of axonal parameters with respect to onset of axonal oscillation. While the leakage current has no effect on axonal oscillation, increasing internodal sodium conductance as well as increasing internodal membrane capacitance can facilitate axonal oscillation. Increasing the conductance of internodal sodium ion channels increases the excitability of the axon and therefore also the chance for back propagation leading to axonal oscillation. Increasing the capacitance of internodal membrane affects axons in two aspects. First, an increasing capacitance leads to a slower propagation speed and thus an increase in the time an action potential takes to propagate between node one and node two or node one and some other internodal active site and back to node one. If this time is large enough, re-excitation of node one leads to backfiring and possibly to persistent axonal oscillations. The other aspect is that it increases the charge carried by the back propagated action potential. We furthermore find that one node connected with an axon is sufficient to induce axonal oscillation if sufficient numbers of sodium channels are present along the axon. In order to investigate the oscillation mechanism, we first chose the simplest model, two nodes connected by an axon. We also simulated systems with three nodes and four nodes, and got similar qualitative results.

The mechanism of oscillation, tonic oscillation, and tonic spiking described in this

chapter is facilitated by back-propagation of action potentials on the axon. This mechanism is similar to that of oscillation in cortical cells, where the back propagation of action potentials by the dendritic tree causes the oscillation activity (94; 95). But it is different from the mechanism of oscillation in thalamic cells, where the somatic low-threshold calcium current induces the oscillation activity(96; 97). In Pinsky and Rinzel's model(98) for CA3 pyramidal cells, oscillation is due to the interaction between the lower threshold, fast, sodium currents in the soma compartment and the higher threshold, slower Ca and Ca dependent currents in the dendrite compartment. In models of sensory neurons(99), there is a saddle-node bifurcation of periodic orbits that separates tonic spiking from oscillation. A ping-pong effect described by Pinsky & Rinzel(98) and Laing & Longtin(99) is similar in appearance to the one we report along the axon in this chapter. Different physical properties of the two compartments are the cause for the ping-pong of excitation between soma and dendrites. In this chapter, we study axonal dynamics only and find a ping-pong effect along the axon under specified physiological conditions and specified spatial distributions of ion channels.

Chapter 8

Effect of clustered ion channels along unmyelinated axon

In most unmyelinated axons, the ion channels are distributed uniformly along the axon to facilitate stable propagation of action potentials. In this case, the conduction in the axon is continuous, and the excitability along the membrane is constant. Some experimental papers show that ion channels also locate in clusters in some unmyelinated axons. Widely dispersed clusters of potassium ion channels were observed in the axonal membrane of squid giant axons(5; 100; 101). Punctuate domains of potassium ion channels were also observed in the axoplasm and were localized into 25-50 μm-wide columns down along the axon longitudinally(5; 100; 101). In Aplysia axonal membrane, sodium ion channels are localized in clusters, and the distance between clusters is on the order of 5-15 μm(96). Sodium ion channel clusters are also observed in pyramidal cell dendrites of Apteronotus(102) and frog sartorius muscle(103). The distance between clusters in these two kinds of membrane are on the order of 5-15 μm and 10-20 μm respectively. Regional node-like membrane specializations were also found in unmyelinated axons of rat retinal

nerve fiber layer(86).These experimental results demonstrate that conduction in some unmylinated axons may occur in a non-uniform rather than in a continuous manner.

The mechanisms and special functions of ion channel clusters along unmyelinated axons are unclear. In this chapter, we investigate theoretically the effect of localization of ion channels along unmyelinated axons. It is well known that the propagation speed of the action potential is important for fast signaling. Experimental papers show that half of the metabolic energy for the neural system is consumed by the pumps that exchange sodium and potassium ions across cell membranes. We use the terminology "action potential propagation efficiency" to describe the energy consumption to propagate action potentials. If the energy consumption to propagate action potentials is decreased, the action potential propagation efficiency is increased, and vice versa. So for a specific potassium channel conductance, decreasing the minimal required sodium channel conductance for successful action potential propagation will increase action potential propagation efficiency and decrease metabolic energy consumption. We will focus on the effect of ion channel localization along an unmyelinated axon in two areas: action potential propagation efficiency and action potential propagation speed. We will investigate the effect of axonal parameters on action potential propagation efficiency, and try to construct an unmyelinated axon with better propagation efficiency. Upon further research, the results of this chapter will be submitted to Physics Review E.

8.1 Model

We use the deterministic HH equations and cable equations to investigate this problem. The model has 101 compartments in total. External current is injected at compartment one to initiate an action potential. The axonal parameters are listed in Table.8.1.

Table 8.1: Axonal parameters

compartment number	101
compartment length	2 μm
axon diameter	1-8 μm
cytoplasmic resistivity	30-130 $\Omega - cm$
membrane capacitivity	1 $\mu F/cm^2$
conductance of leakage current	0.3 mS/cm^2
reversal potential of sodium ion channel	50.0 mV
reversal potential of potassium ion channel	-77.0 mV
reversal potential of leakage current	-54.4 mV
transition rate of α_n	$\frac{0.01(55+v)}{-exp(-(55+v)/10)+1}$
transition rate of β_n	$0.125exp(-(v+65)/80)$
transition rate of α_m	$\frac{0.1(v+40)}{-exp(-(40+v)/10)+1}$
transition rate of β_m	$4.0exp(-(v+65)/18)$
transition rate of α_h	$0.07exp(-(v+65)/20)$
transition rate of β_h	$\frac{1.0}{exp((-35-v)/10)+1}$

8.2 Results

8.2.1 Effect of potassium channel localization

First we test the effect of potassium channel localization on action potential propagation efficiency. The axonal diameter is $2\mu m$, and the cytoplasmic resistivity is 70 Ωcm. Initially, potassium ion channels are distributed uniformly along the axon, with a conductance density of 20 mS/cm^2. The minimal required conductance of sodium channels to support stable action potential propagation is 23 mS/cm^2. Then we keep the total potassium channel number constant, localize potassium ion channels gradually into clusters, and measure the minimal required sodium ion channel conductance to support stable action potential propagation. There is one potassium ion channel cluster every five compartments. Potassium ion channels with lower density are distributed uniformly between clusters. As Fig.8.1 shows, potassium channel localization increases the propagation efficiency, and the minimal required sodium conductance can decrease 15%.

Next we test the effect of the axon diameter on propagation efficiency. We keep the cytoplasmic resistivity at 70 Ωcm, change the axon diameter from 1 μm to 8 μm, and leave the potassium channel conductance at 20 mS/cm^2. We test two cases. In case one, 96% of potassium channels are localized in clusters; in case two, potassium ion channels are distributed uniformly along the axon. With a change in the axon diameter, the minimal required sodium conductance is almost the same in both cases. This shows that the axon diameter does not affect the propagation efficiency.

Now we test the effect of cytoplasmic resistivity on propagation efficiency. The axon diameter is 2 μm. Cytoplasmic resistivity ranges from 30 Ωcm to 130 Ωcm. We test the same two cases that are described above, and calculate the ratio of the minimal required

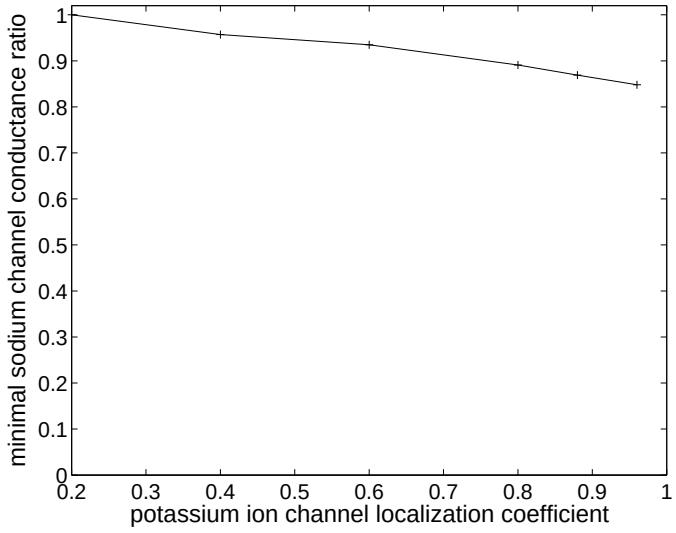

Figure 8.1: The effect of potassium ion channel localization on propagation efficiency. The x axis represents the potassium ion channel localization coefficient which is the number of potassium ion channels in clusters divided by the total number of potassium ion channels. The y axis represents the minimal required sodium channel ratio, i.e. the minimal required sodium conductance divided by the minimal required sodium conductance when potassium ion channels are distributed uniformly.

sodium conductance of the two cases. The results are shown in Fig.8.2. As the cytoplasmic resistivity is increased, the localization of potassium channels has a more dramatic effect on the propagation efficiency.

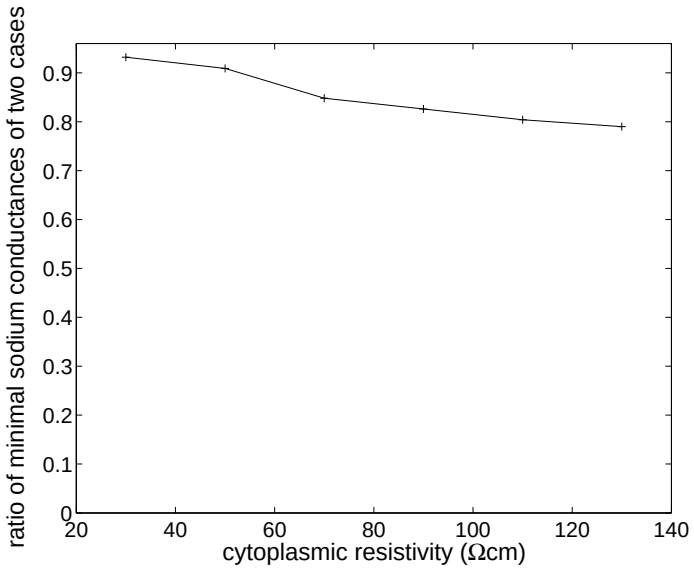

Figure 8.2: The ratio of minimal required sodium conductances of two cases. In case one, 96% of the potassium channels are located in clusters. In case two, potassium channels are distributed uniformly along the axon. The average potassium conductance of the two cases is 20 mS/cm^2. The minimal required sodium conductance of case one is the numerator, and that of case two is the denominator.

Now we change the conductance of potassium channels, and calculate the ratio of minimal required sodium conductances in the two cases. The two cases are the same as above. The axon diameter is 2 μm, and the cytoplasmic resistivity is 70 Ωcm. Fig.8.3 shows the ratio of the minimal required sodium conductance in the two cases. It shows that the effect of potassium channel localization on propagation efficiency is more dramatic as potassium conductance is increased.

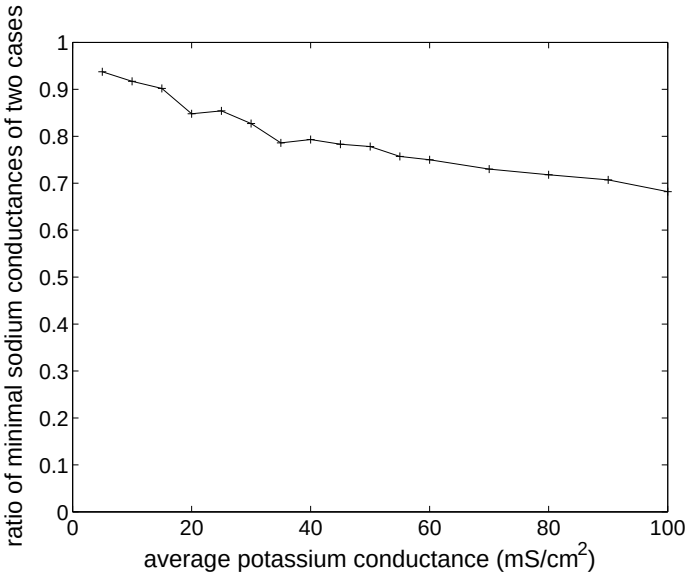

Figure 8.3: The ratio of the minimal required sodium conductance.
The ratio of the minimal required sodium conductance in the two cases versus potassium channel conductance. In case one, 96% of potassium channels are localized in clusters. In case two, potassium channels are distributed uniformly. In both cases, the average potassium channel conductance is the same. The minimal required sodium conductance of case one is the numerator, and that of case two is the denominator.

Now we change the compartment number between potassium clusters then change the distance between two potassium clusters, and calculate the ratio of minimal required sodium conductance in the two cases. The two cases are again the same as above. The axon diameter is 2 μm, and the cytoplasmic resistivity is 70 Ωcm. The average potassium channel conductance in the two cases is 20 mS/cm^2. The minimal required sodium conductance of the case when potassium channels are distributed uniformly is 23 mS/cm^2. Fig.8.4 shows that as one increases the distance between potassium channel clusters, the effect of potassium channel localization on propagation efficiency becomes large. When the distance between potassium channel clusters reaches 26 μm, the ratio of minimal required sodium conductance in the two cases reaches a minimal value.

Now, we test the effect of potassium channel localization on action potential propagation speed. The axon diameter is 2 μm, and the cytoplasmic resistivity is 70 Ωcm. The average potassium channel density is 20 mS/cm^2. We test four different sodium channel conductances:23 mS/cm^2, 30 mS/cm^2, 40 mS/cm^2 and 50 mS/cm^2. For each sodium conductance, we first calculate the propagation speed for different potassium channel localization, then divide the results by the propagation speed when potassium channels are uniformly distributed, to obtain the speed ratio. When potassium channels are uniformly distributed, the propagation speeds of the different sodium channel conductances 23 mS/cm^2, 30 mS/cm^2, 40 mS/cm^2 and 50 mS/cm^2 are 0.12 m/s, 0.15 m/s, 0.18 m/s and 0.2 m/s, respectively. As shown in Fig.8.5, the propagation speed increases for increasing potassium channel localization. As sodium conductance is increased, the effect of potassium channel localization on propagation speed decreases.

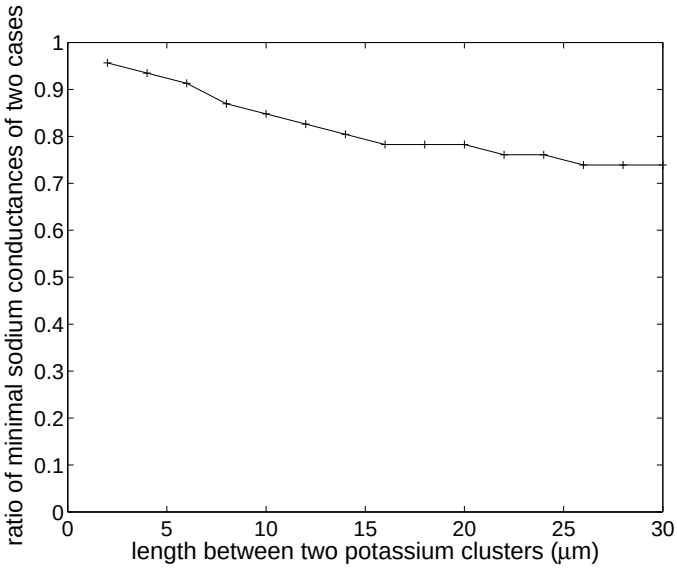

Figure 8.4: The ratio of minimal required sodium conductance.
The ratio of minimal required sodium conductance in the two cases versus distance between potassium channel clusters. In case one, 96% potassium channels localize in clusters. In case two, potassium channels distribute uniformly. In the two cases, the average potassium channel conductance is 20 mS/cm^2. The minimal required sodium conductance of case one is the numerator, and that of case two is the denominator.

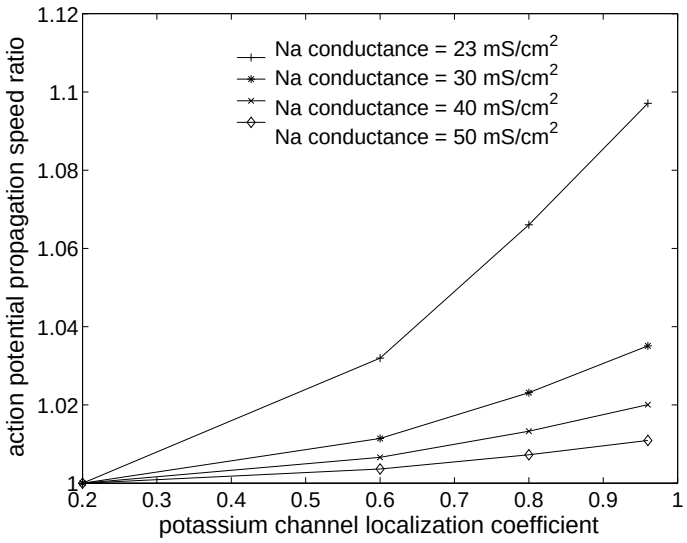

Figure 8.5: The effect of potassium channel localization on propagation speed.

8.2.2 Effect of sodium channel localization

Now we test the effect of sodium channel localization. The axon diameter is 2 μm, and the cytoplasmic resistivity is 70 Ωcm. For different potassium conductances, we calculate the ratio of minimal required sodium conductances in two cases. In case one, there is one sodium channel cluster for every five compartments, and all the sodium channels are localized in the clusters. In case two, sodium channels are distributed uniformly along the axon. The ratio of minimal required sodium conductance is plotted in Fig.8.6. As shown in Fig.8.6, when the potassium conductance is low, sodium channel localization will reduce the minimal required sodium conductance. When the potassium conductance is high, sodium channel localization will increase the minimal required sodium conductance. Localization of sodium channels is advantageous to propagation efficiency only when the potassium conductance is low.

Now we test the effect of the distance between sodium channel clusters on the propagation efficiency. The axon diameter is 2 μm, and the cytoplasmic resistivity is 70 Ωcm. The length of each sodium channel cluster is 2 μm. We calculate the ratio of the minimal required sodium conductance in both cases versus distance between the two clusters. The two cases are the same as above. The result is shown in Fig.8.7. As shown in Fig.8.7, the ratio of minimal required sodium conductance first decreases, reaches a minimal value, and then increases again for increasing distance between the clusters. There is an optimal distance which the propagation efficiency is best.

Now we test the effect of sodium cluster length on the ratio of minimal required sodium conductance in both cases. The two cases are the same as above. The distance between sodium channel clusters is 10 μm, the axon diameter is 2 μm, the cytoplasmic resistivity is 70 Ωcm, and the potassium channel conductance is 20 mS/cm^2. The ratio of mini-

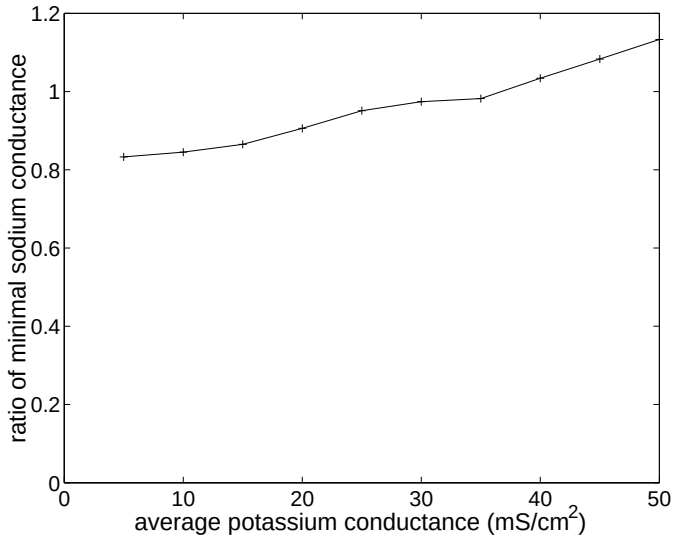

Figure 8.6: The ratio of minimal required sodium conductances.
The ratio of minimal required sodium conductances in two cases versus different potassium conductance. In case one, every fifth compartment has one sodium cluster, and all the sodium channels localize in the clusters. In case two, sodium channels distribute uniformly along the axon. The minimal required sodium conductance of case one is the numerator, and that of case two is the denominator.

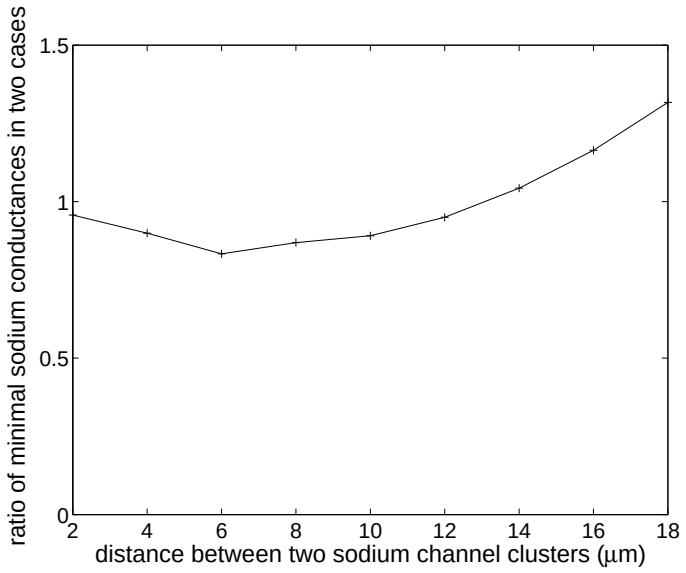

Figure 8.7: The ratio of minimal required sodium conductances.
The ratio of minimal required sodium conductances in two cases versus different distances between sodium channel clusters. In case one, every fifth compartment has one sodium cluster, and all the sodium channels localize in the clusters. In case two, sodium channels are distributed uniformly along the axon. The minimal required sodium conductance of case one is the numerator, and that of case two is the denominator.

mal required sodium channel conductances is plotted in Fig.8.8. As shown in Fig.8.8, for increasing sodium channel cluster length, the ratio of minimal required sodium channel conductances increases. When the length of sodium channel clusters is less than 3.5μm, localization of sodium channels is advantageous to propagation efficiency, otherwise, localization of sodium channels is disadvantageous to propagation efficiency.

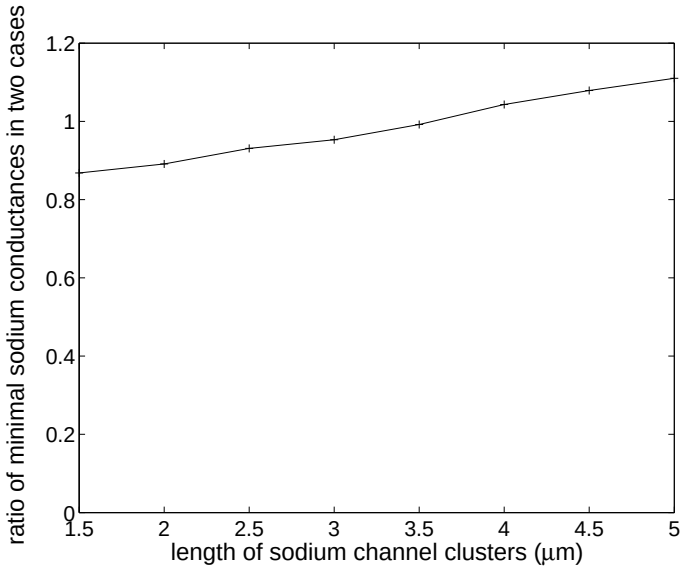

Figure 8.8: The ratio of minimal required sodium conductances.
The ratio of minimal required sodium conductances in two cases versus different sodium channel cluster length. In case one, every fifth compartment has one sodium cluster, and all the sodium channels localize in clusters. In case two, sodium channels are distributed uniformly along the axon. The minimal required sodium conductance of case one is the numerator, and that of case two is the denominator.

Now we test the effect of cytoplasmic resistivity on the ratio of minimal required sodium channel conductance in two cases. The two cases are the same as above. The axon diameter is 2 μm, and the potassium channel conductance is 20 mS/cm^2. The ratio of

minimal required sodium channel conductances is plotted in Fig.8.9. As shown in Fig.8.9, with increasing cytoplasmic resistivity, the ratio of minimal required sodium channel conductance increases. When the cytoplasmic resistivity is less than $120\Omega cm$, localization of sodium channels is advantageous to propagation efficiency, otherwise, localization of sodium channels is disadvantageous to propagation efficiency.

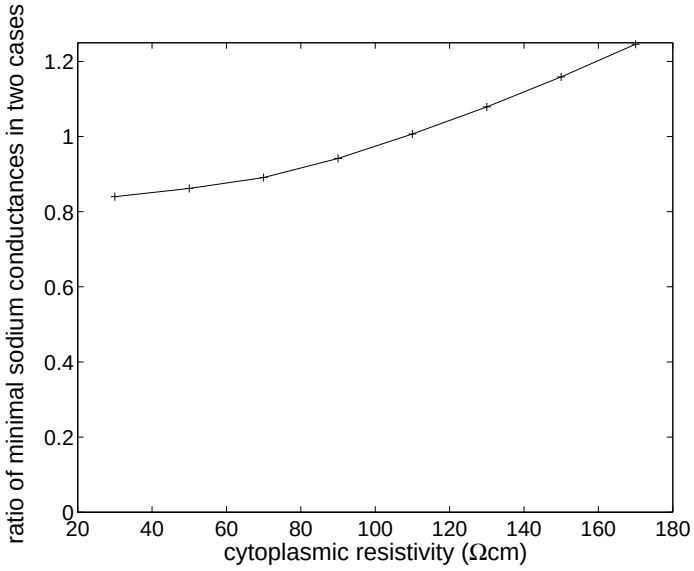

Figure 8.9: The ratio of minimal required sodium conductances.
The ratio of minimal required sodium conductances in two cases versus cytoplasmic resistivity. In case one, every fifth compartments has one sodium cluster, and all the sodium channels localize in clusters. In case two, sodium channels are distributed uniformly along the axon. The minimal required sodium conductance of case one is the numerator, and that of case two is the denominator.

We also have tested the effect of sodium channel localization on the action potential propagation speed. Our results show that localization of sodium channels has only a weak effect on the action potential propagation speed.

8.3 Discussion

Localization of ion channels in myelinated axons is accompanied by the formation of myelin. The cells responsible for myelin formation are different for CNS (Oligodendrocytes) and PNS (Schwann cells). The thickening of myelin and Na channel localization will increase the propagation speed of action potential. But the mechanisms and effects of ion channel localization in unmyelinated axon are unclear. In this chapter, we investigated theoretically the effect of localization of ion channels along unmyelinated axons. We mainly focused on two aspects: propagation efficiency and propagation speed. Our results show that potassium channel localization is beneficial for increasing propagation efficiency and propagation speed of action potentials. Localization of sodium channels is advantageous to propagation efficiency only when axonal parameters are in a specific range. Potassium ion channels play an important role in the modulation of excitability(3). In their pioneering work on neuronal excitability, Hodgkin and Huxley(23) demonstrated that potassium ion channels play an important role in the repolarization of action potential in the squid giant axon.

There are two kinds of functions for internodal potassium ion channels in myelinated axons. One is that they stabilize the paranodal axolemma against nodal back-firing after a single impulse(45). The other is to maintain a resting potential under the myelin(47; 48). Localization of potassium channels decreases the potassium conductance of the axon between potassium clusters, and affects the repolarization of action potentials, the electrical stability at the resting potential of the axonal membrane and the resting potential of the axonal membrane. In order to counterbalance the effect of potassium ion channel localization, it is necessary to decrease the sodium conductance of the axonal membrane between potassium channel clusters. Then localization of potassium ion channels and sodium ion

channels at the same sites can not only increase the propagation efficiency but also maintain the electrical stability of the axonal membrane.

According to the results of this chapter, we can construct a better axon for better propagation efficiency with sufficient electrical stability. For the same potassium channel localization, increasing cytoplasmic resistivity, distance between potassium channel clusters and average potassium conductance all will increase the propagation efficiency. For the same sodium channel localization, increasing cytoplasmic resistivity, distance between sodium channel clusters and average potassium conductance, will decrease the propagation efficiency. There are optimal values of cytoplasmic resistivity, distance between channel clusters and average potassium conductance to optimize the propagation efficiency and electrical stability of unmyelinated axons with ion channel clusters. In future research, I will try to find the series of optimal values.

Chapter 9

Conclusion and outlook

We have compared the average interspike interval and the relative fluctuations of trains of action potentials generated by small and large clusters of ion channels. For large ion channel clusters, action potentials are elicited when the fraction of open sodium channels exceeds a threshold value. The fraction of open channels is mainly determined by the magnitude of the synaptic noise. For small ion channel clusters, channel noise dominates over synaptic noise. Action potentials are generated at a frequency that is determined by the single channel kinetics and is only weakly dependent on the synaptic noise. We have further shown that at the size of the ion channel cluster at which a maximum spontaneous spiking rate is observed, the spike trains exhibit maximum temporal periodicity.

Synchronization is a basic phenomenon in science, and has many applications in living systems. In neurons, the spiking frequency and time of action potentials can be synchronized by weak interactions. Ion channels are usually distributed uniformly along the unmyelinated axon to support stable action potential propagation. In some cases, however, ion channels are also distributed in clusters along unmyelinated axons. The ion channel clusters along the unmyelinated axon generates spontaneous spiking due to channel noise.

If the ion channel clusters are coupled by an axonal cable, then the spontaneous spiking of the clusters can be synchronized. In order to measure the synchronization strength, we calculate the average consecutive number of synchronized spikes. Increasing the axonal diameter, decreasing the specific membrane capacitance and the specific electrical resistivity will increase the synchronized spiking number dramatically. It is also shown that the homogeneous distribution of ion channel clusters produces the maximal number of synchronized spikes. It is also shown that there is an optimal size of ion channel clusters to produce a maximal number of synchronized spikes.

An important requirement for the evolution of organisms is the stable, efficient and fast propagation of action potentials. An elegant solution of this problem is the development of the myelinated axon. The nodes of Ranvier are distributed along the axon where the myelin is interrupted at distances ranging from $50\mu m$ to $1000\mu m$ for different nerves. These spatial axonal domains differ dramatically from internodal axon regions. Sodium channels can be found in the nodes of Ranvier at a much larger density than in the internodal region. Potassium channels are excluded from nodes of Ranvier; they are clustered beneath the myelin shealths in juxtaparanodes. We simulated the action potentials of two nodes connected by an axon. Our simulations show that blockage of internodal potassium ion channels can induce axonal oscillations in the developing axon, but has no effect on the action potential of normal mature axons. These results are consistent with experimental observations. Our simulations also show that internodal potassium ion channels stabilize the internodal axolemma, and prevent axonal oscillation in developing axons. We tested the effect of axonal parameters with respect to the onset of axonal oscillation. While the leakage current has no effect on axonal bursting, increasing internodal sodium conductance as well as increasing internodal membrane capacitance can facilitate axonal oscillation.

The mechanism and function of ion channel localization along an unmyelinated axon is unclear. In this thesis, I performed a theoretical investigation of the effect of ion channel localization along unmyelinated axons. I mainly focused on two aspects: propagation efficiency and propagation speed. Our results show that localization of potassium channels can improve propagation efficiency and speed. Average potassium conductance, size of sodium channel clusters and cytoplasmic resistivity can affect the effect of sodium channel localization on propagation efficiency. In a specific range of the above parameters, sodium channel localization increases the propagation efficiency. But if one of the above parameters exceeds this range, sodium channel localization is detrimental to the propagation efficiency. Sodium channel localization has a minor effect on the propagation speed.

In the future, I will carry out research in the following aspects. In myelinated axons, although most sodium channels are localized in nodes of Ranvier to regenerate action potentials, sodium channels can not be excluded from internodal regions completely(41; 42; 43; 45). The density of internodal sodium channels is approximately 5% of that of nodes of Ranvier(41; 42; 43; 45). In the past, the function of internodal sodium channels has been neglected, however, our preliminary research results show that internodal sodium channels play an important role in action potential propagation. Because the density of internodal sodium channels is low, it is more valid to use the stochastic HH equations to investigate this problem. In the future, I will use deterministic HH equations (for nodes of Ranvier), stochastic HH equations (for internodal sodium channels) and the cable equation to investigate the function of internodal sodium channels on action potential propagation and firing pattern. In chapter 6, I found that there is an optimal length of ion channel clusters along unmyelinated axons for which the consecutive synchronized spiking number is maximal. This result inspires me to investigate whether there is an optimal length of nodes of Ran-

vier along myelinated axons for which the valid propagation distance of action potentials is maximal. In the future, I will use deterministic HH equations and the cable equation to investigate this problem, and try to find the optimal length of nodes of Ranvier and the effects of axonal parameters on the optimal length. In chapter 8, I demonstrated that in order to guarantee electrical stability and increase the propagation efficiency of action potentials of unmyelinated axons, it is necessary to localize sodium ion channels and potassium ion channels. For the same potassium channel localization, increasing cytoplasmic resistivity, distance between two potassium channel clusters and average potassium conductance all will increase the propagation efficiency. For the same sodium channel localization, increasing cytoplasmic resistivity, distance between two sodium channel clusters and average potassium conductance, will decrease the propagation efficiency. There are optimal values of cytoplasmic resistivity, distance between two channel clusters and average potassium conductance to optimize the propagation efficiency and electrical stability of unmyelinated axons with ion channel clusters. In future research I will try to find the series of optimal values.

Bibliography

[1] E. R. Kandel and J. H. Schwartz,*Principles of Neural Science*, Elsevier (1985)

[2] E. Neher and B. Sakmann, Nature **260**, 779 (1976)

[3] B. Hille, *Ionic Channels of Excitable Membranes*, Sinauer Associates (1992)

[4] C. Hildebrand and S. G. Waxman, Brain Research **258**, 23 (1983)

[5] J. R. Clay and A. M. Kuzirian, Journal of Neurobiology **45**(3), 172 (2000)

[6] W. L. Johnston, J. R. Dyer, V. F. Castellucci, and R. J. Dunn, J. of Neurosci. **16** 1730 (1996)

[7] F. Bezanilla, Biophys. J. **52**, 1087 (1987)

[8] J. M. Bekkers et al., J. Physiol. **377**, 463 (1986)

[9] I. Llano, C. K. Webb and F. Bezanilla, J. Gen. Physiol. **92**, 179 (1988)

[10] C. C. Chow and J. A. White, Biophys. J. **71**, 3013 (1996)

[11] E. Schneidman, B. Freedman and I. Segev, Neural Computation **10**, 1679 (1998)

[12] P. Jung and J. W. Shuai, Europhys. Lett, **56**, 29 (2001)

[13] C. Koch, *Biophysics of Computation: Information Processing in Single Neurons* Oxford University Press (1999)

[14] S. G. Waxman and J. M. Ritchie, Science **228**, 1502 (1985)

[15] S. Y. Chiu and J. M. Ritchie, J. Physiol.**322**, 485 (1982)

[16] T. Brismar, J. Physiol. **298**, 171 (1980)

[17] A. F. Huxley and R. Stampfli, J. Physiol. **108**, 315 (1949)

[18] I. Tasaki, *Nervous Transmission*, Springfield, Illinois (1953)

[19] J. Roper and J. R. Schwarz, J. Physiol. **416**, 93 (1989)

[20] B. V. Safronov, K. Kampe, and W. Vogel, J. Physiol. **460**, 675 (1993)

[21] B. Neumcke and R. Stampfli, J. Physiol. **329**, 163 (1982)

[22] A. Scholz, G. Reid, W. Vogel, and H. Bostock, J. Neurophysiol. **70**, 1274 (1993)

[23] A. L. Hodgkin and A. F. Huxley, J. Physiol. **117**, 500 (1952)

[24] E. Skaugen and L. Walloe, Acta Physiol. Scand **107**, 343 (1992)

[25] L. J. DeFelice and A. Isaac, J. Statist. Phys. **70**, 339 (1992)

[26] P. N. Steinmetz, A. Manwani and C. Koch, Journal of computational Neuroscience **9**, 133 (2000)

[27] R. F. Fox and Y. N. Lu, Phy. Rev. E. **49**, 3421 (1994)

[28] R. F. Fox, Biophysical Journal **72**, 2068 (1997)

[29] J. A. White, J. T. Rubinstein and A. R. Kay, Trends Neurosci. **23**, 131 (2000)

[30] F. M. Rieke, D. de Ruytervan Stevenick and W. Bialek, *Spikes: Exploring the Neural code* (MIT, Cambridge, MA, 1997)

[31] W. A. Catterall, Ann. Rev. Biochemistry **64**, 493 (1995)

[32] J. Keener and J. Sneyd, Mathematical Physiology, Springer Verlag (2000)

[33] D. A. Doyel et al., Science **280**, 69 (1998)

[34] S. Einheber, G. Zanazzi, W. Ching, S. Scherer, T. A. Milner, E. Peles and J. L. Salzer, J. Cell Biol. **149**, 491 (1997)

[35] W. A. Catterall, Science **242**, 50 (1988)

[36] W. A. Catterall, Physiol. Rev. **72**, 515 (1992)

[37] H. Baba, H. Akita, T. Ishibashi, Y. Inoue, K. Nakahira, and K. Ikenada. Journal of Neuroscience Research **58**:752-764 (1999)

[38] J. L. Dupree, T Coetzee, A Blight, K. Suzuki, and B. Popko, J. Neurosci. **18**:1642-1649 (1998)

[39] S. D. Novakovic, A. G. Koszowski, S. R. Levinson, and P. Shrager, J. Neurosci. **15**:492-503 (1995)

[40] R. L. Friede and W. Beuche, J. Neuropathol. Exp. Neurol. **44**, 60 (1985)

[41] P. Shrager, J. Physiol. **392**, 587 (1987)

[42] P. Shrager, J. Physiol. **404**, 695 (1988)

[43] P. Shrager, Brain Res. **483**, 149 (1989)

[44] S. Y. Chiu, J. M. Ritchie, R. B. Rogart and D. Stagg, J. Physiol. **292**, 149 (1979)

[45] S. Y. Chiu, J. M. Ritchie, J. Physiol. **313**, 415 (1981)

[46] H. Wang, D. D. Kunkel, T. M. Martin, P. A. Schwartzkroin and B. L. Tempel, Nature **365**, 75 (1993)

[47] S. Y. Chiu and J. M. Ritchie, J. Physiol. **322**, 485 (1982)

[48] S. Y. Chiu and J. M. Ritchie, Proc. R. Soc. Lond. B **220**, 415 (1984)

[49] I. Vabnick, S. D. Novakovic, S. R. Levinson, M. Schachner and P. Shrager, J. Neurosci. **16**, 4914 (1996)

[50] M. N. Rasband, E. Peles, J. S. Trimmer, S. R. Levinson, S. E. Lux, and P. Shrager, J. Neurosci. **19**, 7516 (1999)

[51] M. Menegoz, P. Gasper, M. L. Bert, T. Galvez, F. Burgaya, C. Palfrey, P. Ezan, F. Arnos, and J. Girault, Neuron **19**, 319 (1997)

[52] C. V. Melendez-Vasquez J. C. Rios, G. Zanazzi, S. Lambert, A. Bretscher, and J. L. Salzer, Proc. Natl. Acad. Sci. USA **98**, 1235 (2001)

[53] J. Rosenbluth, J. Neurocytol. **28**, 251 (1999)

[54] K. J. Rhodes, B. W. Strassle, M. M. Michael, Z. Bekele-Arcuri, M. F. Matos and J.S. Trimmer, J. Neurosci. **17**, 8246 (1997)

[55] M. N. Rasband, J. S. Trimmer, J. Comp. Neurol. **429**, 166 (2001)

[56] M. N. Rasband, J. S. Trimmer, E. Peles, S. R. Levinson, S. E. Lux and P. Shrager, J. Neurocytol. **28**, 319 (2001)

[57] M. N. Rasband, J. S. Trimmer, T. L. Schwarz, S. R. Levinson, M. H. Ellisman, M. Schachner, and P. Shrager, J. Neurosci. **18**, 36 (1998)

[58] H. Wang, M. L. Allen, J. J. Grigg, J. L. Noebels, and B. L. Tempel, Neuron **15**, 1337 (1995)

[59] M. N. Rasband and P. Shrager, J. Physiol. **525**, 63 (2000)

[60] A. L. Hodgkin and A. F. Huxley, J. Physiol. **116**, 449 (1952)

[61] A. L. Hodgkin and A. F. Huxley, J. Physiol. **116**, 473 (1952)

[62] A. L. Hodgkin and A. F. Huxley, J. Physiol. **116**, 497 (1952)

[63] A. L. Hodgkin and W. A. H. Rushton, Proc. R. Soc. London B **133**, 444 (1946)

[64] A. Pikovsky, M. G. Michael, G. V. Osipov, and J. Kurths, Physica D **104**, 219 (1997)

[65] L. Davis and R. Lorente de No, Studies from the Rockefeller Institute for Medical Research **131**, 442 (1947)

[66] W. Rall, Cable theory for dendritic neurons. In: *Methods in Neuronal Modelling.* C. Koch and I. Segev editors, pp. 9-62. MIT Press: Cambridge, Massachusetts (1989)

[67] I. Segev, and R. E. Burke, In *Methods in Neuronal Modeling: From Ions to Networks.* C. Koch, and I. Segev editors, pp. 93-136. The MIT Press. Cambridge, Massachusetts, London, England, (1998)

[68] D. H. Perkel and B. Mulloney, American Journal of Physiology **235**, 93 (1978)

[69] Shangyou Zeng, and Peter Jung, Phy. Rev. E **70**, 011903 (2004)

[70] W. Rall, R. F. Reiss editor In: *Neural Theory and Modelling* (Stanford University Press: Palo Alto, 1964)

[71] P. C. Bressloff, Phy. Rev. E **50** 2308 (1994)

[72] J.R. Clay and L. J. DeFelice, Biophys. J. **42**,151 (1983)

[73] N. Brunel, F. S. Chance, N. Fourcaud and L. F. Abbott, Phy. Rev. Lett, **86**, 2186 (2001)

[74] G. Schmid, I. Goychuk and P. Hänggi, Europhys. Lett., **56**, 22 (2001)

[75] A. Manwani and C. Koch, Neural Computation **11**, 1797 (1999)

[76] D. Bramble, and D. Carrier, Science **219**, 251 (1983)

[77] M. Rosenblum, A. Pikovsky, C. Schafer, P. A. Tass, J. Kurths, *Neuro-Informatics and Neural Modelling* (North-Holland, Elsevier 2001)

[78] C. Hayashi, *Nonlinear Oscillations in Physical Systems* (McGraw-Hill, New York, 1964)

[79] P. Landa, *Nonlinear Oscillations and Waves in Dynamical Systems* (Kluwer Academic Publishers, Dordrecht, Boston, London, 1996)

[80] M. Rosenblum, A. Pikovsky, and J. Kurths. Phys. Rev. Lett. **76**, 1804 (1996)

[81] L. Glass, and M. C. Mackey, *From Clocks to Chaos: The Rhythms of life* (Princeton University Press, Princeton, NJ, 1988)

[82] J. Sturis, C. Knudsen, N. M. O'Meara, J. S. Thomsen, E. Mosekilde, E. Van Cauter, and K. S. Polonsky, Chaos **5**,193 (1995)

[83] A. Neiman, X. Pei, D. Russell, W. Wojtenek, L. Wilkens, F. Moss, H. A. Braun, M. T. Huber, and K. Voigt, Phys. Rev. Lett. **82**, 660 (1999)

[84] W. Singer, and C. Gray. Annu. Rev. Neurosci. **18**, 555 (1995)

[85] C. Gray, and W. Singer. Soc. Neurosci. **404**, 3 (1987)

[86] C. Hildebrand, and S. G. Waxman, Brain Research **258**, 23 (1983)

[87] R. Nossal, and H. Lecar, *Molecular and Cell Biophysics.* Addison-Wesley. Redwood City, CA.

[88] J. M. Ritchie, Proc. Roy. Soc. Lond. B **217**, 29 (1982)

[89] R. B. Rogart, and J. M. Ritchie, *Physiological basis of conduction in myelinated nerve fibers* Plenum Press. New York, 1977

[90] C. M. Bowe, J. D. Kocsis and S. G. Waxman, Proc. R. Soc. Lond. B **224**, 355 (1985)

[91] J. D. Kocsis, S. G. Waxman, C. Hildebrand and J. A. Ruiz, Proc. R. Soc. Lond. B **217**, 77 (1982)

[92] I. Vabnick, J. S. Trimmer, T. L. Schwarz, S. R. Levinson, D. Risal and P. Shrager, J. of Neuroscience **19**, 747 (1999)

[93] C. C. Mcintype, A. G. Richardson and W. M. Grill, J. Neurophysiol. **87** 995 (2002)

[94] D. Franceschetti, E. Guatteo, F. Panzica, G. Sancini, E. Wanke and G. Avanzini, Brain Res. **696** 127 (1995)

[95] R. Azouz, M. S. Jensen and Y. Yaari, J. Physiol. **492** 211 (1996)

[96] H. Jahnsen and R. Llinas, J. Physiol. **349** 205 (1984)

[97] W. Guido and T. Weyand, J. Neurophysiol. **74** 1782 (1995)

[98] P. F. Pinsky and J. Rinzel, Journal of Computational Neuroscience **1** 39 (1994)

[99] C. R. Laing and A. Longtin, Phy. Rev. E **67** 51928 (2003)

[100] J. R. Clay, and A. M. Kuzirian, Mol Biol Cell **10**:1312 Suppl. (1999)

[101] J. R. Clay, and A. M. Kuzirian, Biophys J. **76**(1):A223 (1999)

[102] R. W. Turner, et. al. J. Neurosci. **14** 6453 (1994)

[103] W. Almers, P. R. Stanfield and W. Stuhmer. J. Physiol. **336** 261 (1983)